The effect of Cold Atmospheric Plasma (CAP) on the molecular mechanism of wound healing

I n a u g u r a l d i s s e r t a t i o n

zur

Erlangung des akademischen Grades eines

Doktors der Naturwissenschaften (Dr. rer. nat.)

der

Mathematisch-Naturwissenschaftlichen Fakultät

der

Universität Greifswald

vorgelegt von

Debarati Shome

geboren am 15.03.1992

in Kolkata, India

Greifswald, den 15.06.2020

Dekan: Prof. Dr. Gerald Kerth

1. Gutachter: Prof. Dr. Katharina Riedel

2. Gutachter: Prof. Dr. Michael Lalk

3. Gutachter: Prof. Dr. Steffen Emmert

Tag der Promotion: 02.11.2020

Contents

Contents

Abbreviations

ANOVA	Analysis of Variances
BMP	Bone Morphogenic Protein
BSA	Bovine Serum Albumin
CAP	Cold Atmospheric Plasma
CCR	C-C chemokine receptor
cDNA	Complementary Deoxyribo Nucleic Acid
CO_2	Carbon di Oxide
CTGF	Connective Tissue Growth Factor
CXCR	Chemokine Receptor
Cyr61	Cysteine Rich Angiogenic Inducer 61
ECM	Extracellular Matrix
EDTA	Ethylenediaminetetraacetic acid
EGF	Epidermal Growth Factor
ELISA	Enzyme Linked Immuno Sorbent assay
EPO	Erythropoietin
ERK	Extracellular signal Regulated Kinase
ETS	E26 transformation-specific or E-twenty-six
FAK	Focal Adhesion Kinase
FCS	Fetal Calf Serum
FGF	Fibroblast Growth Factor
FOXO	Forkhead family of transcription factors
GM Fbs	GM00637 Fibroblasts
GM-CSF	Granulocyte Macrophage Colony Stimulating Factor
GSH	Reduced Glutathione
H_2O_2	Hydrogen peroxide
HaCaT	Human adult low calcium temperature keratinocytes
HB EGF	Heparin Binding EGF line Growth Factor
HGF	Hepatocyte Growth Factor
HIF 1α	Hypoxia-Inducible Factor 1-alpha
ICAM-1	Intercellular Adhesion Molecule 1
IGF	Insulin like Growth Factor
IgG	Immunoglobulin G
IL	Interleukins
IR	Infrared Radiation
ITAC	Interferon–inducible T Cell Alpha Chemoattractant
KEAP-1	Kelch-like ECH-Associated Protein 1
LATS	Large tumor suppressor kinase
MCP-1	Monocyte Chemoattractant Protein-1

MEK	Map Kinase Kinase
MIP-1	Macrophage Inflammatory Protein
MMP	Matrix Metallo Proteinase
MST	Macrophage-stimulating protein
mTOR	mechanistic Target of Rapamycin
NAC	N-acetyl L- Cysteine
NaCl	Sodium Chloride
NADPH	Nicotinamide Adenine Dinucleotide Phosphate Hydrogen
NRF2	Nuclear factor erythroid 2–Related Factor 2
PBS	Phosphate Buffered Saline
PCR	Polymerase Chain reaction
PDGF	Platelets Derived Growth Factor
PI3K	Phosphoinositide 3-kinases
PTEN	Phosphatase and Tensin Homolog
PVDF	Polyvinylidene fluoride
qPCR	Quantitative Polymerase Chain Reaction
Ras	Proto-oncogene protein p21
Redox	Oxidation Reduction
RNA	Ribo Nucleic Acid
RNS	Reactive Nitrogen Species
RONS	Reactive Oxygen and Nitrogen Species
ROS	Reactive Oxygen Species
RPMI	Roswell Park Memorial Institute
SDS	Sodium Dodecyl Sulphate
SLM	Standard Liters Per Minute
SOD	Superoxide Dismutase
TBS	Tris Buffered Saline
TBST	Tris Buffered Saline Tween
TEA	Transcriptional enhancer factor TEF-1
TGF	Transforming Growth Factor
TIMP	Tissue Inhibitor of Metallo Proteinases
TNF	Tumor Necrosis Factor
UV	Ultraviolet
VEGF	Vascular Endothelial Growth Factor
VUV	Vacuum Ultra Violet
YAP	Yes Associated Protein

1. Introduction

1.1   Human Skin

The human skin is the largest organ of the body. The skin and its accessory structure make up the integumentary system which protects the body against mechanical, physical and chemical stress [1]. The skin is composed of two main layers: the epidermis, made of closely packed epithelial cells, and the dermis, made of dense, irregular connective tissue that houses blood vessels, hair follicles, sweat glands, and other structures. Beneath the dermis lies the hypodermis, which is composed mainly of loose connective and fatty tissues. Figure 1.1 illustrates the human skin comprising the epidermis, dermis and hypodermis. The epidermis is divided into the layers stratum basale, stratum spinosum, stratum granulosum and stratum corneum [2]. Except stratum basale, the cells in all the other epidermal layers are called keratinocytes, consist >90% of the total epidermis and are at various differentiation stages in different layers. During this process of differentiation, the keratinocytes flatten more and more and at the stratum corneum they lose their cell nuclei [2]. The stratum basale is a single cell layer primarily made of basal cells. Two other cell types are found interspersed among basal cells, i.e., merkel cell and melanocytes. The dermis might be considered as the core of integumentary system and contains blood and lymph vessels, nerves, and other structures, such as hair follicles and sweat glands. The dermis is made of two layers of connective tissue that compose an interconnected mesh of elastin and collagenous fibers, produced by fibroblasts [2]. In our study, we focused on the two major cell types of epidermis and dermis, keratinocytes and fibroblasts, respectively.
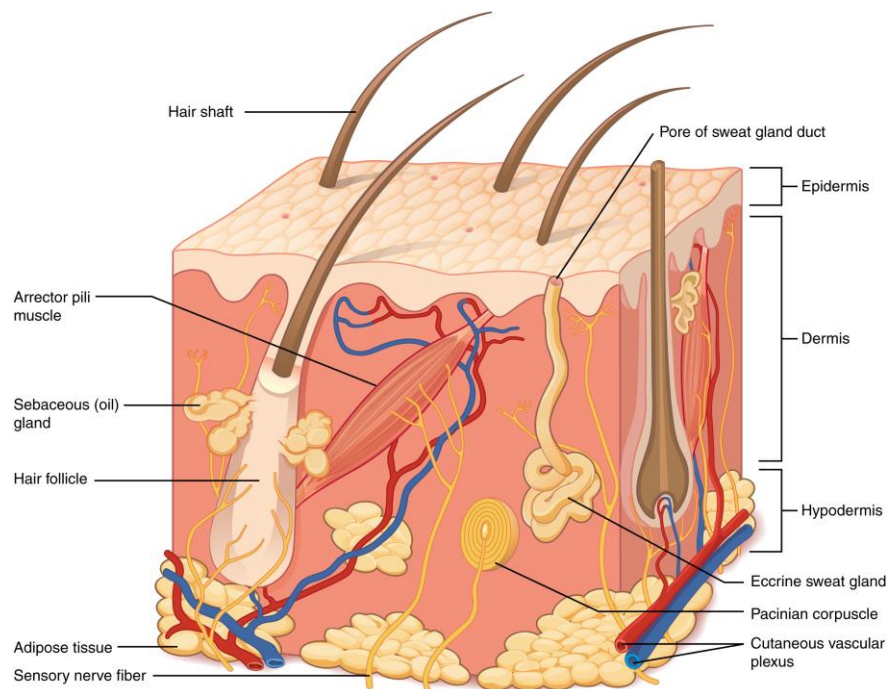
Figure 1.1 Layers of human skin, comprised of epidermis, dermis and hypodermis. The figure is adapted from Open Stax, Anatomy and physiology [2].

1.2 Wound Healing

Wound healing is one of the well-orchestrated complex processes within the human body and consists of four interdependent and overlapping phases namely hemostasis, inflammation, proliferation and remodeling [3, 4]. Figure 1.2 illustrates the sequential stages of wound healing. Over these four intertwined phases, spatial and temporal synchronization of various cell types resolves the wound. The hemostasis phase is characterized by platelet aggregation, degranulation, vascular constriction and fibrin formation. The inflammatory phase is caused by invading microorganisms and starts with the infiltration of neutrophils at the wound bed followed by macrophages and leucocytes. The proliferation phase is highly overlapping with the inflammatory phase and is characterized by angiogenesis where new blood vessels are formed, collagen synthesis for extracellular matrix deposition and re-epithelialization. The final stage of wound healing is remodeling, where the collagen and vascular structure are restructured. In case, a cutaneous wound is formed, wounds are healing anywhere from within a few days up to a few weeks. However, when wounds do not follow these "routine steps" and do not show any sign of resolution even after 4 weeks, are designated as non-healing or chronic wounds. It is often referred that a prolonged inflammatory phase leads to chronic wounds [5]. We will now discuss the acute and chronic wound separately.

Figure 1.2 Sequential illustration of wound healing stages. The figure is adapted and modified from www.biodermis.com and Akbik et al. [6].

1.3   Acute Wounds

Acute wounds result from surgical wounds or trauma such as burns, excoriations, animal bites etc. [7]. A complete wound healing is characterized by 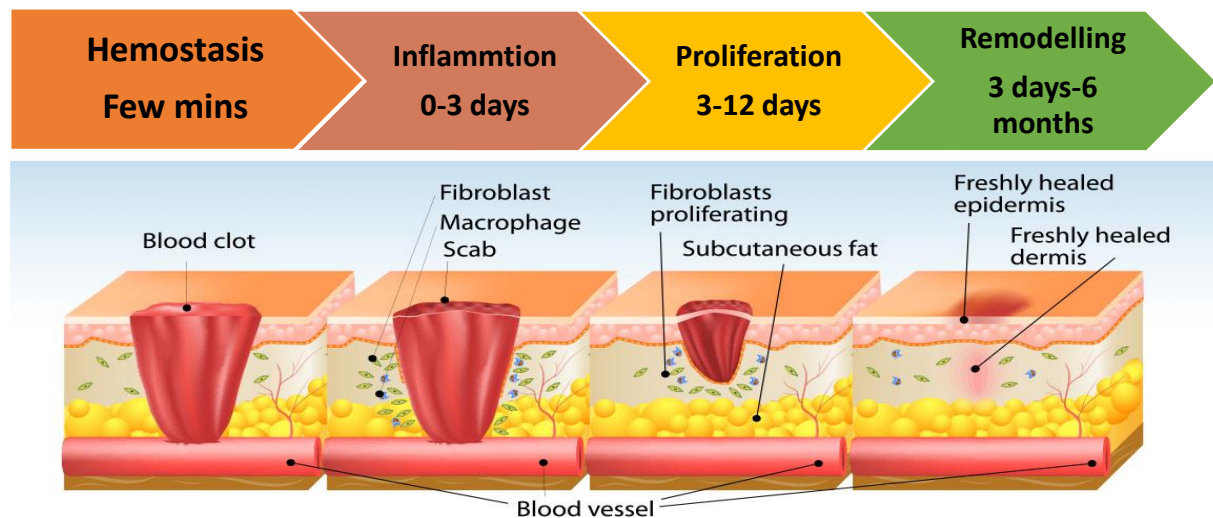four interdependent and overlapping phases where different cell types like keratinocytes, fibroblasts, immune surveillance cells, microvascular cells play an important role in tissue repair and regeneration [8, 9]. Immediately after injury, platelets aggregate at the wound site, begin a hemostatic reaction and induces a blood clotting cascade which constrains excessive blood loss. Platelets attracts the first horde of immune cells like neutrophils, leucocytes and monocytes/macrophages by releasing key chemotactic molecules like PDGF, TGF-α1 and α2 [10, 11]. Neutrophils are the first to appear at the wound site in large numbers. Once in the wound site, the integrin receptors at the surface of neutrophils enhance cell matrix interactions and enables the neutrophils to kill and phagocytose bacteria and wound debris [11, 12]. Mast cells at the wound site also release histamines, leukotrienes, cytokines and proteases which are additional signals for leukocyte recruitment [13]. Monocytes are the most important immune cells for the later stages of inflammation resolution. At the wound site, they are recruited in response to chemotactic factors like MCP-1[14] and MIP-1 [15] and are differentiated to macrophages. Extracellular matrix degradation products like collagen and fibronectin fragments also attract monocytes [16]. Macrophages mediate the subsequent obliteration by killing remaining pathogenic organisms, scavenging tissue debris and killing any remaining neutrophils which have not initiated apoptosis [11]. Macrophages are the source of cytokines and growth factors that initiate cell migration, proliferation and re-epithelialization. First keratinocytes at the wound edge change their shape, become flatter

and elongated [3]. Important signaling molecules like FGF-7, EGF, TGF-α, TGF-ß, GM-CSF, matrix metalloproteinase and several cytokines induce keratinocyte migration and proliferation [3, 4]. These cytokines and growth factors also activate fibroblasts which proliferate and migrate into the granulation tissue, initiates collagen formation and wound constriction [17]. Fibroblasts can transform into myofibroblasts and contract the connective tissue at the wound site [3]. Concurrently, paracrine and autocrine interactions between different cell types, ECM and peripheral nerves leads to a hypoxic environment at the wound site, which is the major trigger for angiogenesis [10]. Hypoxic environment stimulates the production of HIF-1α from fibroblasts [18, 19], keratinocytes [20], macrophages [21, 22] and vascular endothelial cells [23]. The release of pro angiogenic factors from macrophages and fibroblasts like VEGF, VEGF-A, FGF-2, PDGF and TGF-ß1 and the metabolic switch in endothelial cells promote neovascularization [24]. Finally the fibroblasts proliferate and deposit ECM which sustains the newly formed blood vessels [19, 25]. The last and the longest phase of acute wound healing is the remodeling phase [3]. In this stage, the granulation tissue is diminished, metalloproteinase released from fibroblasts and macrophages destroy collagen III in the granulation tissue and replaces it with collagen I [10]. This stage can last up to a few months. The acute wound healing is illustrated in figure 1.3.
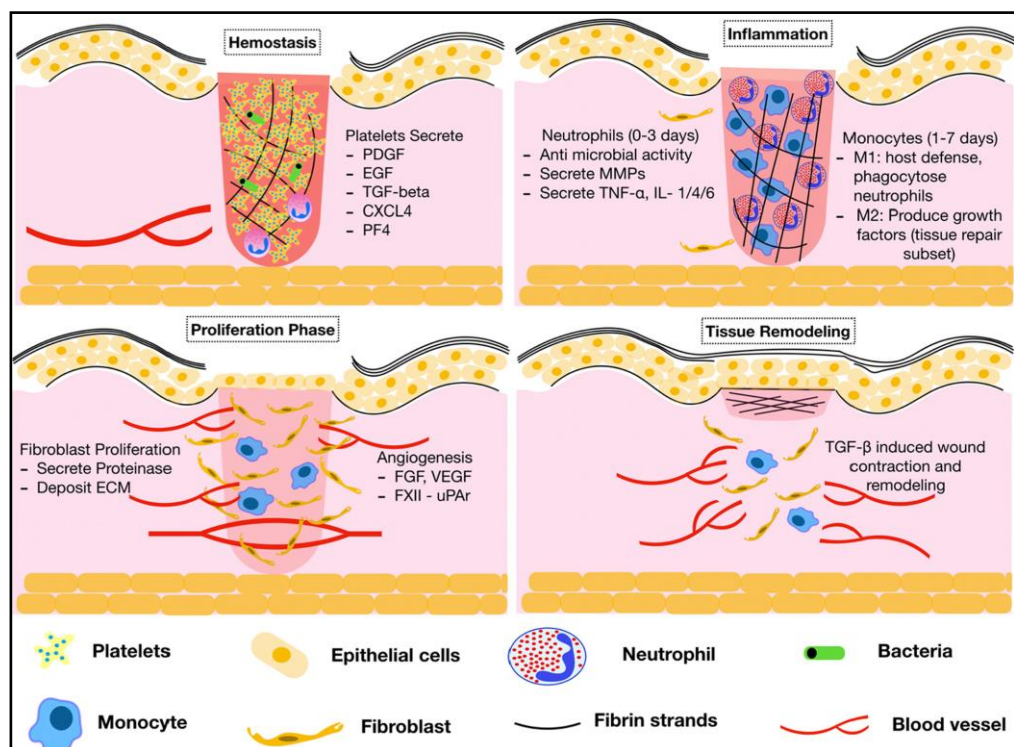

Figure 1.3 Illustration of relevant cell types and soluble mediators engaged in acute wound. The figure is adapted from Openja et al [26].

1.4   Chronic Wounds

Chronic wounds do not adhere to the standard course of wound healing. Venus leg ulcers, ischemic leg ulcer, diabetic foot ulcer and pressure sores are the most common examples of chronic wounds. Despite differences in molecular etiology, most of these chronic wounds share similar features with stalled inflammation, persistent infection, resistant microbial biofilm formation at the wound site and dermal cells failing to respond to a reparative stimulus [27-30]. Chronic wounds are characterized by prolonged and persistent infiltration of macrophages [31]. Loots et al., observed a higher population of CD8+T cells compared to CD4+ T cells, which resulted in an increased infiltration of macrophages, B cells and plasma cells in the chronic wound bed compared to acute wounds [31]. The reason for the increased infiltration of immune cells could be attributed to the higher level of pro inflammatory cytokines and growth factors at the chronic wound environment [32-35]. Healing ulcers correlated with the reduction of pro inflammatory cytokines like IL-1, IL-6 and TNF-α in wound fluid; [34] but also with TGF-beta increase in wound fluid [33]. Moreover, a distinct cytokine and chemokine expression signature have been also investigated. Chronic wound fluids showed a differential expression of well-known wound healing biomolecules like IL-1ß, PDGF, VEGF, bFGF, TGF-α, IL-6, IL-8, and IL-18 compared to acute wound fluids. However, lesser reported molecules in context of wound healing like RANTES, IL-17A, I-TAC, IL-23, IP-10 and EPO were differentially expressed in the two wound states [36]. Chronic wounds also display higher load of bacterial colonization at the wound site. Bacterial infection is an extrinsic factor that delays wound healing [37].   Bacteria and the infiltrated immune cells produce proteases which degrade the ECM and the growth factors [38]. Biofilms are prevalent in chronic wound [8, 39] and delays epithelialization [40].

Another characteristics of chronic wounds are phenotypic abnormalities of epidermis and dermis-derived cells [38]. Compared to healthy skin fibroblasts, fibroblasts isolated from chronic wounds show decreased mortality and have lower mitogenic potential in response to PDGF-AB, EGF, bFGF and IGF [38]. Keratinocytes also show lower migratory potential in chronic wounds. This phenomenon has been attributed to the lower production of laminin 332, which is an important substrate of ECM and therefore could be a reason for delayed re-epithelialization [41]. These keratinocytes also display an increased activation of A-catenin/c-myc pathway and do not express keratin 10 and 2, markers of differentiation [42]. Chronic wounds are also infiltrated with senescent fibroblasts. Diabetic patients often show matrix glycation, which could be a reason for premature senescence in fibroblasts, angiogenic sprout formation, decreased cell proliferation and migration [38, 43]. On one hand, matrix glycation can disrupt the matrix assembly and the interaction between collagen and the matrix binding partners. On the other hand, high glucose in diabetic patients induces the production of high MMPs by fibroblasts, macrophages and endothelial cells, thus contributing to matrix instability and therefore further delaying the wound healing [38, 44, 45].

5

Low levels of ROS are essential in all phases of wound healing. Low concentration of ROS are essential for the fight against invading microorganisms or redox signaling resulting in cell survival signaling [46]. Physiological concentration of ROS drives cell proliferation, migration and wound repair [46]. A balance between antioxidants and reactive species is therefore significant for wound healing. Elevated and sustained oxidative stress is frequently associated with chronic wounds. This is majorly due to the elevated production of ROS by infiltrated immune cells, which could lead to an imbalance between redox species and antioxidants in the wound resulting in oxidative stress at the wound situate [47]. Wound fluids collected from chronic wound patients also show a decrease in antioxidants, in fact chronic wounds show a lower expression of natural antioxidants Vitamin A and E [48] and glutathione [49]. Elevated ROS levels can damage endothelial cells, thus inhibiting angiogenesis [50]. High ROS levels at the chronic wound milieu can induce the expression of MMPs in fibroblasts and inactivate the TIMPs, thus ensuing in a highly proteolytic environment in the wound site and finally delaying wound healing [47, 51-54]. The chronic wound healing is shown in figure 1.4.
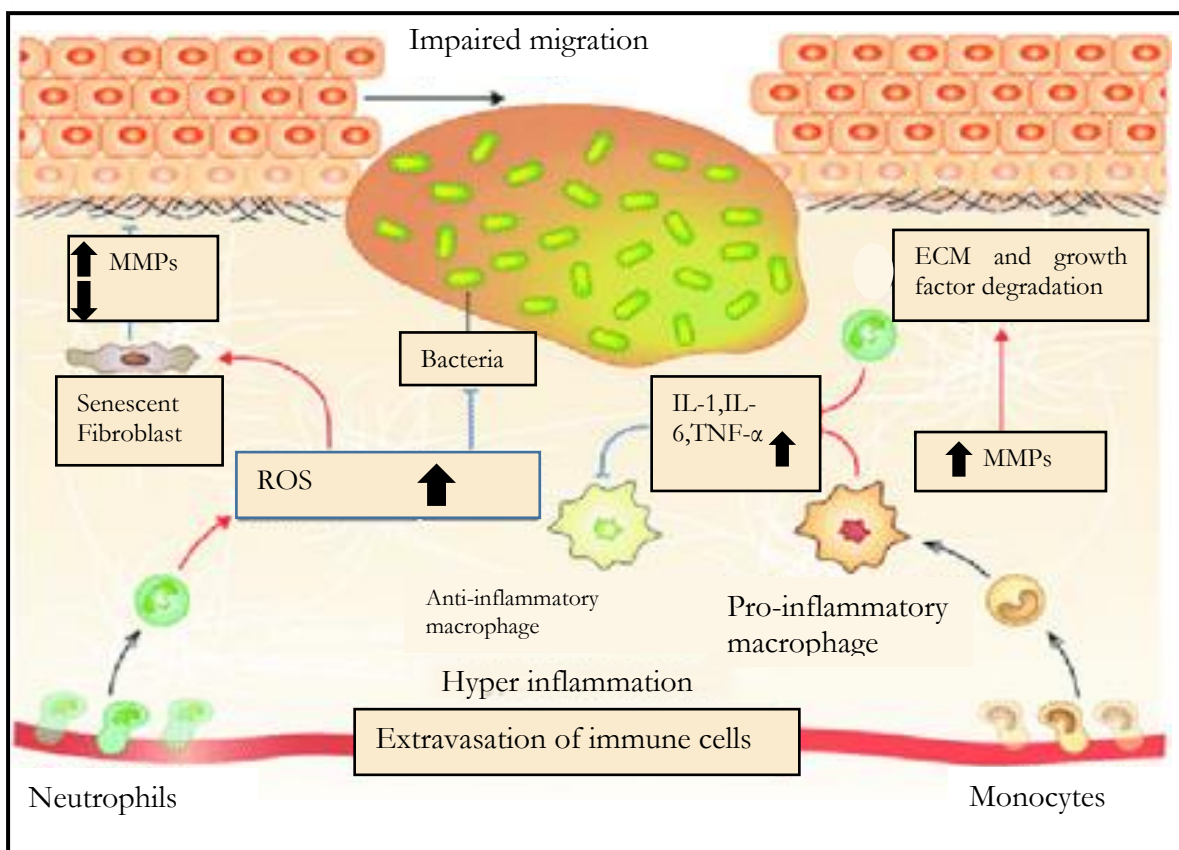

Figure 1.4 Illustration of chronic wound. Adapted from Larouche et al. [55].

1.5   Signal Transduction

Signal transduction is the process by which a physical or chemical stimulus is transmitted through a cell as a series of molecular events. External stimuli can be physico-chemical (like pH, oxidative stress, temperature) or biological (cytokines, chemokines etc.) [56]. Most often, the environmental signal is first processed by a cell membrane bound receptor protein. These receptors have an intracellular and extracellular domain. The signals bind to the 'binding site' of the extracellular domain and generates a signaling cascade. The first signals are often called primary messengers; upon binding of these messengers the receptor-ligand complex undergoes a structural change. This structural change is not sufficient to elicit a response from the cells, as the numbers of membrane bound receptors are very few. However, secondary messengers transmit the signal from the receptor-ligand complex and can affect the cascade by two ways; first they are small molecules which can freely diffuse in the nucleus and influence the transcription factors for downstream gene expression. Secondly, they can be amplified significantly and can work as the 'input' for other signaling pathways leading to multiple cross talk. ROS play a central role as secondary messengers and determines cell fate and several other cellular processes.

1.6   HIPPO Signaling Pathway

The HIIPPO signaling pathway was first identified in *Drosophila melanogaster* and is a regulator of organ size, proliferation and is highly conserved in vertebrates and arthropods [57]. The core HIPPO cascade which consists of four kinase cassette, was first identified through genetic screens for tumor suppressor genes in Drosophila. The cascade includes Warts (Wts) [58, 59], the WW domain containing protein Salvador (Sav1/WW45) [60, 61], the Ste20- like protein kinase Hippo (Hpo) [62-64] and the adaptor protein Mob as tumor suppressor (Mats) [65]. In mammals, the core kinase cascade contains two Hpo homologs which are Mst1 and Mst2, two Wts homologs (LATS1 and LATS 2), one Sav homolog (WW45 or Sav1) and two Mats homologs (MOBKL1A and MOBKL1B) [57].

The Hippo pathway can be stimulated by multiple types of cellular stress, including mechanical stress, and reactive oxygen species [66]. Mst1/2 bind to their regulatory protein WW45/Sav1 and activates it which in turn phosphorylates and activates LATS1/2 kinases [67, 68]. Mst1/2 also activates and phosphorylates MOB1A/B [69]. The MOB1A/B-LATS1/2 complex in turn phosphorylates the two major transcriptional coactivators of the HIPPO cascade, Yes associated protein (YAP) and transcriptional coactivator with PDZ-binding motif (TAZ) [70-72]. YAP and TAZ have HXRXXS/T motifs which are phosphorylated by LATS1/2 kinases [73]. Upon phosphorylation, these two effectors undergo cytoplasmic sequestration or ubiquitin mediated protein degradation by binding to 14-3-3 proteins [72, 74].

When LATS1/2 is inactive (de-phosphorylated), YAP/TAZ are not phosphorylated and translocate to the nucleus (figure 1.5 right part). In the nucleus, YAP/TAZ bind to TEAD domain family members (TEAD 1-4) and mediate the transcription of target genes such as Connective Tissue Growth Factor (CTGF) and Cysteine rich angiogenic inducer 61 (Cyr61) [75]. These downstream genes code for CCN family proteins regulating cell growth, proliferation, migration and survival [74, 76-78]. These extracellular matrix associated angiogenic regulators are heparin binding proteins, share 47% amino acid identity [79, 80] and are synthesized during cutaneous wound healing in dermal fibroblasts [81]. YAP, CTGF and Cyr61 are the main focus for this thesis. Apart from TEAD family transcription factors, YAP/TAZ interacts with several other transcription factors like Smad family members (1, 2/3, 7), RUNT related transcription factors (RUNX1, RUNX2), T box transcription factors (TBX5) and p73 [79].
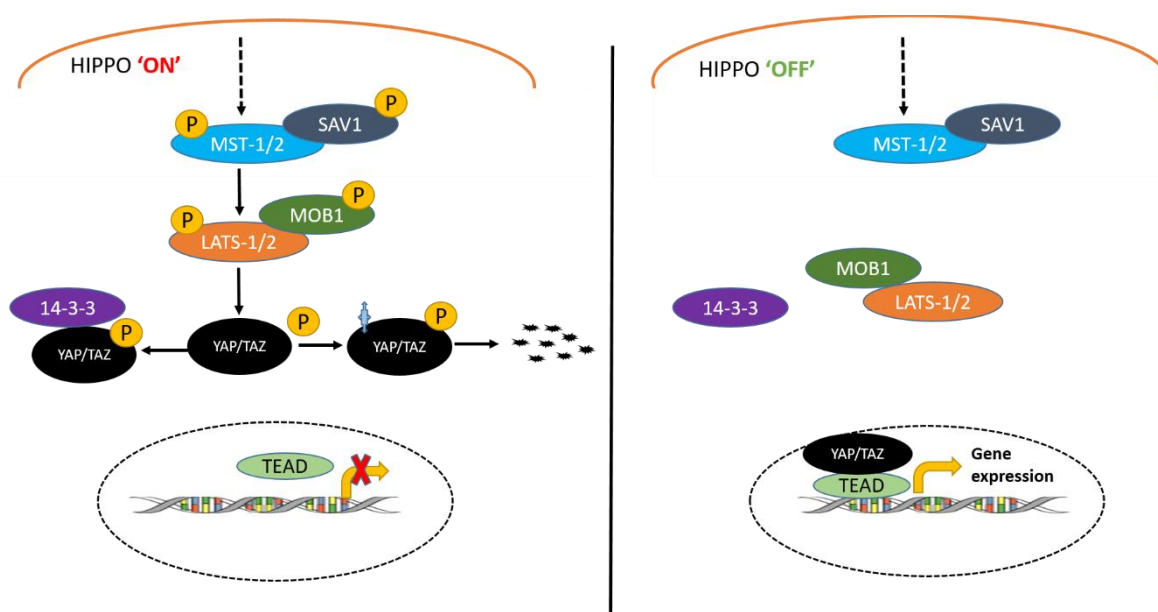
Figure 1.5 On/off state of HIPPO signaling pathway. The figure is adapted from Boopathy et al. [79].

There are numerous examples of redox-mediated activation of HIPPO signaling pathway. MST-1 is activated upon oxidative stress and phosphorylates FOXO3 leading to neuronal cell death due to FOXO3 mediated Bim expression [82]. YAP also mediates ROS triggered signaling. In cardiomyocytes, YAP acts as a transcriptional co-activator of FOXO1 and upregulates the expression of antioxidant genes like catalase and Mn-SOD [83]. GABP (an ETS family member) mediated YAP expression is also correlated with oxidative stress in the liver [84]. YAP also acts as a functional link between HIPPO and PI3K-mTOR pathway. YAP inhibits PTEN by inducing miR-29 and thus activates the mTOR signaling pathway which is involved in cellular growth and proliferation [85]. Furthermore, YAP binds to HIF-1α and promotes sustained HIF-1α protein stability [86]. Moreover, YAP and TAZ are also involved in wound healing and tissue regeneration. The localization of YAP and TAZ in

nucleus is important for cutaneous wound healing and knockdown of these two genes can cause potential delay in wound closure [87]. In the basal layer of epithelial cells, expression of YAP and TAZ increases post wounding; however wound healing is markedly decreased in YAP/TAZ double conditional knockout mice [88]. Taken together, these results already indicate the role of YAP-TAZ in cutaneous wound healing.

CTGF is a 40 kDA, matricellular protein and has been reported to interact with several cytokines and growth factors like IGF-1, BMP-4, BMP-7,TGF-ß and VEGF [89]. It is also described that CTGF interacts with cell-surface receptors and integrin receptors [89]. Moreover, CTGF interacts with matrix proteins such as fibronectin or heparine sulphate proteoglycans [89]. Due to its ability to interact with several growth factors, cytokines and receptors, CTGF possess the potential to regulate several biological processes including cell migration, adhesion, proliferation, angiogenesis, early wound healing and repair [90-93]. Several studies provide evidence that CTGF is linked to wound healing cascade. For example, application of recombinant human CTGF (10-100 ng/cm^2) in non-human primate burn wound induced faster healing and proliferation compared to the control group [94]. Topical application of CTGF on diabetic rodent wounds showed a faster wound closure rate, accumulation of collagen IV at the wound site and increased expression of alpha smooth muscle actin expression and macrophage infiltration [95]. CTGF is induced in tissue repair and constitutive CTGF expression is a hallmark of fibrogenesis. Kapoor et al. also observed that CTGF promoter activity is absent in normal skin, but post wounding the promoter activity is induced in myofibroblasts [96].

Like CTGF, Cyr61 has also been reported to affect several cellular activities including cell migration, proliferation, angiogenesis and apoptosis [81, 90, 97, 98]. Cyr61 is a cell adhesion protein and binds to several integrin receptors including αvβ3, αvβ5, αIIbβ3, α6β1, and αMβ2 in different cell types [99]. Cyr61 is involved in cell migration of fibroblasts and epithelial cells. Zhang et al. showed that Cyr61 mediates PDGF-induced cell migration via Cyr61-integrin-FAK signaling cascade in smooth muscle cells [100]. It also regulates matrix remodeling by inducing metalloproteinases during angiogenesis and wound healing in dermal fibroblasts [101]. Moreover, it has been also shown to induce fibroblast senescence in response to cutaneous wound healing to restrain fibrosis during tissue repair [102]. Oxidative stress plays an important role in activation of Cyr61 downstream the HIPPO cascade. Qin et al. found that Cyr61 expression is induced by oxidative stress and that a positive feedback loop continues to generate ROS and upregulate Cyr61 in fibroblasts [103].

Present literature suggests that reactive species is an important modulator of HIPPO signaling cascade and downstream angiogenic proteins. Therefore, in this study we wanted to investigate the role of HIPPO signaling in wound healing upon plasma treatment.
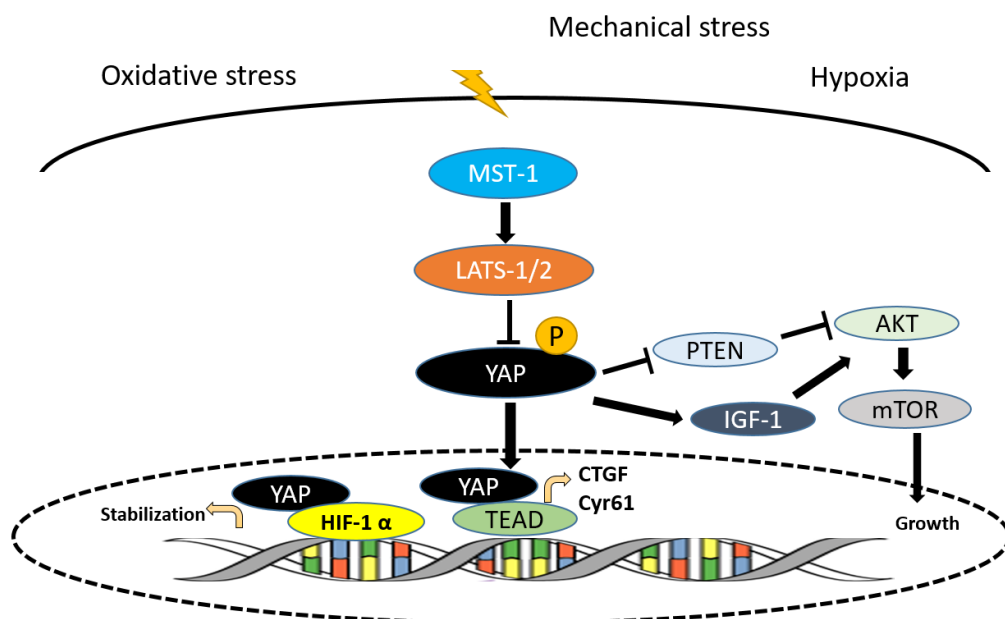
Figure 1.6 Simplified version of HIPPO signaling pathway. The figure is combined and adapted from Boopathy et al. [79], Zhang et al. [86], Tumaneng et al. [85] and Mao et al. [104].

1.7   Plasma

Plasma is the fourth fundamental state of matter after solid, liquid and gas and was first described by the American physicist and chemist Irving Langmuir in the nineteen- twenties [105]. Irvine Langmuir first coined the term in 1928 [106]. Plasma is a partially or completely ionized gas. Gas atoms collide with other gas atoms and free electrons and becomes ionized; this happens when the kinetic energy of the collision is higher than the ionization energy. Upon increase of gas temperature, the kinetic energy also increases which results in higher probability of ionized collision [107]. Therefore, the transition from gas to plasma is quite transient and continuous. Figure 1.7 describes the transition from solid to plasma. Visible matters such as lightning, *Aurora boraelis*, stars etc. are in state of plasma. In fact, it is supposed, that 99 % of the matter in the universe is plasma. Plasma can be manmade and is nowadays exploited in a variety of processes e.g. environmental remediation, agriculture or surface modification to name a few. Plasma medicine is the latest application of plasma research. It is a new field at the intersection of physics, engineering, biology and medicine. Plasma is generated by energizing gas up to a critical point at which electrons dissociate from atoms [56]. The resulting partially ionized gas contains charged particles, while the overall charge remains electrically neutral. Typical particles being generated include ions, electrons, or reactive oxygen and nitrogen species (ROS/RNS) [56]. Electric and magnetic fields, light (visible, infrared, UV), and neutral particles are also generated [108]. The physicochemical properties of plasma is complex and depends upon a variety of

parameters which includes the type and composition of the gas or gas mixture used for plasma generation, the applied energy and electrode configuration, the pressure, and the environment [108].
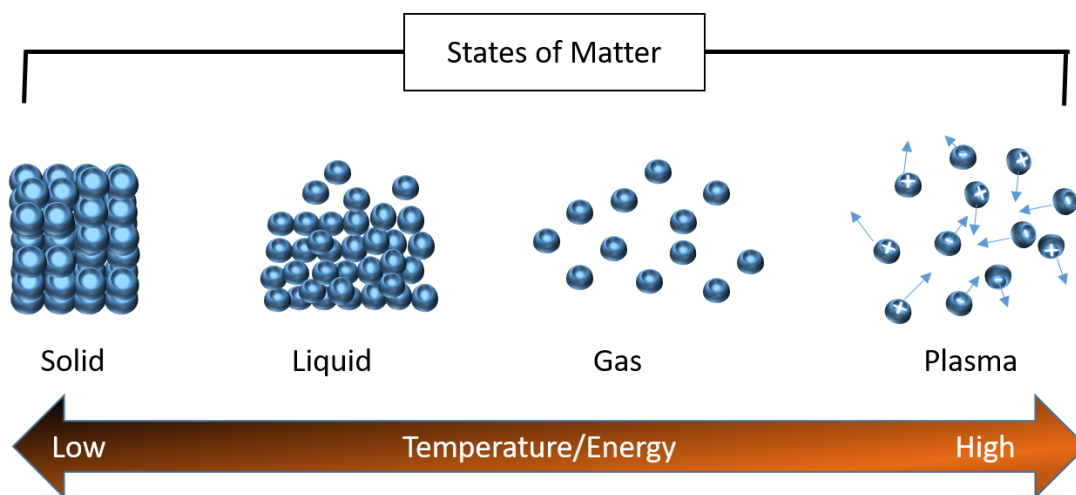

Figure 1.7 States of matter: generation of plasma. Plasma is the fourth state of matter after solid, liquid and gas. Plasma is composed of large number of unbound charged particles.

In the history of plasma technology thermal plasma with temperature higher than 80°C has been used for tissue ablation, destruction and sterilization purposes [109]. In thermal plasma, temperatures of the electrons and ions are equal and remains in thermal equilibrium [110]. However, for medical purposes, since the 1990s, technologies for stable and reproducible plasma generation at low temperature under atmospheric conditions are available on a larger scale, facilitating the generation of so-called non-thermal plasma or cold atmospheric plasma (CAP). Most cold atmospheric plasmas (CAP) for biomedical applications are generated by applying electrical energy to a not directly biologically effective gas (argon, helium, oxygen, nitrogen, air, or gas mixtures). The electrical energy is mostly transmitted to excite free electrons whereas the majority of gas atoms, molecules and ions remain in a low energy state resulting in a low plasma temperature [111]. In contrast to thermal plasma, CAP is characterized by low degree of ionization (about 1%). Hot free electrons ($Te \geq 10^4$ K) which are responsible for the ionization initiation are surrounded by neutral gas molecules with relatively low temperatures ($Tg \leq 10^3$ K) [112]. Therefore, lower energy levels are transferred to the ions, molecules and atoms of the plasma leading to a composition which is not at thermal equilibrium and the total plasma temperature is a few hundred K [113]. For biomedical applications, plasma sources which emits minimum thermal output and does not exceed 40°C at target site are considered for medical purposes [114].

Excited atoms and molecules interact with each other for the open atmospheric conditions and with neighboring media and generate primary and secondary reactive species with

biological potential at the genome, transcriptome and proteome level. Electromagnetic radiation ((UV/VUV, visible light, IR/heat, electric fields) is also emitted [111]. The generation of reactive species vastly depend on each plasma source and device parameters like working gas, power input and temperature [115]. Figure 1.8 illustrates the generation of short- and long-lived redox species by plasma.
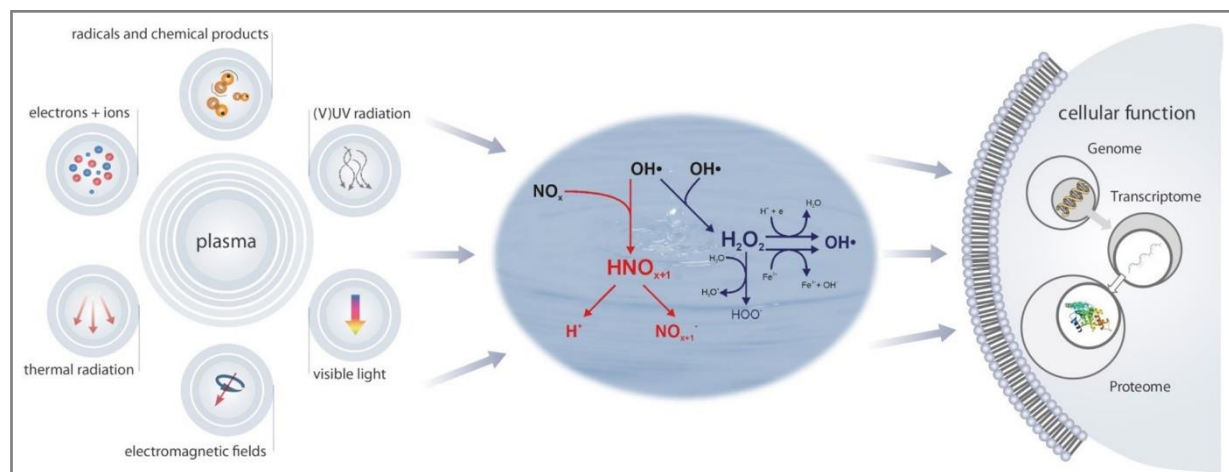

Figure 1.8 CAP generates reactive species with biological potential. This figure is adapted from Weltmann et al. [116].

1.8 Plasma Medicine

Plasma medicine has emerged as one of the exciting new field at the interface of physics and life sciences. CAP, due to its operation at atmospheric pressure and low temperature is apt for treatment of viable tissues and thus has become a focus of medical research over the past years [117]. The modern era of plasma medicine started with the application of CAP on cultivated cells which induced separation of cells from a uniformed cell structure without killing the cells. This was the first direction for a non-lethal selective application of CAP on living cells [118].

Plasma medicine follows an interdisciplinary research approach, where physics describes the physical parameters of plasma production, life science investigates the basic effect of CAP on microorganisms, tissues and eukaryotic cells and finally plasma medicine aims to describe the effect of cold plasma in clinical use [119]. A variety of different CAP devices has been developed for research and therapeutic applications. While some of them are already used in clinics as certified medical devices, some CAP devices are still used in benches. Majorly, there are two different type of CAP discharges, direct (Dielectric Barrier Discharge: DBD) and indirect (APPJ: Atmospheric Pressure Plasma Jet). Figure 1.9 illustrates the two types of plasma source. With the DBD, plasma is ignited in the gap

between an isolated dielectric high voltage electrode and the tissue to be treated. Here, the tissue/cells work as the counter electrode. Most of the DBD devices use atmospheric air as the feed gas [111]. In contrast, APPJ consists of a gas nozzle with one or two electrodes. The plasma is ignited inside the nozzle and transported outside to the object with a preassembled working gas (mostly neutral gas or gas mixture) [111]. Since 2013, four devices have been medically certified for its use in clinical purposes: Argon gas operated Jet based devices kINPen MED (Neoplas Tools GmbH) and SteriPlas (ADTEC, Hunslow, UK) as well as the DBD-based devices PlasmaDerm (CINOGY GmbH Duderstadt, Germany) and plasma care (terraplasma medical GmbH Garching, Germany), the latter two using atmospheric air as working gas [108].
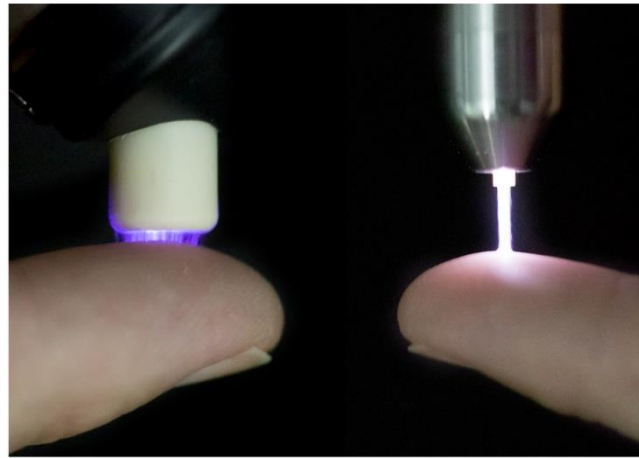

Figure 1.9 Volume DBD and Plasma Jet in contact with fingertip. The figure is adapted from Weltmann et al. [116].

Various studies have focused on the anti-microbial, anti-inflammatory, anti-neoplastic and wound healing promoting properties of CAP [120-123]. Several in vitro studies have elucidated CAP mediated effective inactivation of bacteria and have shown its potential as an effective tool for disinfection [107, 124-128]. The antiseptic properties of CAP have also been shown in clinics by microbial load reduction in wounds and tissues [129-133].

One of the starting points in plasma medicine focused on the use of CAP in wound healing due to its antimicrobial activity. Several experimental *in vitro* studies demonstrate a direct impact of CAP on cell proliferation and migration as well as on angiogenesis [134-142]. The results of this basic research details that CAP mediated wound healing does not only depend on the microbial load reduction, but also on the direct stimulation of tissue regeneration [119]. CAP treatment leads to upregulation of Nrf2-Keap-1 signaling axis which in turn stabilizes the architecture of F-actin cytoskeleton and focal adhesions and increases granulation tissue formation and matrix deposition [123, 143]. Activation of the Nrf2 also mediates the upregulation and secretion of inflammatory molecules and therefore recruit immune cells for which activates the wound healing signaling [123]. In fact, CAP supports angiogenesis by stimulating the secretion of Keratinocyte Growth Factor (KGF),

Vascular Endothelial growth factor (VEGF), basic Fibroblast Growth Factor (bFGF), Epidermal Growth Factor (EGF) etc [136, 137, 144, 145]. Several groups and clinicians now are interested in the role of CAP in acute and chronic wound management in vivo and in patient trials. A study of burn wounds in mice showed that plasma treatment enhanced angiogenesis [146]. Full-thickness cutaneous wound healing was found to be accelerated after exposure to CAP as well [142]. In several randomized pre-clinical trials and case studies, CAP has shown to reduce the wound size faster than the established treatments and accelerate wound healing processes as a preliminary result [116, 147]. CAP is also able to influence the inflammatory and immune cell signature in a chronic wound environment. Taken together, CAP treatment leads to an accelerated healing in acute and chronic wound [123]. Besides wound healing, other CAP application in dermatology have been reported, mainly in the treatment of pathogen-based and/or inflammatory skin irritations and diseases [109, 148, 149]. The role of CAP in dentistry also falls under the umbrella of plasma medicine; possible dental application of CAP include inactivation and removal of biofilm on teeth, disinfection of tooth root canal, plasma-assisted cleaning and optimization of tooth and implant surfaces to improve bone integration [150].

1.9   The atmospheric pressure argon plasma jet *kINPen MED*

The kINPen MED® is a commercially available atmospheric pressure argon plasma jet. Its concentric, light-weighted, and pen-like design was developed for biomedical applications and allows precise and arbitrary 3D movements. Due to its easy handling, this device can be used for both a direct treatment of cold plasma on the cells and indirect treatment of liquids [151]. The hand-held unit is operated using a power supply and a gas supply unit. In this work kINPen MED was used as the only plasma source. The electrical safety of the kINPen was certified and complies with EU standards [151]. This is the first jet worldwide to be accredited as a medical device class IIa according to European Council Directive 93/42/EEC for use in wound treatment and this device lacks mutagenic and genotoxic effects [151-153].In its metal housing a central rod like capillary is shielded by a dielectric quartz capillary connected to a grounded ring electrode. Figure 1.10 depict the physical structure of kINPen MED. The plasma is generated by applying a sinusoidal voltage (2–6 kVpp) with a frequency of 1.0–1.1MHz to the central electrode (power: <3.5W in the hand-held unit).The typical plasma effluent length is 9–12mm and 1mm in diameter [151]. The complete physical parameters of kINPen MED is provided in table 1.1. High spatial and temporal optical resolution of the plasma revealed that it propagates in a bullet-like manner [154]. Argon is primarily used as feed gas, but other molecular gases can be also admixed [155]. In particular, the plasma in the effluent region interacts with the ambient air and generates non-reactive species (like H_2O_2,ozone) or radical species (like hydroxyl radical, nitrogen monoxide) [156]. A gas curtain can also be used to shield the plasma, which generates a more controlled environment influencing the plasma chemistry in contact with liquids [157].

Figure 1.10 Atmospheric pressure plasma jet kINPen MED. Physical structure and application on skin. The figure is adapted from Bekeschus et al. [151].

Table 1. 1 Physical parameters of kINPen MED. The table is adapted from Bekeschus et al [151].

Properties	kINPen MED
Recommended feed gas and flux	Argon (5±1 l/min)
Frequency	1 MHz
Feed gas flow control	Yes (Integrated)
Mode of operation	Pulsed 2.5 kHz
Duty cycle	Plasma on/off = 1:1
Power	<8W of the whole system <3.5W of the handheld device
Typical effluent length	9-11 mm
Recommended working distance	8-10 mm
Temperature at recommended working distance	35-38°C
UV irradiation at working distance	UV A : 5-15μW/ cm2 UV B : 5-15 μW/ cm2
Plasma stabilization during plasma generation	Automatic: PLL-circuit

1.10 Wound healing is subject to redox control

The redox environment of wound site has an important influence in cutaneous wound healing. ROS are critical secondary messengers that orchestrate the wound healing processes by regulating the immune response, angiogenesis and optimal perfusion of blood at wound site [158]. Redox state at the wound site regulates thrombosis and blood coagulation [158, 159] .The inflammatory stage is profoundly affected by the redox environment; H_2O_2 directly regulates the monocyte function which are recruited at the wound site [160]. ROS induce the production of MIP-1A, MIP-2 and MCP-1 [161, 162]; chemotactic molecules which recruits immune cells at the wound site. H_2O_2 also modulates leucocyte adhesion molecule expression [163] and transcriptional expression of MCSF-1, which drives the monocyte adherence to the extracellular matrix [164]. Several chemokines at the wound site respond to ROS. ROS induce CCR5 and CXCR4 mRNA expression [165]. Low concentration of H_2O_2 sensitizes the mRNA expression of CCR2, CCR5, and CXCR4 mRNA [165]. H_2O_2 also increases cell migration in response to MIP1 [165]. Re-epithelialization is also influenced by redox species; at lower concentration, ROS induces epithelial cell proliferation and migration [166, 167]. Studies have shown that, H_2O_2 supports wound healing in keratinocytes by inducing VEGF production [168]. In fact, Roy et al. showed that even though, high doses of H_2O_2 have an adverse effect on wound healing; at lower doses it induces FAK phosphorylation at wound edge tissues and drives H_2O_2 mediated angiogenesis in vivo [169]. Studies have also shown that H_2O_2 induced-VEGF-A transcription is driven by the Ras-Raf-MEK1-ERK1/2 pathway [170]. CAP generates a plethora of redox species, which similar to H_2O_2 influence the physiological stages of wound healing i.e. cell migration [171], viability [172, 173], proliferation [174], inflammation [175] and dermal regeneration and re-epithelialization [176]. CAP also triggers the nuclear translocation of Nrf2, basic leucine zipper (bZIP) protein that regulates the expression of antioxidant genes against redox damage [143]. Upon its translocation and activation, Nrf2 and its downstream targets affect angiogenesis [120], oxidation of lipid layers [143] and TGF-ß signaling during wound healing [177].

1.11 Aim of the work

During the past few years, plasma medicine has emerged as an important field in biomedical science. Cold atmospheric plasma generates a mixture of reactive oxygen and nitrogen species, including singlet oxygen, atomic oxygen, hydroxyl radicals, and hydrogen peroxide, as major (secondary) contributors. In recent years, CAP has been used for the management of acute and chronic wounds in clinics; however, the mechanistic insight of CAP-mediated wound healing responses remain still largely unexplored.

In clinics, through observational study, efficacy of kINPen MED in wound healing has been demonstrated [151]. In fact, plasma-mediated wound closure has also been observed in monoculture of keratinocytes by an accelerated production of growth factors and neovascularization [145]. CAP could also promote proliferation and migration of human dermal fibroblasts as well as production of cytokines and collagen [135]. Yet, for simulation of cross talk of diverse cell types in wounds, it has to be investigated how CAP affects single cell types and their cross talk. However, studies on the effect of CAP on synergistic interaction of dermal keratinocytes and fibroblasts remain scarce. Activation of anti-oxidant pathways upon cold plasma treatment has been also described in keratinocytes and animal model [123, 178]. Nevertheless, not much studies have focused on the regenerative and remodeling signaling potential of cold plasma. Therefore, this study aimed to investigate the stimulatory potential of cold plasma and addressed the following questions:

1. How does CAP affect the coculture of dermal keratinocytes and fibroblasts in terms of cell migration and cell viability/metabolic activity?

2. How does CAP affect the regenerative signaling (HIPPO signaling) pathway and extracellular matrix and adhesion molecules?

3. What is the impact of CAP on the paracrine interaction between keratinocytes and fibroblasts?

To this end, we first optimized the coculture of keratinocytes and dermal fibroblasts *in vitro*. Next, we performed cell viability studies and 'scratch assays' to characterize and distinguish plasma activities on skin cell monocultures and the coculture of keratinocytes and fibroblasts. Subsequently, plasma-modulated regenerative signaling molecules and extracellular matrix and adhesion molecules were identified. Finally, this research aimed to study the paracrine cross talk between keratinocytes and fibroblasts post plasma treatment. Altogether, this thesis contributed to a more detailed picture on plasma-mediated molecular mechanisms in wound healing.

2. Materials

Table 2.1 Chemicals used in this study

Chemicals	Supplier
2,2-Azino-bis(3-ethylbenzothiazoline-6-sulfonic acid)	Sigma Aldrich
Amplex^{TM} UltraRed Reagent	Thermo Fisher Scientific
Argon gas (purity 99.999 %)	Air Liquide
dH$_2$O, PCR grade	Roche Applied Science
Dimethyl sulfoxide(DMSO)	Sigma Aldrich
EDTA	AppliChem
Ethanol, absolute	Sigma Aldrich
FCS	Sigma Aldrich
H$_2$DCF-DA	Life Technologies
H$_2$O$_2$ (30 %)	Sigma Aldrich
L-Glutamine	Pan Biotech
Mini Protein TGX TM Precast Gels	Bio rad
PageRulerTM Prestained Protein Ladder	Thermo Fisher Scientific
PBS (10 x, w/o Ca^{+2}/ Mg$^{+2)}$	Corning
Penicillin/Streptomycin	Pan Biotech
Protease and Phosphatase Inhibitor Cocktail	Thermo Fisher Scientific
Recombinant Human CTGF	Peprotech GmbH
Recombinant Human Cyr61	Peprotech GmbH
Resazurin	Alfa Aesar
RIPA Lysis Buffer System	Santa Cruz Biotechnology
RPMI 1640	Corning
Super Signal^{TM} West Femto Maximum Sensitivity Substrate	Thermo Fisher Scientific
Trypsin/EDTA	Corning
Western Blot Stripping Buffer	Sigma Aldrich

Table 2. 2 Laboratory equipment

Equipment	Supplier
Beakers	Sarstedt
Cell culture flask (175 cm^2)	Sarstedt
Cell culture flask (75 cm^2)	Sarstedt
Cell Scrapers	Sarstedt
Dispenser tips	Sarstedt
E swabs	Copan Diagnostics
Eppendorf (0.5ml,1.5 ml, 2ml)	Sarstedt
Falcon tubes (15ml,50ml)	Sarstedt
Glass bottles	Sarstedt
LightCycler 480 sealing foil	Sarstedt
Multiwall plates (6well, 12 well, 24 well, 96 well), sterile	Sarstedt
Parafilm	Curwood
Pasteur pipettes	Labsolute
PCR tubes (8 strips, 0.2ml)	Sarstedt
Pipette filter tips (2-20μl, 20-200μl, 200-1000μl)	Biosphere Plus
Pipette tips	Sarstedt
Pipettes	Eppendorf
PVDF membrane	Bio-Rad
Quantstudio 1 sealing foil	Applied Biosystems
Serological Pipettes (5ml,10ml,25ml)	Sarstedt
Trans blot turbo transfer pack	Bio-Rad
Transparent PCR plate (25 µl)	Applied Biosystems
White PCR plate (25 µl)	Sarstedt

Table 2. 3 Laboratory instrument

Instruments	Supplier
Argon plasma jet kINPen MED	Neoplas Tools
Autoclave	Systec
Centrifuge	Eppendorf
Clean bench	Thermo Fisher Scientific
CO_2 incubator	Thermo Fisher Scientific
Freezer (-80° C)	Thermo Fisher Scientific
Gel tank	Bio Rad
Image quant Las 4000	GE Healthcare
Incucyte S3	Essen Bioscience
LighCycler 480	Roche Diagnostics
Microscale	Sartorius
Microscopy	Leica
Nano drop	Thermo Fisher Scientific
pH meter	Sartorius
Plate reader (M200 pro, F200 pro)	Tecan
Refrigerator	Liebherr
Sonicator	Labsonic M
Tabletop Centrifuge Mini Spin	Eppendorf
Thermoblock	Eppendorf
Thermocycler	Biometra
XYZ table	CNC-Stop Ell

Table 2.4 Kits/Antibodies

Kits	Supplier
Anti-mouse IgG, Alexa-Fluor 488	CST, catalog no 4408s
Anti-mouse IgG, HRP Linked Antibody	CST, catalog no. 7076s
Anti-rabbit IgG, HRP Linked Antibody	CST, catalog no. 7074s
CTGF antibody (E-5)	Santa Cruz Biotechnology, Catalog no. sc-365970
CYR61 (D4H5D) XP® Rabbit mAb	CST, Catalog no. 14479
High-Capacity cDNA Reverse Transcription Kit	Thermo Fisher Scientific
Human CTGF Mini ABTS ELISA Development Kit	Peprotech GmbH
Human Cyr61/CCN1 ELISA - 96 strip-wells	Raybiotech
Human Cyr61/CCN1 Quantikine ELISA Kit	R&D BioSystems
Phospho-YAP (Ser127) Antibody	CST
Primers	Biotez
RNA mini kit	Bio & Sell
RT^2 First Strand Kit	Qiagen
RT^2 Profiler PCR array	Qiagen
RT^2 Sybr Green mix	Qiagen
ß actin Mouse mAb	CST, catalog no. 3700s
ß actin Rabbit mAb	CST, catalog no 4970s
YAP antibody (63.7)	Santa Cruz Biotechnology, Catalog no. sc-101199

23

Table 2.5 Software

Software	Supplier
GraphPad Prism 8	GraphPad software
Image J Software	Image J
Image Studio Lite ver 5.2	Image Studio
Incucyte S3 2018A	Essen Bioscience
LightCycler 480 SW 1.5.1	Roche Applied Diagnostics
MS Office	Microsoft
Quant studio Design & Analysis	Applied Biosystems group
Tecan iControl	Tecan group
ZEN 2.1	Zeiss group

3. Methods

3.1 Cell Culture

Human skin keratinocytes HaCaT (Cell Lines Service, catalog no. 300493) and immortalized skin fibroblast cell line GM00637 (GM Fbs, Coriell Institute, New Jersey, USA) were cultured in Roswell Park Memorial Institute 1640 cell culture medium (RPMI 1640), supplemented with 10% fetal calf serum (FCS), 0.1 mg/ml penicillin/streptomycin, and 2 mM L-glutamine (Pan Biotech) at 37°C, 95% humidity and 5% CO_2. For sub cultivation of cells, GM Fbs were washed with 5 ml of PBS-EDTA (0.5mM EDTA) and HaCaT cells were incubated with the mentioned volume of PBS-EDTA for 10 minutes. Afterwards, both the cell lines were trypsinzed with 3 ml Trypsin-EDTA (Corning), detached cells were suspended with 5 ml culture medium. Then, the cells were centrifuged at 500 g for 3 minutes, supernatant was discarded and cell pellets were suspended in 5 ml new culture medium. For GM fibroblasts, a starting density of 2-4×10^6 cells and for HaCaT cells a density of 2 ×10^6 cells were seeded in a new culture flask of 75 cm^2, supplemented with 10 ml culture medium. The sub cultivation was performed twice in a week.

3.2 Plasma Source

CAP treatment was performed using an atmospheric argon plasma jet kINPen MED (Neoplas tools, Greifswald, Germany). The electrical safety of the kINPen was certified and complies with EU standards [151]. This is the first jet worldwide to be accredited as a medical device class IIa according to European Council Directive 93/42/EEC for use in wound treatment and this device lacks mutagenic and genotoxic effects [151-153]. The simple pen like design was developed for biomedical applications. The jet was operated at a voltage of 2-6 kVpp and a frequency of 1.0-1.1 MHz. The gas flow rate was set at 5 Standard Liter per Minute (SLM) and the plasma had a visible plume of 9-12 mm in length and 1 mm in diameter. For our experiments, we operated the jet only with argon gas.

3.3   Indirect Plasma treatment

The plasma jet kINPen Med, as depicted in figure 3.1 was operated with argon gas at a flow rate of 5 SLM (standard liters/minute) as controlled by a Mass Flow Controller (MFC). The kINPen Med was fixed with a computer controlled xyz table (CNC Machines, Germany) that conducted a P shaped movement over the liquid surface to ensure equal distribution of plasma generated species in the liquid. In most cases, 5 ml of RPMI 1640 supplemented with 1 % FCS in a 60-mm dish was treated for 10, 30 and 60 s depending on the experimental type. CAP treated media was used immediately to treat the cells for further experiments. Cells incubated with untreated RPMI medium served as negative controls for all experiments.
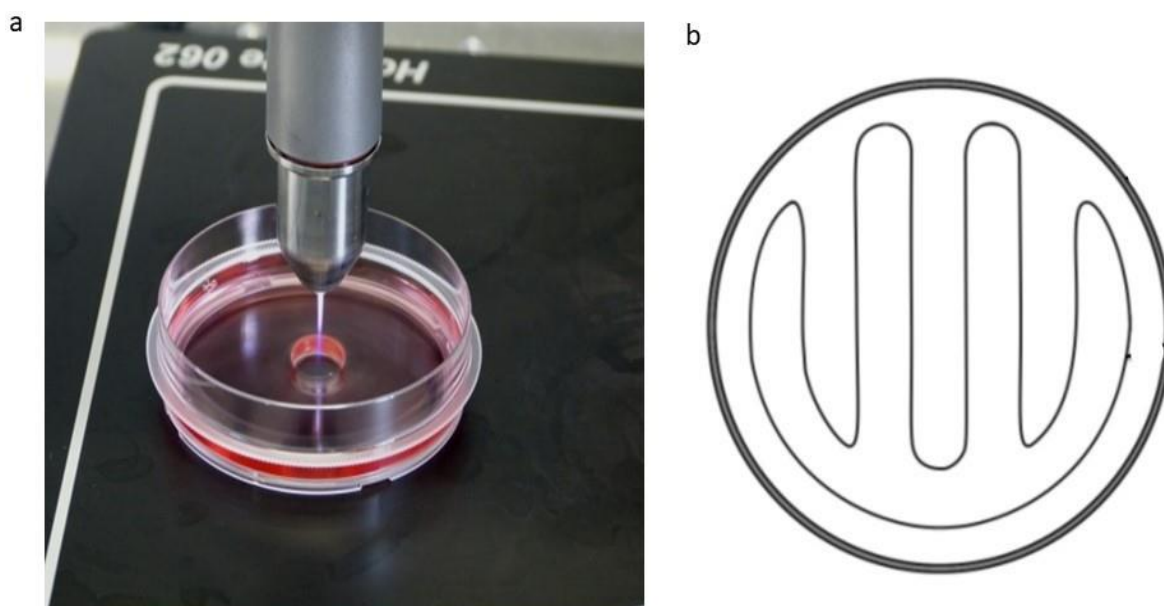
Figure 3.1 kINPen MED. a. Picture of indirect plasma treatment with kINPen MED. b. Moving track of the kINPen MED. 5 mL cell culture medium in a 60 mm dish was plasma-treated with the jet along the P-shaped track by a computer controlled xyz table.

3.4   Direct Plasma Treatment:

For direct plasma treatment, cells were seeded in a 96 well plate; before the treatment only 50 µl of cell culture volume was kept per well. Then the kINPen MED was operated with argon gas at a gas flow rate of 5 SLM for 10 and 30 seconds. For control, no treatment was performed. The kINPen was fixed with a computer controlled xyz table, and the plate was moved manually per well. After the plasma treatment, cells were loaded with 150 µl/well RPMI 1640 medium and incubated for the required hours.

3.5   Coculture with keratinocytes & fibroblasts

Direct coculture of HaCaT and GM Fbs was set up for cell migration assays and metabolic assays, as illustrated in figure 3.2. For coculture set up, GM Fbs were seeded first into a 96 well plate, and once they adhered to the plate, depending on the experimental type, the indicated number of HaCaT cells were seeded on top of GM Fbs. The exact cell numbers are described in the respective methods section.
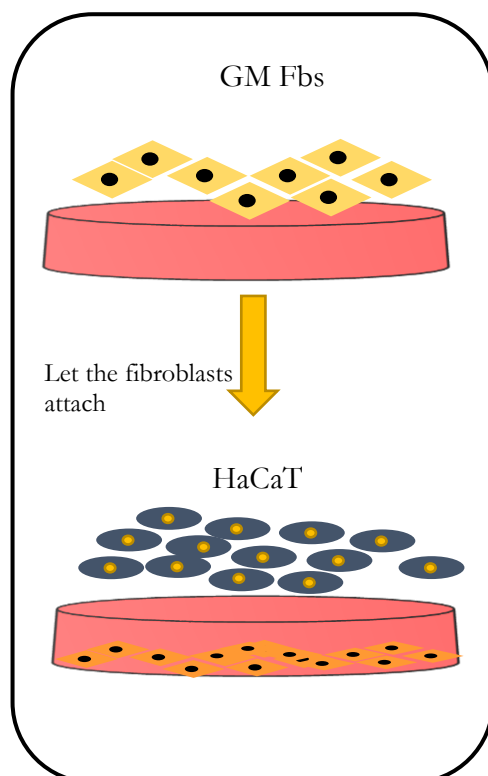

Figure 3.2 Coculture set up of HaCaT cells and GM Fbs. GM Fbs are seeded on the bottom, following which HaCaT cells are seeded on the top.

3.6   Harvest of GM Fbs conditioned medium

In a 24 well plate, 0.1×10^6 GM Fbs were seeded per well in complete RPMI medium, supplemented with 10% FCS. The cells were grown till 80-85% confluence after which the medium was replaced with 1% FCS containing RPMI medium. The cells were incubated in starving medium for another 16-18 hours. Next, fibroblasts were incubated with untreated or CAP treated medium (10, 30s) for another 18 hours. Following the incubation, conditioned medium was harvested, centrifuged for 5 min at 2000 rpm, filtered through a 0.22 µm syringe filter and stored at -80°C until further use.

3.7 Metabolic Activity assay

2.1×10^4 cells (in monoculture of HaCaT or GM Fbs) were seeded on a 96 well plate (Sarstedt) 24 hours before the experiment. For coculture, 0.7×10^4 GM Fbs were seeded first, followed by 1.4×10^4 HaCaT cells. Cells either in monoculture or coculture were incubated with untreated or CAP treated medium for 3 and 24 hours. As positive control, cells were treated with 10-30 µM H_2O_2. After the mentioned incubation hours, wells were loaded with 100 µM of resazurin (Alfa Aesar) that is transformed to fluorescent resorufin by metabolically active cells. The plate was incubated at 37°C for 2 hours and the fluorescence was measured at λ_{ex} 535 nm and λ_{em} 590 nm using a Tecan plate reader. CAP and H_2O_2 treated fluorescence values were normalized against untreated control.

3.8 Intracellular ROS production with H₂DCFDA assay

Changes of intracellular redox levels were determined using H_2DCF-DA. 15000 cells were seeded into a 96 well plate and cultured at cell culture conditions for 24 hours. Afterwards, cells were stained with 1 µM of dye for 20 min, prior to plasma-treated medium was added, and the conversion from DCFDA to DCF was measured 10 minutes thereafter by reading the plate at λ_{ex} 485 nm and λ_{em} 530 nm.

3.9 Amplex Red Assay for H₂O₂ measurement

The concentration of hydrogen peroxide was determined by reaction of H_2O_2 with amplex red in the presence of HRP (Horse Radish Peroxide) that leads to the production of resorufin, a fluorescence active product. Amplex Red/HRP reagent consists in 100 µM of Amplex Red and 0.25 U/mL HRP in double ionized water. Since the higher concentration of H_2O_2, able to be processed properly by this reagent is around 10 µM of H_2O_2, plasma-treated medium was diluted 10 times previously to the addition of the reagent. 50 µL of the Amplex Red/HRP reagent was added to 200 µL of the 10-fold diluted plasma treated medium in a 96-well plate and incubated for 30 min at 37 °C. Subsequent fluorescence measurements were performed by Tecan reader at λ_{ex} 560 nm and λ_{em} 590nm.

3.10 Cell migration assay

The cell migratory behavior of HaCaT cells and GM Fbs was assayed by a cell migration assay using Essen Bioscience wound maker. For this assay, monoculture of HaCaT, GM Fbs, and coculture of HaCaT and GM Fbs were used. For the mono culture, 6×10^4 HaCaT

cells/well and GM Fbs/ well were seeded in an Essen Bioscience 96 well Image lock plates. For the co-culture, 2×10^4 GM Fbs/well were seeded into image lock plates and incubated until the fibroblasts attach to the plates, and then 4×10^4 HaCaT cells/well were seeded onto the top of the fibroblasts at a ratio of 1:2 fibroblasts: keratinocytes within the coculture. A ratio of 1:3 and 1:5 fibroblasts: keratinocytes were also tested for the cell migration assay. Finally, for further experiments a ratio of 1:2 GM Fbs: HaCaT cells were used. After complete adherence of HaCaT cells, GM Fbs and coculture, the cells were starved to 1% FCS 16-18 hours prior to the experiment. Just prior to make the scratches, the old medium was replaced with 100 µl of new RPMI medium. Essen Bioscience wound maker was used to make the scratches, afterwards cells were incubated with either 10 or 30 s plasma treated medium or untreated medium as indicated. For direct plasma treatment, after making the scratches 50 µl of medium was taken out, plasma treatment was carried out and the medium was replaced with 150 µl new medium.

For other experiments, recombinant CTGF (10-50 ng/ml) and Cyr61 (0.1-1 µg/ml) and GM-Fb-conditioned media were used on HaCaT mono culture seeded at a density of 4×10^4 cells/well.

The migration rate was monitored with Incucyte S3 live cell analysis system until 24 hours. The relative wound density was measured with the in-built software of Incucyte S3 2018A. The relative wound density (%) is the ratio of the occupied area of the initially scratched area with respect to the total scratched area. The graphs are plotted as a function of relative wound density (%) in y-axis with respect to time at x-axis. The migration assay set up is shown in figure 3.3.
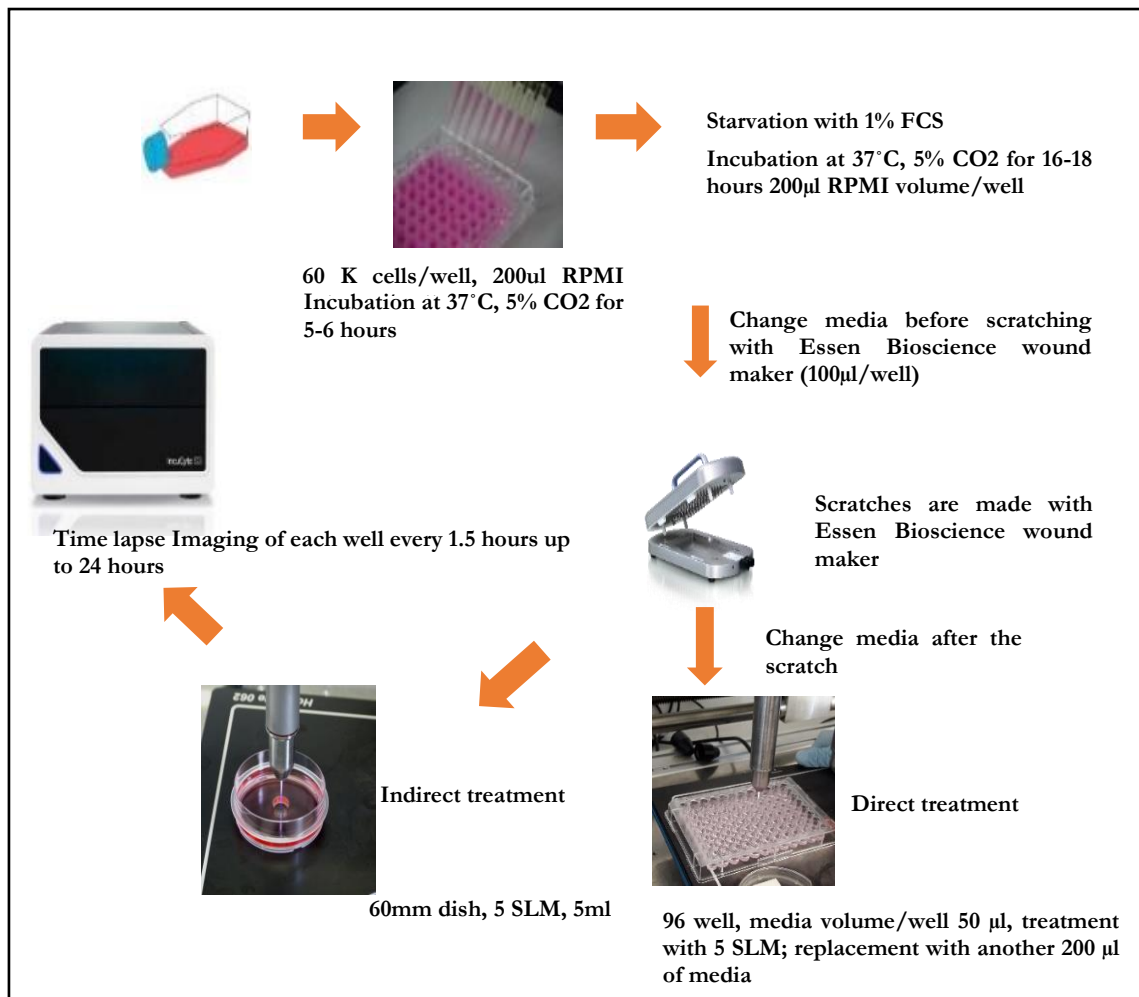
3. Methods

Figure 3.3 Cell migration assay set up

3.11   Gene expression analysis

3.11.1 RNA isolation

0.5×10^6 HaCaT cells or GM Fbs were seeded into a 6 well plate, and once the monocultures reached confluence, the cells were starved for 16-18 hours, scratches were made using a 10µl pipette tip and the cells were subsequently incubated with CAP treated medium or untreated control medium for indicated incubation hours. After that, the cells were washed with 1ml of ice-cold PBS and total RNA was isolated with RNA mini kit (Bio & Sell, Germany). Briefly, after washing with PBS, 400 µl of lysis buffer was added to the cells and either kept at -20°C for later processing or immediately processed with the following steps. Cell lysates were transferred to the blue column and centrifuged at $10,000 \times g$ for 2 minutes. The filtrate was then transferred to the purple column and mixed with equal volume (400 µl) of 70% ethanol and centrifuged again at $10,000 \times g$ for 2 minutes. The supernatant was discarded and 500 µl of wash buffer IT was added into the purple columns and

centrifuged at 10,000 × g for 1 minute. The filtrate was discarded and second wash step was carried out with 700 µl of wash buffer MT and subsequently centrifuged at 10,000 × g for 1 minute. Afterwards, the filtrate was removed and the columns were centrifuged at 10,000 × g for 3 minutes to discard any residual wash buffer. Finally, elution was carried out with 40 µl of nuclease free water by centrifuging at 6000 × g for 2 minutes. The RNA was then quantified with a spectrophotometer (Nanodrop 2000C, Thermo Fisher Scientific) and stored at -20°C for future use.

3.11.2 cDNA transcription

cDNA was synthesized with High-Capacity cDNA Reverse Transcription Kit (Thermo Fisher Scientific) according to manufacturer's protocol. Briefly, a master mix per sample was prepared as mentioned in table 3.1.

Table 3.1 Composition of transcription master mix per sample

Component	Volume
10X RT Buffer	2 µl
100mM dNTP mix	0.8 µl
10X random primers	2 µl
Multiscribe^{TM} Reverse Transcriptase	1 µl
Nuclease free H2O	4.2 µl
Total per reaction	10 µl

10 µl of master mix was admixed with 1 µg of RNA to a final volume of 20 µl and centrifuged shortly to spin down the contents and eliminate any residual air bubbles. Samples were incubated in a thermocycler using the conditions mentioned in table 3.2-

Table 3.2 Thermal cycling conditions

Settings	Step 1	Step 2	Step 3	Step 4
Temp	25°C	37°C	85°C	4°C
Time	10 min	120 min	5 min	∞

3.11.3 Quantitative Polymerase Chain Reaction

Gene expression was analyzed with Fast Start Essential DNA Green Master Mix (Roche). All the steps were carried out on ice. Thawed cDNA samples were diluted 1:10 with nuclease free water and qPCR mix for one reaction was prepared as summarized in the table 3.3.

Table 3.3 Composition of qPCR master mix

Reagent	Volume
2X SYBR Green Master Mix	5 µl
PCR primers	2 µl
Nuclease free water	13 µl
Total volume	20 µl

20 µl PCR mix was pipetted into each well of the PCR plate and 1 µl of cDNA template was added in each well. Subsequently, the multiwall plate was sealed with sealing foil (Sarstedt), centrifuged at 500 × g for 2 minutes and immediately transferred in the LightCycler 480 instrument (Roche). qPCR program was started with the conditions mentioned in table 3.4.

Table 3.4 Light Cycler program for gene expression analysis

Program	Cycle		Analysis mode
Pre-incubation	1.0		None
Amplification	40.0		Quantification
Cooling	1.0		None
Temperature(°C)	Acquisition mode	Hold(hh:mm:ss)	Ramp rate(°C/s)
Pre-incubation			
95	None	00:10:00	4.4
Amplification			
95	None	00:00:10	4.4
58	None	00:00:30	2.2
72	Single	00:00:01	4.4
Cooling			
40	None	00:00:30	2.2

Specific primer sequences (BioTez Berlin GmbH), analyzed in this thesis are mentioned in table 3.5. The house keeping gene ß-actin was used as an internal control. Each sample was measured in technical triplicates and the gene expression analysis was performed with the ΔΔCt method [179]. The final fold change in gene expression upon plasma treatment was determined according to the ratio of expression in the respective sample corresponding to the control.

Table 3.5 Analyzed genes and their primer sequences

Gene	Forward Primer Sequence	Reverse Primer Sequence
YAP	TAGCCCTGCGTAGCCAGTTA	TCATGCTTAGTCCACTGTCTGT
CTGF	CAGCATGGACGTTCGTCTG	AACCACGGTTTGGTCCTTGG
Cyr61	GGTCAAAGTTACCGGGCAGT	GGAGGCATCGAATCCCAGC
ß-actin	CACCAACTGGGACGACAT	ACAGCCTGGATAGCAACG
HIF-1α	ATCCATGTGACCATGAGGAAATG	TCGGCTAGTTAGGGTACACTTC
mTOR	GCAGATTTGCCAACTATCTTCGG	CAGCGGTAAAAGTGTCCCCTG
IGF-1	GCTCTTCAGTTCGTGTGTGG	GCCTCCTTAGATCACAGCTCC
IGF-2	GTGGCATCGTTGAGGAGTG	CACGTCCCTCTCGGACTTG

3.11.4 RT² PCR Profiler Array

The gene expression profile of GM Fbs after CAP treatment was analyzed by Qiagen RT² PCR array. The RNA was isolated as described before and the cDNA was synthesized with the RT² first strand kit (Qiagen). For cDNA synthesis by RT² first stand kit, a gDNA elimination mix was prepared with 2 µl of GE Buffer and 0.5 µg of RNA to a total volume of 10 µl. This mixture was incubated at 42°C for 5 minutes and immediately kept on ice afterwards for at least 1 minute. Subsequently, 10 µl of reverse transcriptase mix was prepared per reaction consisting 4 µl of BC3 buffer, 1 µl of Control P2, 2 µl of RT mix and 3 µl of nuclease free water. This reverse transcriptase mix was then added with gDNA elimination mix and incubated at 42°C for 15 minutes followed by 95°C for 5 minutes in a thermocycler. Afterwards, 91 µl of nuclease free water was added into each reaction and the cDNA was measured by a nanodrop. The cDNA was stored at -20°C for future use or proceeded directly with the qPCR array.

The qPCR array was performed with RT² Profiler™ PCR Array Human Extracellular Matrix & Adhesion Molecules (PAHS-013ZF-6) and RT² Profiler™ PCR Array Human Hippo Signaling (PAHS-172ZF-6). For one cDNA reaction, one 96 well plate was used. These 96 well plates were pre-coated with forward and reverse primer sequences of one gene. Besides housekeeping genes, 84 different genes were analyzed per array. A master mix of 1350 µl of SyBr Green, 1248 µl of nuclease free water and 102 µl of cDNA was prepared; 25 µl of this master mix was therefore aliquoted into each well of one 96 well plate. The plate was then centrifuged at 500g for 1 minute and the qPCR was carried out with Quantstudio 1 (Thermo Fisher Scientific) according to the protocol mentioned in table 3.6. Melting curve analysis was also performed to check the reactivity and specificity of the primer sequences. Data analysis was performed with the online free platform Gene Globe (Qiagen). A fold regulation greater than 2 (up or down) compared to the untreated control sample was

considered significant. The entire gene lists are mentioned in the appendix.

Table 3.6 Quant studio 1 cycling conditions for RT^2 PCR Array

Program	Cycle
Pre-incubation	1
Amplification	40
Melting	1
Temperature(°C)	Hold(hh:mm:ss)
Pre-incubation	
95	00:10:00
Amplification	
95	00:00:15
60	00:01:00
Melt curve	
95	00:00:15
60	00:01:00
95	00:00:01

3.12   Protein expression analysis

3.12.1 Immunoblotting

HaCaT cells and GM Fbs were seeded at a density of 0.5×10^6 cells in a 6 well plate. After the cells reached confluence, they were serum starved for 16-18 hours, scratches were created using a 10 µl pipette tip and the cells were subsequently incubated with CAP treated medium or untreated medium. Cells were washed with 1ml of ice-cold PBS and subsequently lysed with 100 µl of RIPA buffer (composition in the table 3.7 below). Afterwards, this lysate was kept on ice for 20 min, followed by sonication step for 10 seconds per sample in ice. Next, the cell lysate was centrifuged at 15,000g at 4°C for 10 minutes. Supernatants containing the cellular proteins were transferred to another 1.5ml vial and total protein quantification was carried out using DC^{TM} protein assay (BioRad).

3. Methods

Table 3.7 Composition of RIPA Buffer

Reagent	Concentration
PBS (without Ca^{+2},Mg^{+2})	1X
Igepal CA -630 substance	1%
Sodium deoxycholate	0.5%
SDS	0.1%
EDTA	20mM

One tablet each of protease and phosphatase inhibitors (Sigma Aldrich) and 2mM of PMSF (Phenyl Methane Sulfonyl Fluoride, Carl Roth) was added in a freshly prepared 10ml RIPA buffer. This was then used as the RIPA lysis buffer.

25 µg of total protein concentration / per sample was then denatured at 95°C for 7 minutes using lysis buffer (composition summarized below in table 3.8) and proteins were resolved using a 10% precast SDS page gel (BioRad) in 1X running buffer, while a constant voltage of 125V was applied. 5 µl of pre-stained protein ladder was subjected to each gel. Composition of 10X running buffer is also summarized below in table 3.9.

Table 3.8 Composition of sample lysis buffer

Reagent	Concentration
Tris (Sigma Aldrich)	0.25M, pH 6.8
SDS	2%
Glycerol (Carl Roth)	10%
ß-mercaptoethanol	2%
Bromophenol Blue (BPB)	0.004%

Table 3.9 Composition of 10X running buffer

Reagent	Concentration
Tris base(Sigma Aldrich)	30 gm
Glycine (Sigma Aldrich)	144 gm
SDS (Sigma Aldrich)	10 gm
H_2O	1000 ml

The proteins were thereafter transferred and blotted on a PVDF membrane with Trans blot Turbo^{TM} for 7 min at 25V. The membranes were blocked with 2.5% BSA in TBST (Tris Buffered Saline Tween 20, table 3.10) for 1 hour. Subsequently, the membranes were incubated with primary antibodies (table 3.11) at a dilution of 1:1000 in TBST for overnight at 4°C. Next day, the membranes were washed with TBST thrice (10 min washing step each) which was followed by incubation with HRP conjugated secondary antibody (table 3.12, dilution 1:5000 in TBST) for 1 hour at room temperature. Bands were detected with chemiluminescence substrate (Thermo Fisher Scientific, Supersignal^{TM} Femto Substrate) using Image Las 4000 (GE Healthcare). The band intensities were quantified with Image Studio Lite (version 5.2), normalized to housekeeping ß-actin, and expressed as a fold change compared to corresponding untreated control.

Table 3.10 Composition of TBST

Reagent	Concentration
Tris base (Sigma Aldrich)	20 mM
NaCl (Sigma Aldrich)	13.7 mM
Tween 20 (Sigma Aldrich)	0.1%

Table 3.11 List of primary antibodies

Target	Molecular Mass (kDa)	Host animal
YAP	65	Mouse
Phospho YAP(Ser 127)	65	Rabbit
CTGF	38	Rabbit
Cyr61	41	Rabbit

Table 3.12 List of secondary antibodies

Target	Host animal
Mouse IgG	Goat
Rabbit IgG	Mouse
Mouse IgG, Alexa-Fluor 488	Goat

3.12.2 Enzyme linked immunosorbent assay (ELISA)

Secreted proteins (CTGF and Cyr61) in cell culture conditioned media were analyzed by ELISA (table 3.13). Different providers were used and the experiments were performed according to manufacturer's protocol. Here only a general method is overviewed. 96 well plates, pre-coated with capture antibodies were brought to room temperature. Lyophilized standard was reconstituted with assay diluent and serial dilutions were performed to prepare the standard curve. Fibroblast conditioned media was directly added into the wells. About 100 µl of each standard and samples were added into each well in at least duplicates. The wells were covered and incubated for 2-2.5 hour in room temperature. Following which, the samples and standards were discarded and the wells were washed 3-4 times with 1X wash buffer. After each wash, the plates were inverted and blotted against a clean paper towel. 100 µl of protein specific biotinylated detection antibody was added in the wells and incubated for 1-2 hours with gentle shaking. Afterwards, the washing step was again performed 3-4 times. Next, 100 µl of newly prepared HRP conjugated streptavidin solution was added to the wells and incubated for 45min-1 hour with gentle shaking. Subsequently, the solutions were discarded and the washing step was repeated. 100 µl of substrate solution (TMB) was added to the wells and incubated for 30 min in room temperature in dark. Positive samples were now colored in blue. Reaction was stopped with 50 µl of stop solution to each well, for which the color changed from blue to yellow. The absorbance was measured with a multimode plate reader (Tecan M200 pro) at 450nm and the reference was set at 570nm.

Table 3.13 ELISA kits used for extracellular protein detection

ELISA kit	Manufacturer	Catalog No.
CTGF	Peprotech GmbH	900-K317
Cyr61	R& D systems	DCYR10

3.13   Immunofluorescence

Wounded monolayers of HaCaT cells and GM Fbs were incubated with untreated or CAP treated medium for 3 hours. Next, these monolayers were fixed in 4% paraformaldehyde diluted in PBS for 15 minutes. The samples were thereafter rinsed with 1X PBS for 3 times, 5 minutes each wash. The cells were permeabilized with PBS containing 0.3% Triton X-100 for 10 minutes, rinsed with PBS (3 times) and blocked with blocking buffer (1% BSA, 0.1% Tween 20 in 1X PBS) for 1 hour at room temperature. Next, the samples were incubated with mouse anti YAP (1:500, diluted in 1% BSA, 0.1% Tween 20 in 1X PBS,

Santa Cruz Biotechnology, sc-101199) for 1 hour at room temperature. Afterwards, the diluted primary antibody mix was decanted. Anti-mouse IgG (Alexa-Fluor 488, CST 4408S) was diluted 1:2000 in 1% BSA/PBST for 1 hour at room temperature in the dark. Secondary antibody was decanted and the cells were washed with 1X PBS for 3 time, 5 minutes each. Finally, the cells were incubated with 0.2 µg/ml DAPI in PBS for 10 minutes in dark and imaged using an Axio Observer Z1 (Zeiss, Germany).

3.14 Statistics

Graphics and statistics were performed using prism 8.02 (GraphPad PRISM software, San Diego, USA). Mean and standard deviation were calculated and analyzed according to unpaired t-test with Welch's correction and ordinary one-way or two-way analysis of variance (ANOVA). A p value < 0.05 was considered statistically significant ($*p \leq 0{:}05$, $**p \leq 0{:}01$, $***p \leq 0{:}001$, and $****p \leq 0{:}0001$).

4. Results

4.1   Characterization of H_2O_2 production in CAP treated medium

In majority of our experiments, CAP treated RPMI was used as medium (indirect treatment). Previous studies indicate, that amongst the short- and long- lived species produced by kINPen MED at 5 SLM, H_2O_2 is one of the most stable oxidants [180]. Therefore, we quantified the H_2O_2 concentration by the amplex red assay as described in the methods section. We observed a linear increase of the H_2O_2 concentration with treatment time (figure 4.1). 60s, the highest treatment time generated about 13 µM of H_2O_2.
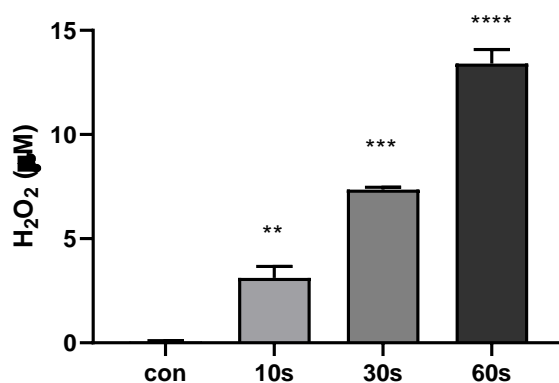
Figure 4.1 CAP generated hydrogen peroxide production in RPMI medium. Concentration of H_2O_2 after 10, 30 and 60s of plasma treatment with kINPen MED operated at 5 SLM with argon flux. No plasma treatment served as the negative control. Data are presented as mean ± S.D. from two independent experiments. Statistical comparisons are performed using one-way ANOVA.

4.2   Intracellular ROS production in HaCaT and GM Fbs

2',7' –dichlorofluorescin diacetate is a cell permeable dye, which is first deacetylated by cellular esterases but later oxidized by ROS into 2', 7' –dichlorofluorescein , a highly

fluorescent compound. We already demonstrated that CAP treatment produces H_2O_2 in RPMI medium. Therefore, we performed the H_2DCFDA assay. We observed an increase in intracellular ROS production in both HaCaT and GM Fbs (figure 4.2). To be precise, compared to untreated negative control, ROS production was 1.2-fold higher in HaCaT cells and1.3-fold higher in GM Fbs with the highest plasma treatment of 60s. 100 µM of H_2O_2 served as a positive control, which showed a significant induction of intracellular ROS in both the cell lines.
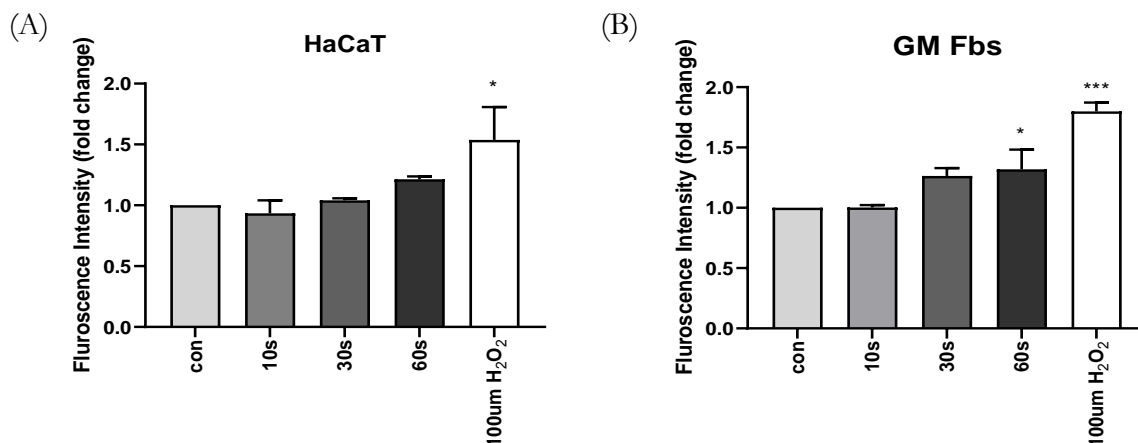
Figure 4.2 Effect of CAP on intracellular ROS levels. Intracellular ROS production was measured by 2, 7′-diclorofluorescein (DCF) fluorescence in (A) HaCaT cells and (B) GM Fbs. Data are presented as mean ± S.D. from two independent experiments, each performed in technical quadruplets. Statistical comparisons were performed using one-way ANOVA.

4.3   Influence of CAP on metabolic activity in mono and coculture

4.3.1 Metabolic activity of mono and coculture after 3 and 24 hours of CAP treatment

The Alamar Blue assay measures the cell viability of metabolically active cells. Alamar Blue assay serves as the redox indicator of cells, is cell permeable, non-toxic and acts as an intermediate electron acceptor in the electron transport chain without interference of the normal transfer of electrons. This is in direct correlation to the NADPH content of cells which further refers to the cells capability to generate ATP. Hence, constant monitoring of cells in culture is possible by Alamar Blue assay.

We performed the Alamar Blue assay with the monocultures HaCaT, GM Fbs and the coculture (figure 4.3). 10 and 30 s CAP treatment did not significantly alter the metabolic activity of HaCaT, GM Fbs and coculture after 3 hours of treatment. However, 60s treatment

could lead to a significant reduction of metabolic activity in all the cell types. 24 hours after the CAP treatment, HaCaT cells and the coculture did not show a further reduction in cell viability, however, in GM Fbs, both 30s and 60s treatment significantly reduced cell viability. Based on these results, we excluded 60s treatment for most of our subsequent experiments.

(A)

(B)
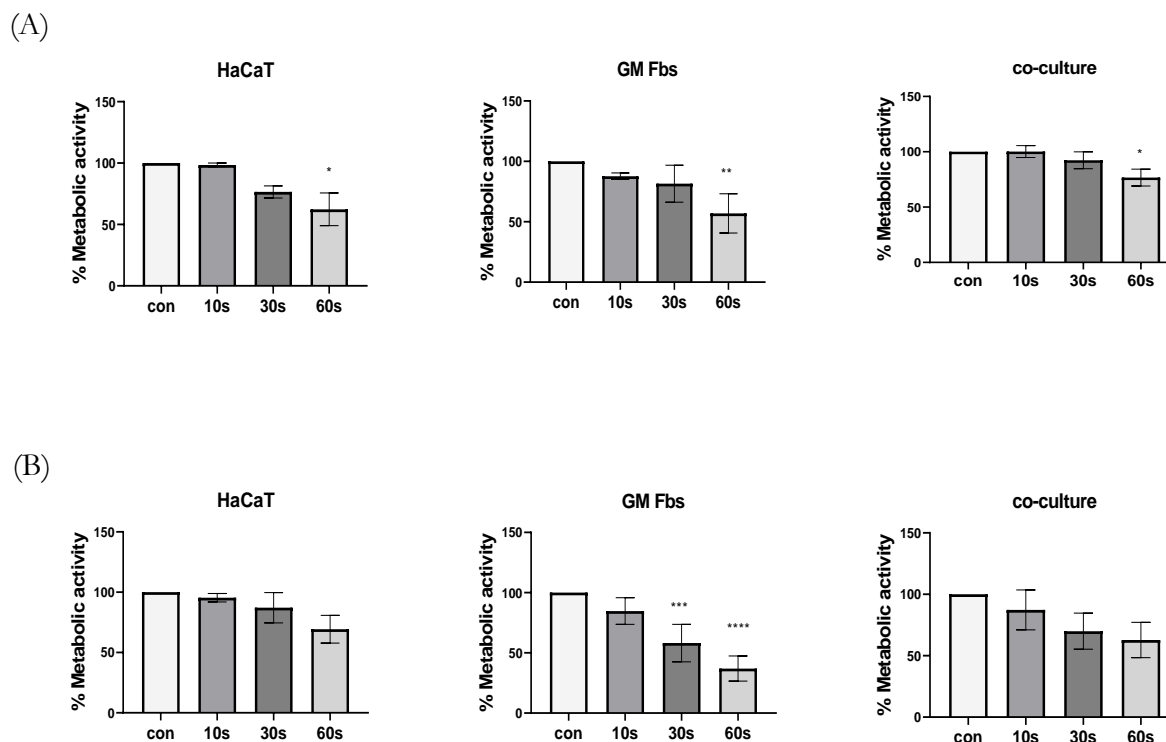
Figure 4.3 Influence of CAP on metabolic activity of mono and coculture. The metabolic activity of HaCaT cells, GM Fbs, and coculture after 3 h in response to 10, 30, and 60s of CAP treatments. Untreated RPMI served as control (A). Metabolic activity of the same cell types after 24 h of CAP treatment (B). Data are presented as mean ± SD of three independent experiments performed in triplicate. Statistical comparisons were performed using one-way ANOVA.

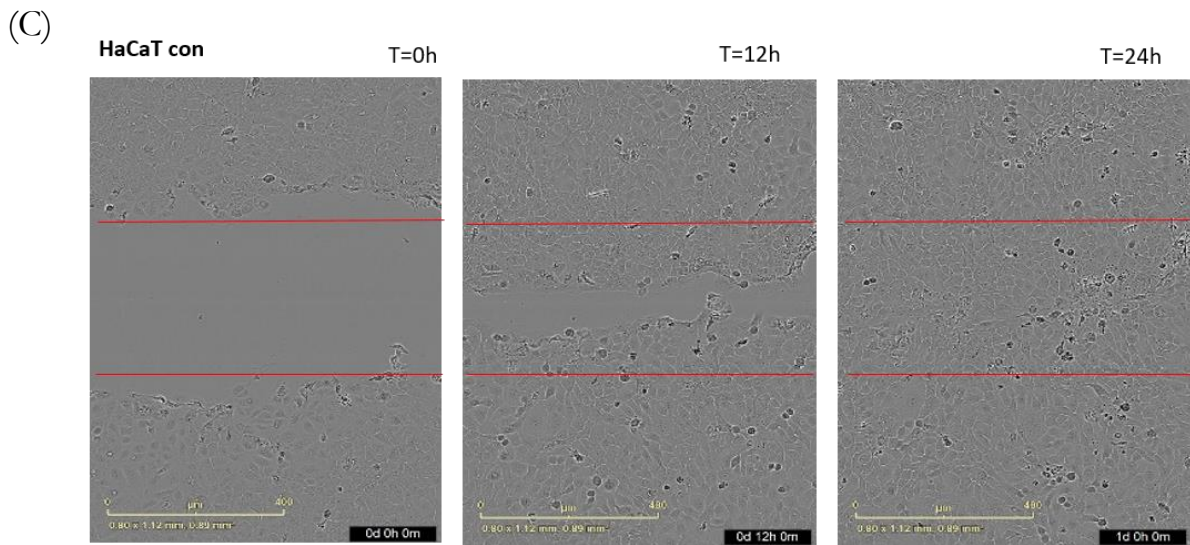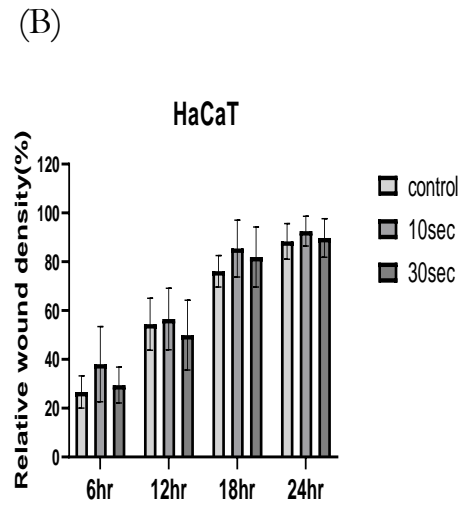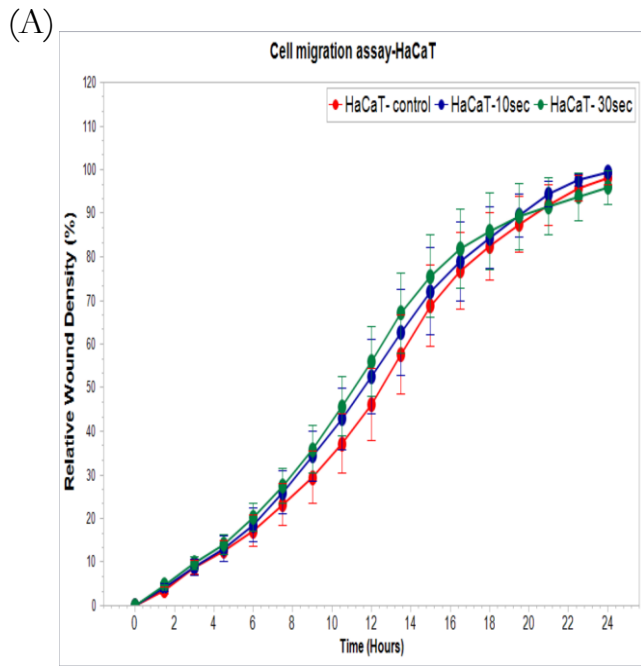## 4.3.2 Influence of NAC on metabolic activity in mono and coculture

NAC or N-acetyl L-cysteine is a precursor of L cysteine, a potent antioxidant and acts directly as a scavenger of free radicals especially oxygen radicals. To determine the effect of CAP produced ROS on metabolic activity, cells were incubated with 2.5 mM NAC alone or in combination with 10, 30 and 60 s CAP treated medium for 3 and 24 hours. 60 µM H_2O_2 alone or in combination with NAC was used as a positive control. As observed in figure 4.4, NAC alone did not significantly increase the metabolic activity in HaCaT and

coculture in 3 hours. However, in GM Fbs, there was a significant increase in metabolic activity when cells were treated with NAC alone. In all the three cell types, NAC treatment in combination with cold plasma restored the metabolic activity within 3 hours. In fact, a significant increase in metabolic activity was observed in both GM Fbs and coculture when NAC was incubated with 60s plasma treated medium. As expected, the positive control H_2O_2 decreased the metabolic activity in all the three cell types, but NAC restored the metabolic activity when treated in combination with H_2O_2. These proves that NAC is able to act as a scavenger in this experimental set up. Due to its antioxidant activity, metabolic activity was restored already after 3 hours of incubation with plasma-treated medium.
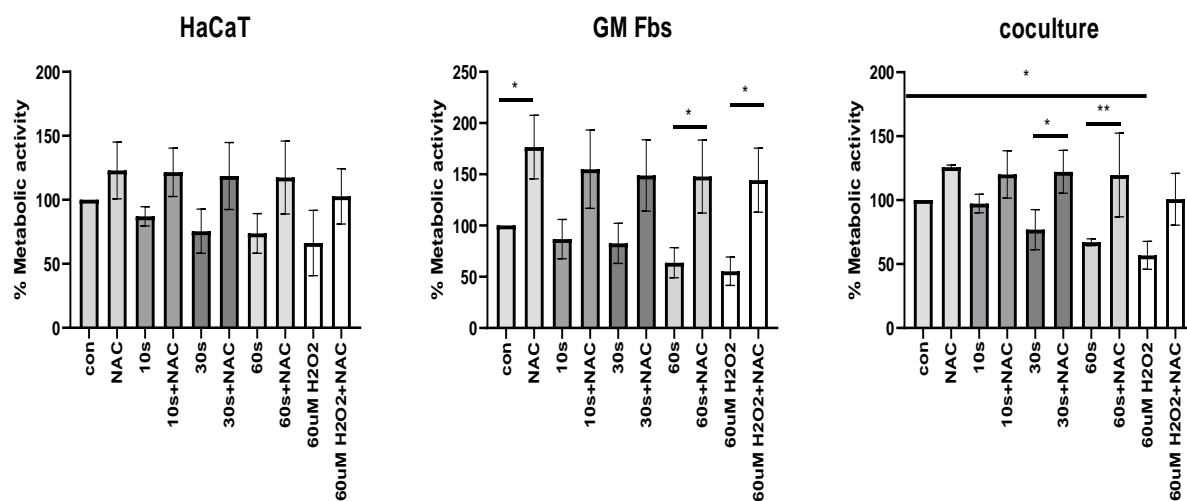
Figure 4.4 Effect of NAC on metabolic activity after 3 h of CAP treatment. Metabolic activity of HaCaT cells, GM Fbs, and coculture after 3 h incubation with 2.5mM NAC alone or in combination with CAP-treated media. Data are presented as mean ± SD from at least three independent experiments performed in triplicate. Statistical analysis was performed using one-way ANOVA.

As observed in figure 4.5, after 24 hours, NAC alone did not significantly alter the metabolic activity in HaCaT cells and coculture. However, metabolic activity was increased in GM Fbs upon incubation with NAC alone. In HaCaT cells, 60s plasma treatment and 60 µM H_2O_2 significantly reduced the metabolic activity in HaCaT cells. But, NAC counteracted plasma and H_2O_2 treatment and restored the metabolic activity. In GM Fbs, as observed before, incubation with plasma treated medium and 60 µM H_2O_2 significantly reduced the metabolic activity. But, NAC counteracted 10, 30, 60 s CAP treatments and H_2O_2 and hence increased the metabolic activity. In coculture, NAC significantly counteracted the effects of 30s of CAP treatment and increased the metabolic activity of these cells.
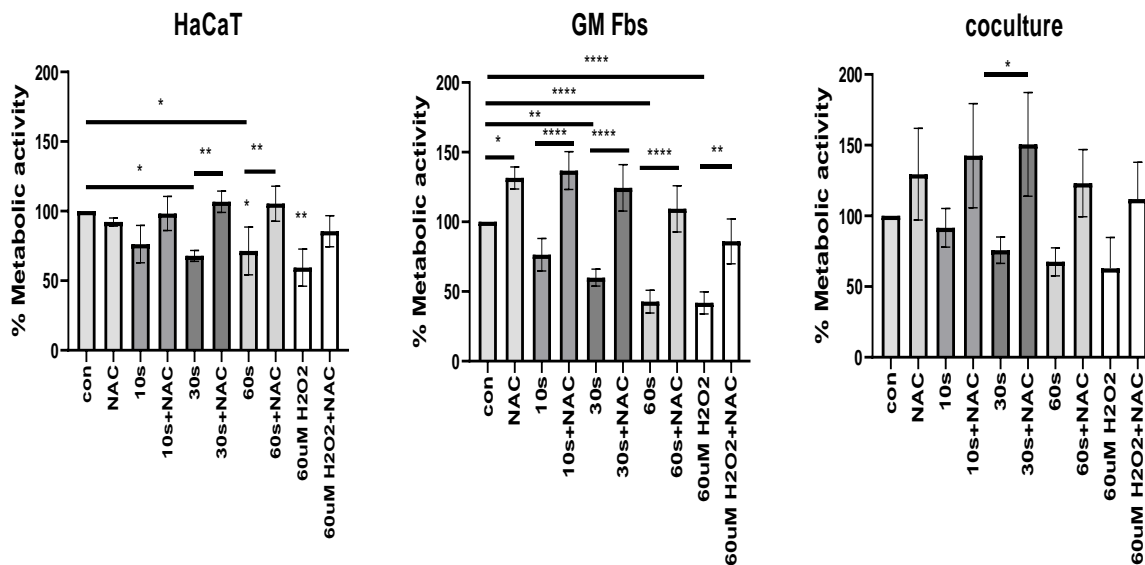
Figure 4.5 Effect of NAC on metabolic activity of CAP treated cells after 24 h. Metabolic activity of HaCaT cells, GM Fbs, and coculture after 24 h incubation with 2.5mM NAC alone or in combination with CAP-treated media. Data are presented as mean ± SD from at least three independent experiments performed in triplicate. Statistical analysis was performed using one-way ANOVA.

4.4 Influence of CAP on cell migration in mono and coculture

One of the most important steps in wound closure is the ability of cells to migrate in the wound bed. The proliferative stage of wound healing is primarily dominated by proliferation and cell migration of dermal keratinocytes and dermal fibroblasts. To exclusively monitor cell migration, we starved the cells for 18-20 hours prior to the experiment. In fact, during the entire process of cell migration assay, only 1% FCS was used. Cell migration was monitored upon indirect and direct plasma treatment as mentioned in the methods section.

4.4.1 Influence of indirect CAP treatment on cell migration

60k cells/ well either in monoculture or in coculture (40K HaCaT, 20K GM Fbs), after making scratches by wound maker, were incubated with 200 µl of untreated or 10-30s CAP treated media until 24 hours. Figure 4.6 and figure 4.7 illustrates that, indirect CAP treatment (10s, 30s) did not significantly modify the relative wound density in HaCaT or GM Fbs. In fact, 30s treatment showed a minor delay in migration in GM Fbs. However, in case of coculture (figure 4.8), CAP treatment could significantly accelerate the relative wound density from 12 hours. This result indicates that the CAP treatment could have a significantly different effect on monocultures and coculture.

4. Results

(A)

Cell migration assay-HaCaT

(B)

HaCaT

(C)

HaCaT con

* Figure continued in the next page

HaCaT 10sec   T=0h   T=12h   T=24h

HaCaT 30sec   T=0h   T=12h   T=24h
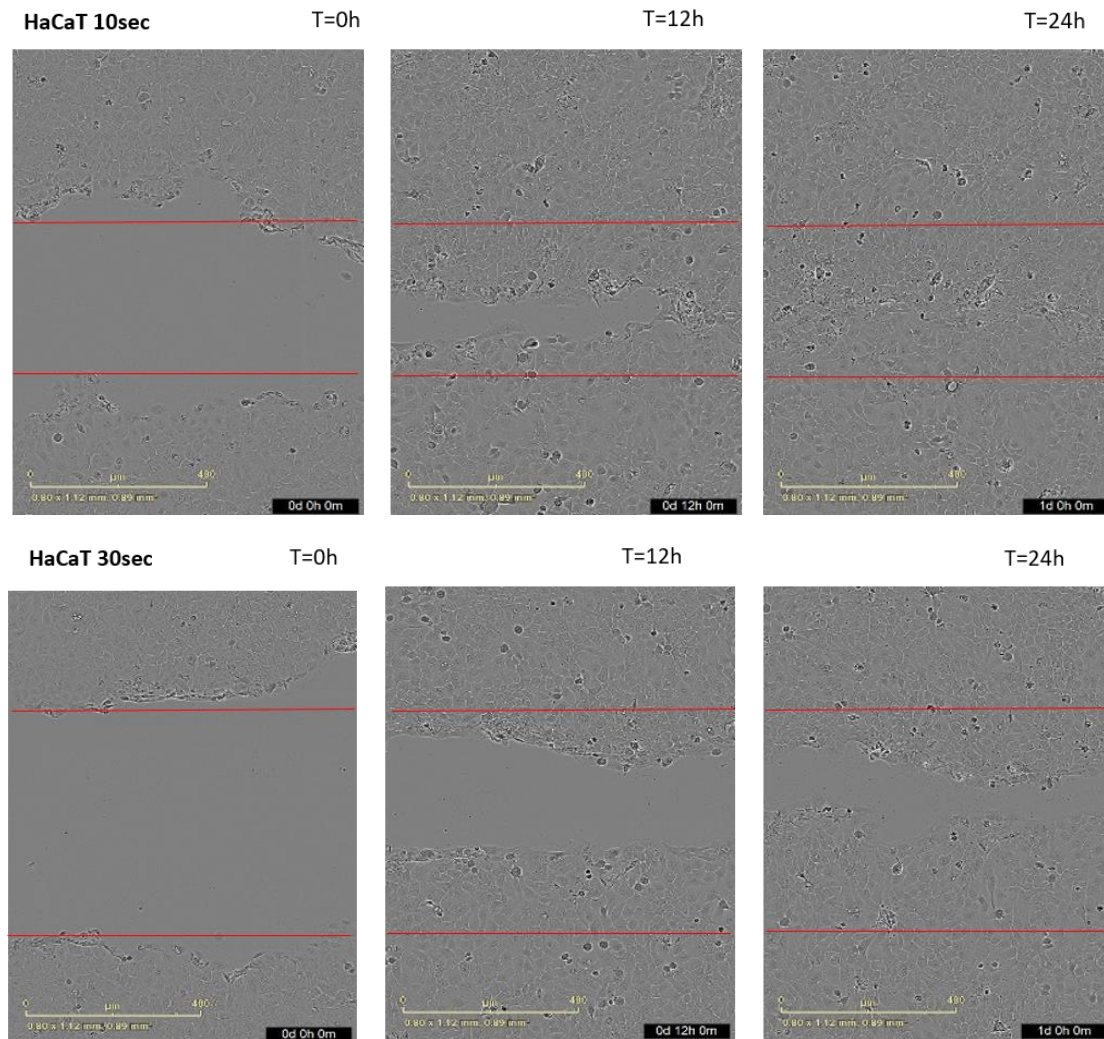
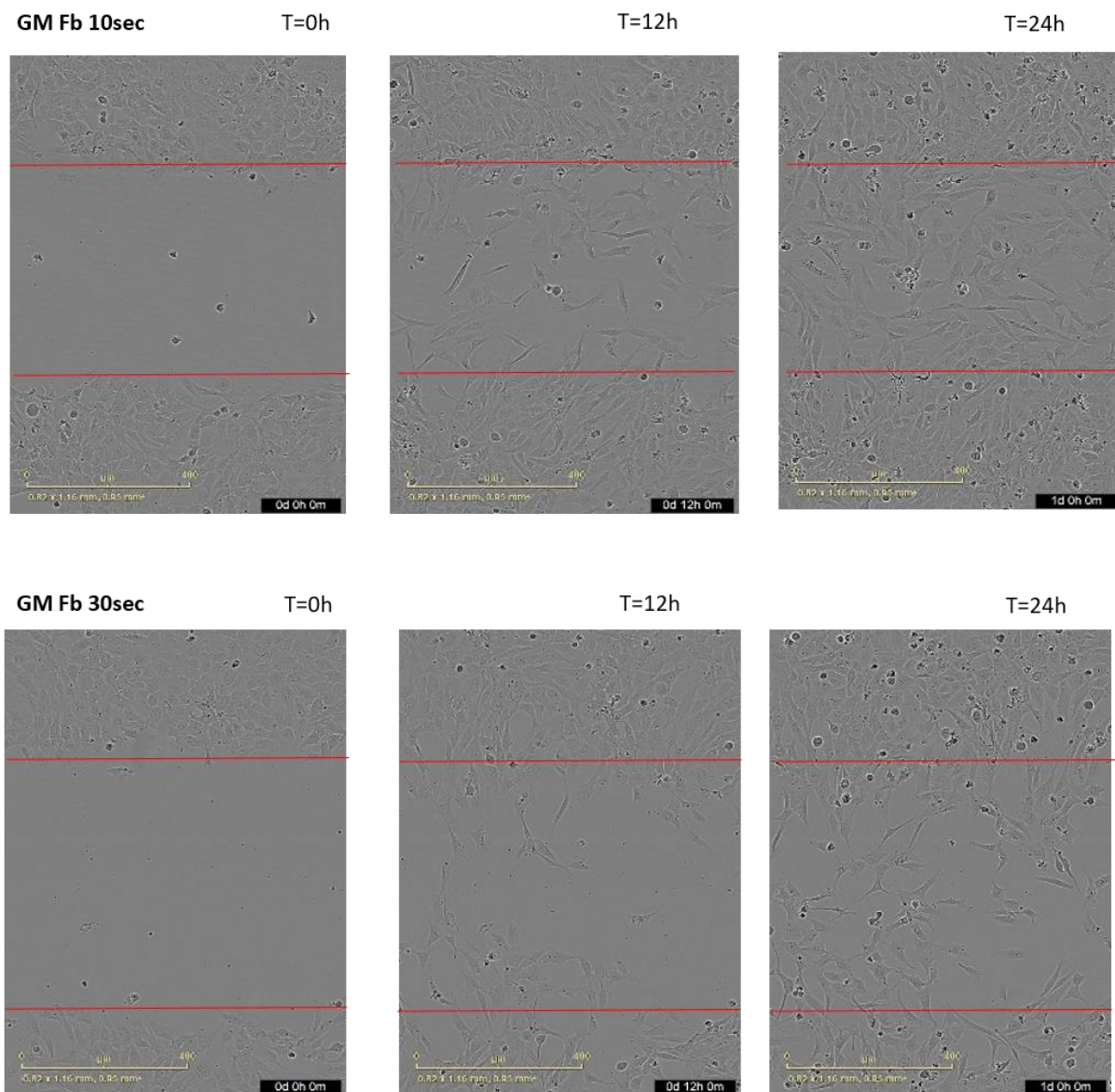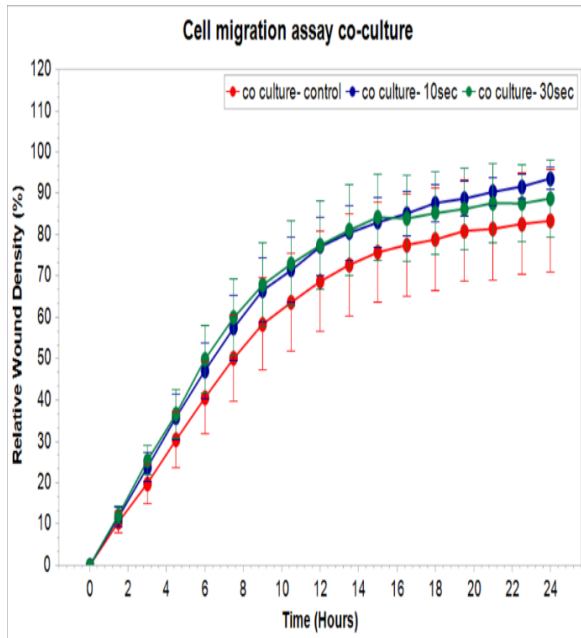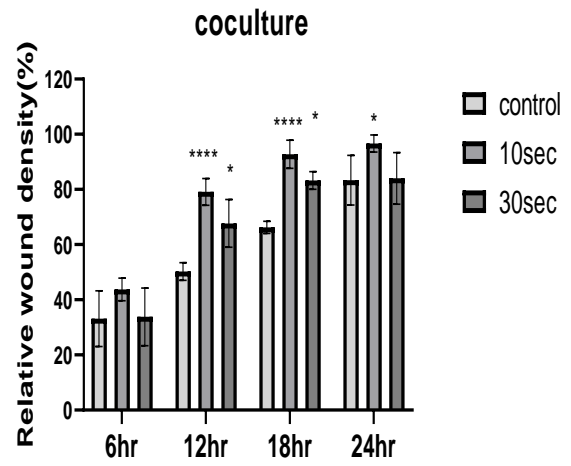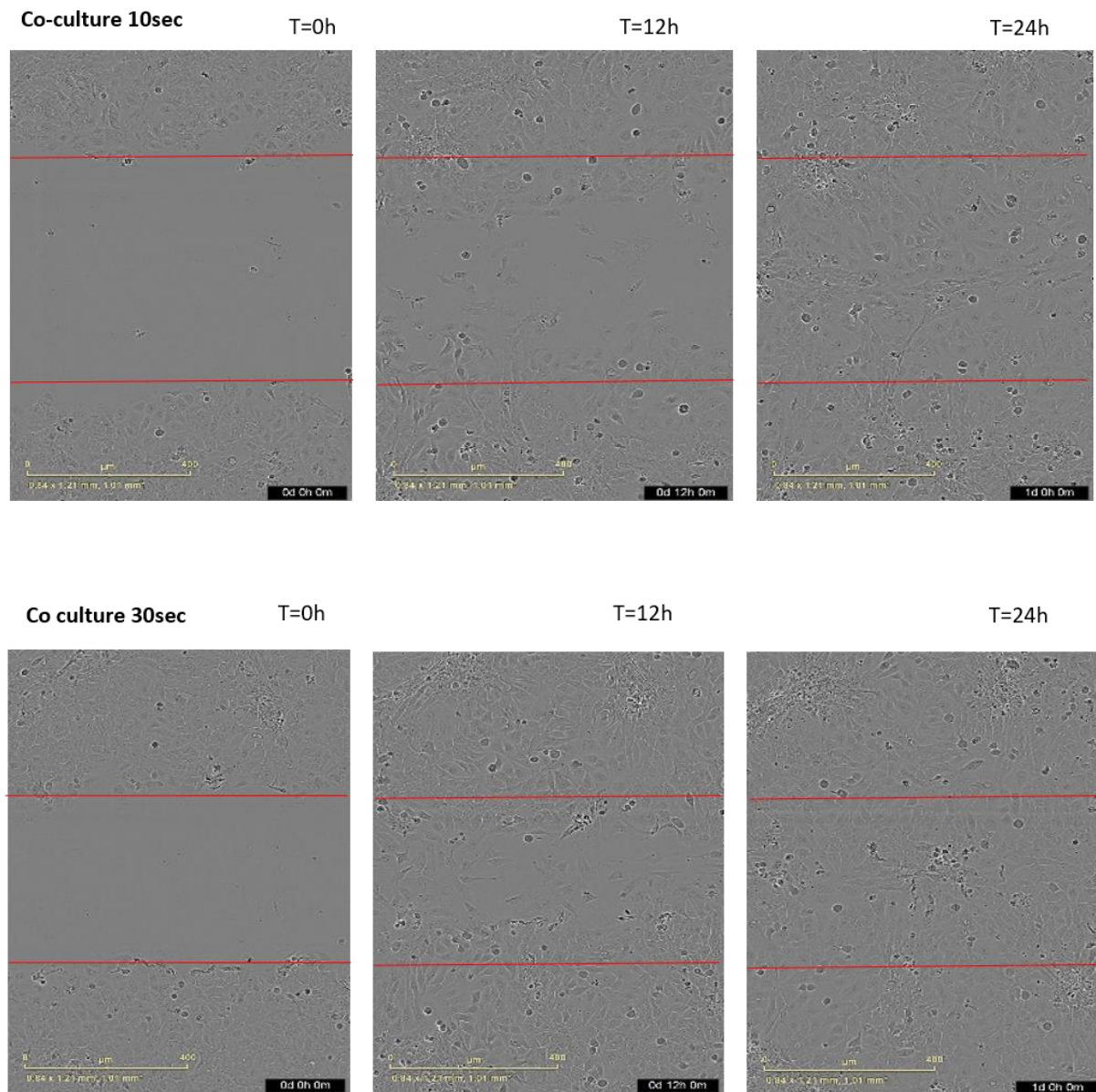**Figure 4.6** Influence of CAP on HaCaT cell migration. The representative time course of wound closure in untreated and indirect CAP treated HaCaT cells is shown in (A). The summation of relative wound density of untreated and CAP treated HaCaT cells are shown at specific time points 6, 12, 18 and 24 h (B). Wound closure images at time 0, 12 and 24 h in untreated and CAP treated HaCaT cells (C). Data are presented as mean± SD from three independent experiments. Statistical comparisons were performed using two-way ANOVA.

4. Results

(A)

Cell migration assay GM00637

(B)

GM Fbs

(C)

GM Fb con   T=0h   T=12h   T=24h

* Figure continued in the next page

46
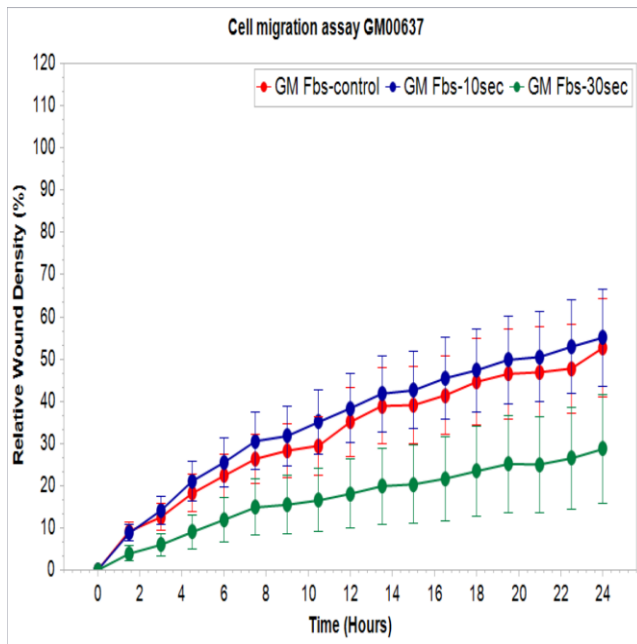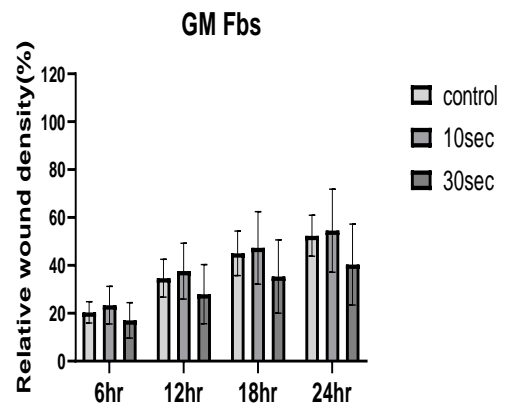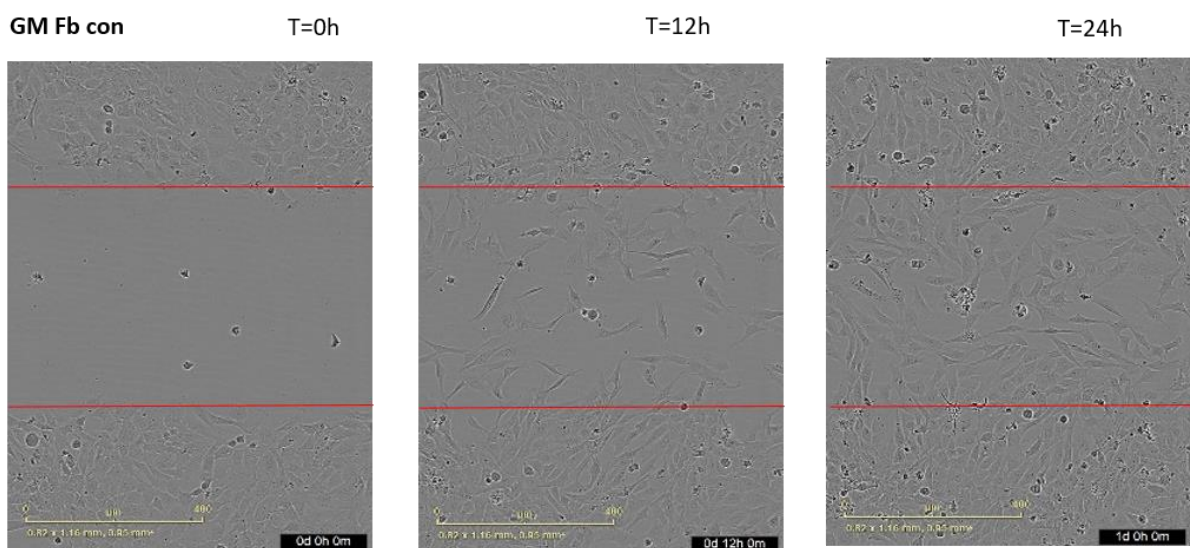
Figure 4.7 Influence of CAP on cell migration of GM Fbs. The representative time course of wound closure in untreated and indirect CAP treated GM Fbs is shown in (A). The summation of relative wound density of untreated and CAP treated fibroblasts are shown at specific time points 6, 12, 18 and 24 h (B). Wound closure images at time 0, 12 and 24 h in untreated and CAP treated GM Fbs (C). Data are presented as mean ±SD from three independent experiments. Statistical comparisons were performed using two-way ANOVA.

4. Results

(A)

(B)

(C)
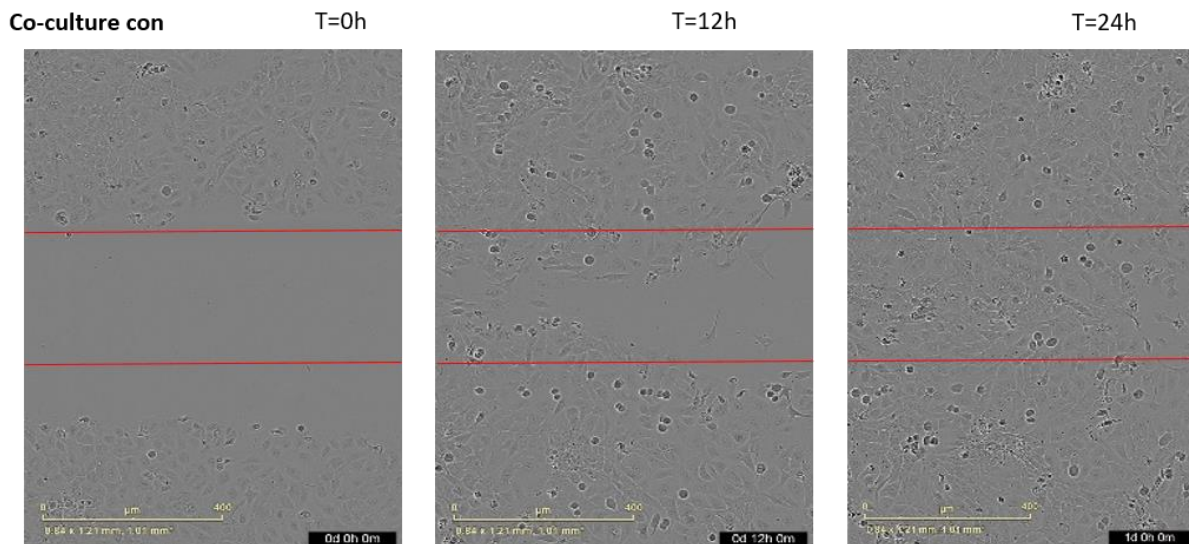
* Figure continued in the next page

Figure 4.8 Influence of CAP on cell migration in coculture. The representative time course of wound closure in untreated and indirect CAP treated coculture is shown in (A). The summation of relative wound density of untreated and CAP treated coculture are shown at specific time points 6, 12, 18 and 24 h (B). Wound closure images at time 0, 12 and 24 h in untreated and CAP treated coculture (C). Data are presented as mean ±SD from three independent experiments. Statistical comparisons were performed using two-way ANOVA.

We also compared the relative wound density between HaCaT cells alone and those cocultured with fibroblasts (figure 4.9), and we observed that, 10s indirect CAP treatment could significantly accelerate relative wound density in coculture compared to HaCaT monoculture alone. 30s CAP treatment also showed similar results where a significant increase in relative wound density in coculture was observed at 12 hours. These results further indicate that, CAP mediated cell migration varies depending on cell type and dermal cell interactions could also significantly alter CAP-mediated cell migratory effect.
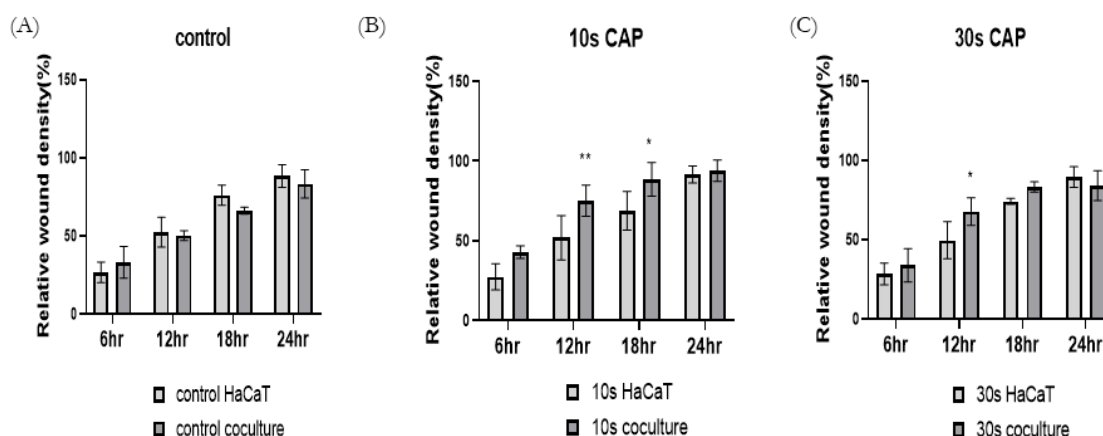
Figure 4.9 Comparison of relative wound density between untreated and CAP-treated HaCaT cells and coculture. (A), (B) and (C) details the comparative analysis of cell migration between HaCaT mono culture and co culture after incubation with untreated , 10s and 30s CAP treated medium at 6, 12, 18 and 24 h. Data are presented as mean ± SD from three independent experiments. Statistical comparisons are performed with two-way ANOVA.

4.4.2 Influence of NAC on cell migration of HaCaT and coculture

HaCaT cells and coculture were incubated with 2.5 mM NAC alone or in combination with CAP treated medium in cell migration assays for 24 hours. Interestingly, we observed that NAC alone did not improve HaCaT cell migration. Upon, CAP treatment, no significant acceleration in relative wound density of HaCaT cells were observed (like figure 4.6). But, upon NAC administration with CAP treated medium, relative wound density of HaCaT cells was reduced as observed in figure 4.10.

In coculture, similar results were obtained, as demonstrated in figure 4.11. Starting from 12 hours, NAC treatment reduced CAP-induced acceleration of relative wound density. At later time point (24 hours), treatment with NAC alone significantly reduced relative wound

density compared to control. NAC reduced CAP mediated cell migration to ~40-50% at later hours (starting from 18 hours) in coculture.
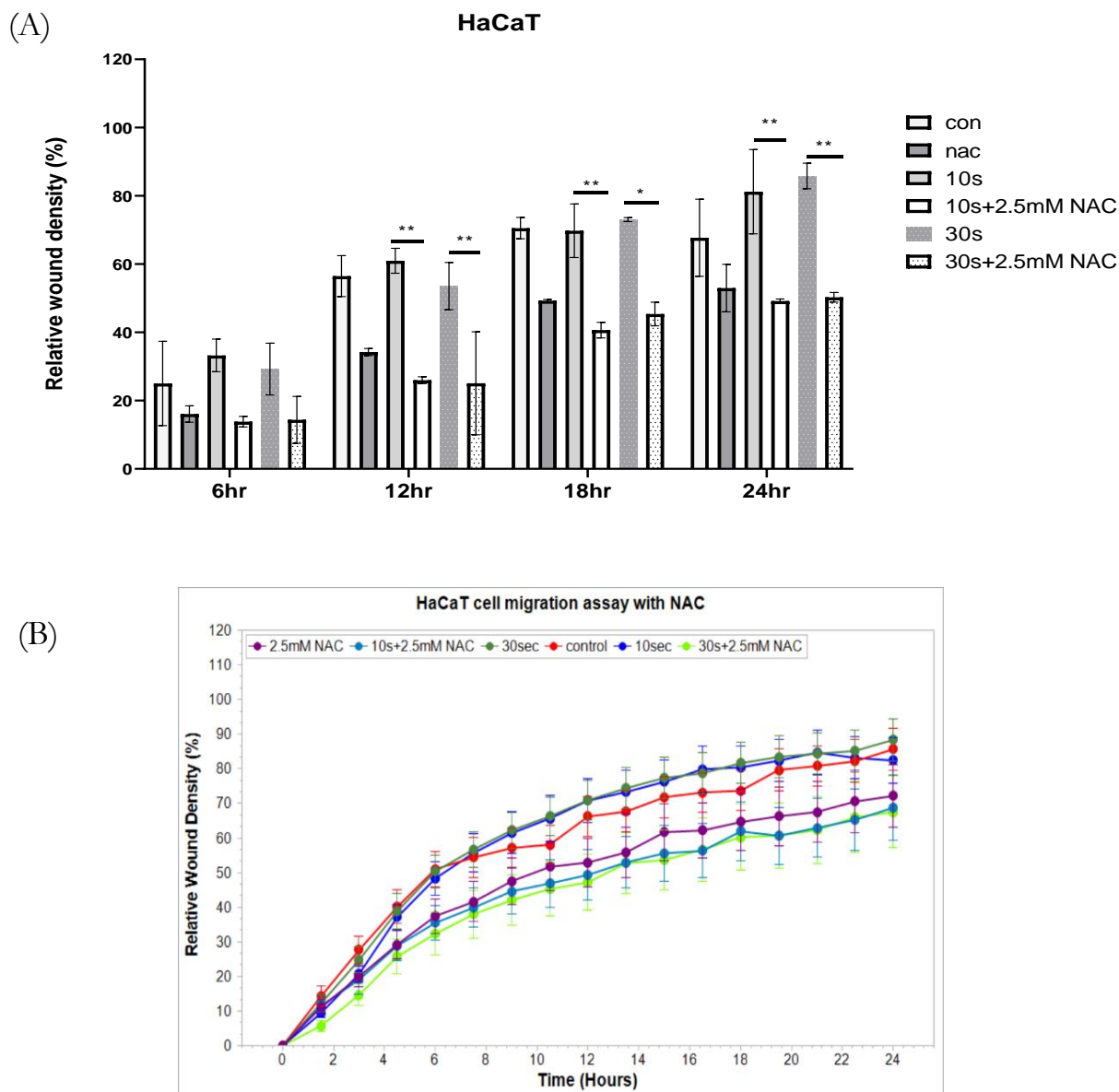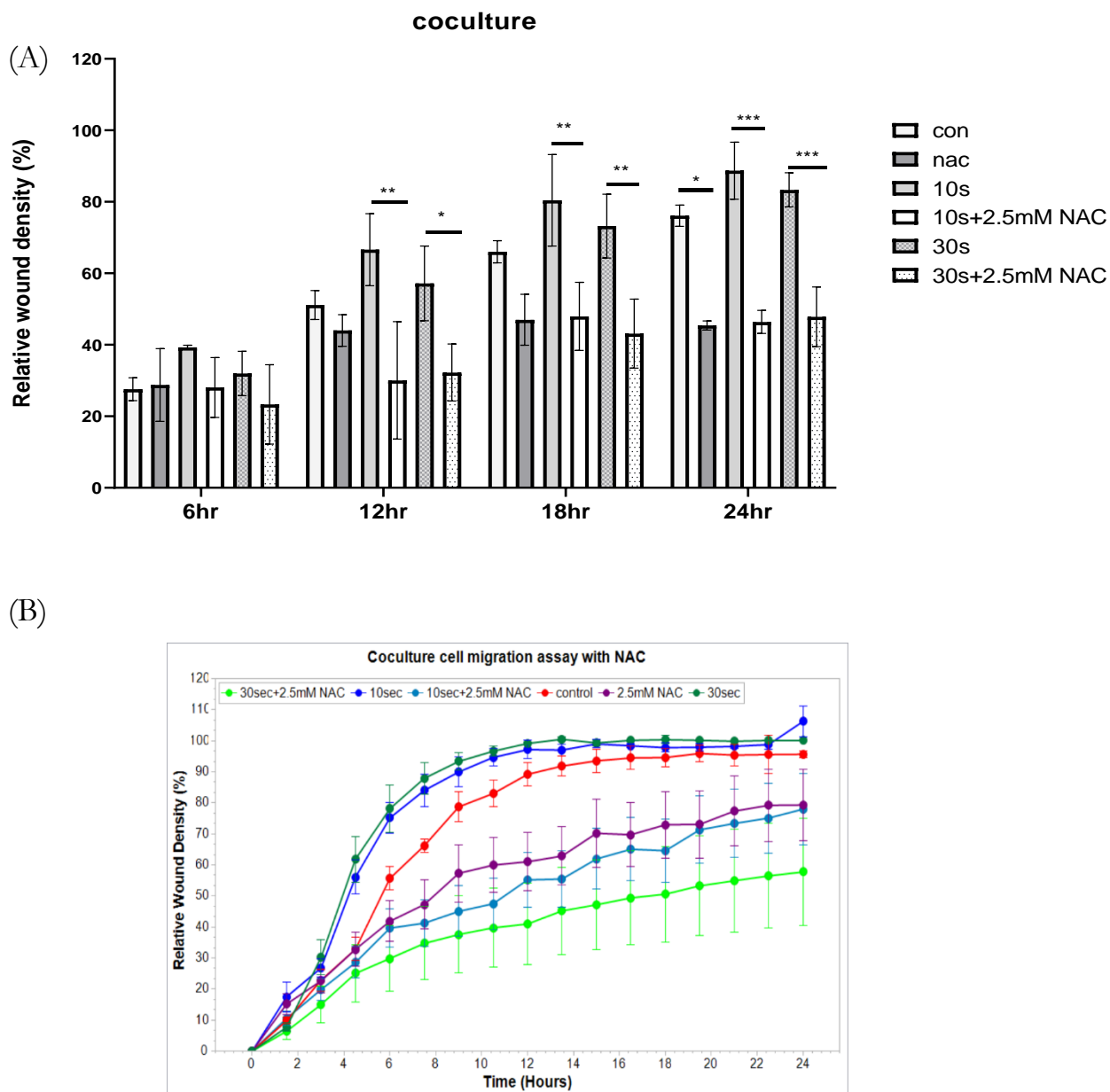
(A)

(B)

Figure 4.10 Effect of NAC on HaCaT cell migration. (A) details the relative wound density of HaCaT cells after treatment with NAC alone or in combination with CAP-treated media at 6, 12, 18, and 24 h. (B) depicts the representative time course of wound closure in HaCaT cells treated with CAP alone or in combination with 2.5mM NAC. Data are presented as mean ± SD of three independent experiments performed in triplicate. Statistical comparisons were performed using two-way ANOVA.

4. Results

Figure 4.11 Effect of NAC on coculture cell migration. (A) details the relative wound density of coculture after treatment with NAC alone or in combination with CAP-treated media at 6, 12, 18, and 24 h. (B) depicts the representative time course of wound closure in coculture treated with CAP alone or in combination with 2.5mM NAC. Data are presented as mean ± SD of three independent experiments performed in triplicate. Statistical comparisons were performed using two-way ANOVA.

4.4.3 Influence of direct CAP treatment on cell migration

HaCaT cells in monoculture or cocultured with fibroblasts were also directly treated with 5 SLM plasma for 10 and 30s with kINPen MED (as mentioned in the methods section) and we analyzed the effect of direct CAP treatment on cell migratory behavior. EGF (10ng/ml) was used as a positive control for cell migration. Figure 4.12 illustrates that direct CAP treatment (both 10 and 30s) did not accelerate relative wound density in HaCaT cells. In fact, both 10 and 30s of direct treatment showed a tentative reduction in relative wound density compared to control starting from 12 hours. However, on the contrary, in coculture, 10s direct CAP treatment accelerated relative wound density compared to control starting from 12 hours. But, 30s direct CAP treatment could not improve the relative wound density. This could be due to long- and short- lived species produced by 30s direct CAP treatment, which could already start to exert an oxidative stress on cells resulting in delayed cell migration. As 10s direct CAP treatment stimulated cell migration in HaCaT cells cocultured with fibroblasts, an effect of CAP on cell-cell interaction during wound healing is indicated.
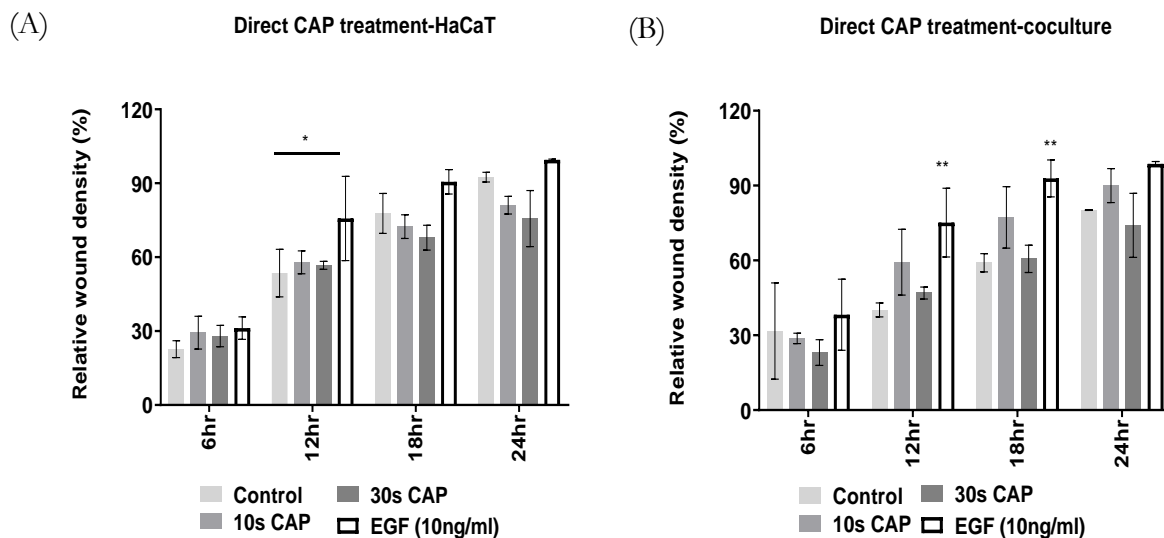
Figure 4.12 Influence of direct CAP treatment on cell migration in HaCaT and coculture. (A) and (B) depicts the summation of relative wound density in HaCaT monoculture and coculture upon untreated, 10 and 30s direct CAP treatment at specific time points 6, 12, 18 and 24 h. EGF (10ng/ml) served as the positive control. Data is presented as mean ± SD from two independent experiments, each with triplicates. Statistical comparisons were performed with two-way ANOVA.

We compared the effect of direct CAP treatment and CAP-treated medium (indirect treatment) on cell migration in figure 4.13. We observed that compared to control and direct CAP treatment, indirect CAP treatment (30s) could significantly accelerate relative wound density in coculture (figure 4.13). In HaCaT cells, there was a tendency of improved cell migration upon 10s indirect CAP treatment compared to direct CAP treatment, but it was not significant. In fact, as shown in figure 4.13 (C, D), compared to control, relative wound density (%) was reduced upon direct CAP treatment in HaCaT cells. The wound closure was faster in response to indirect CAP treatment in mono and coculture compared to direct CAP treatment, therefore, we used indirect CAP treatment for the rest of the thesis.
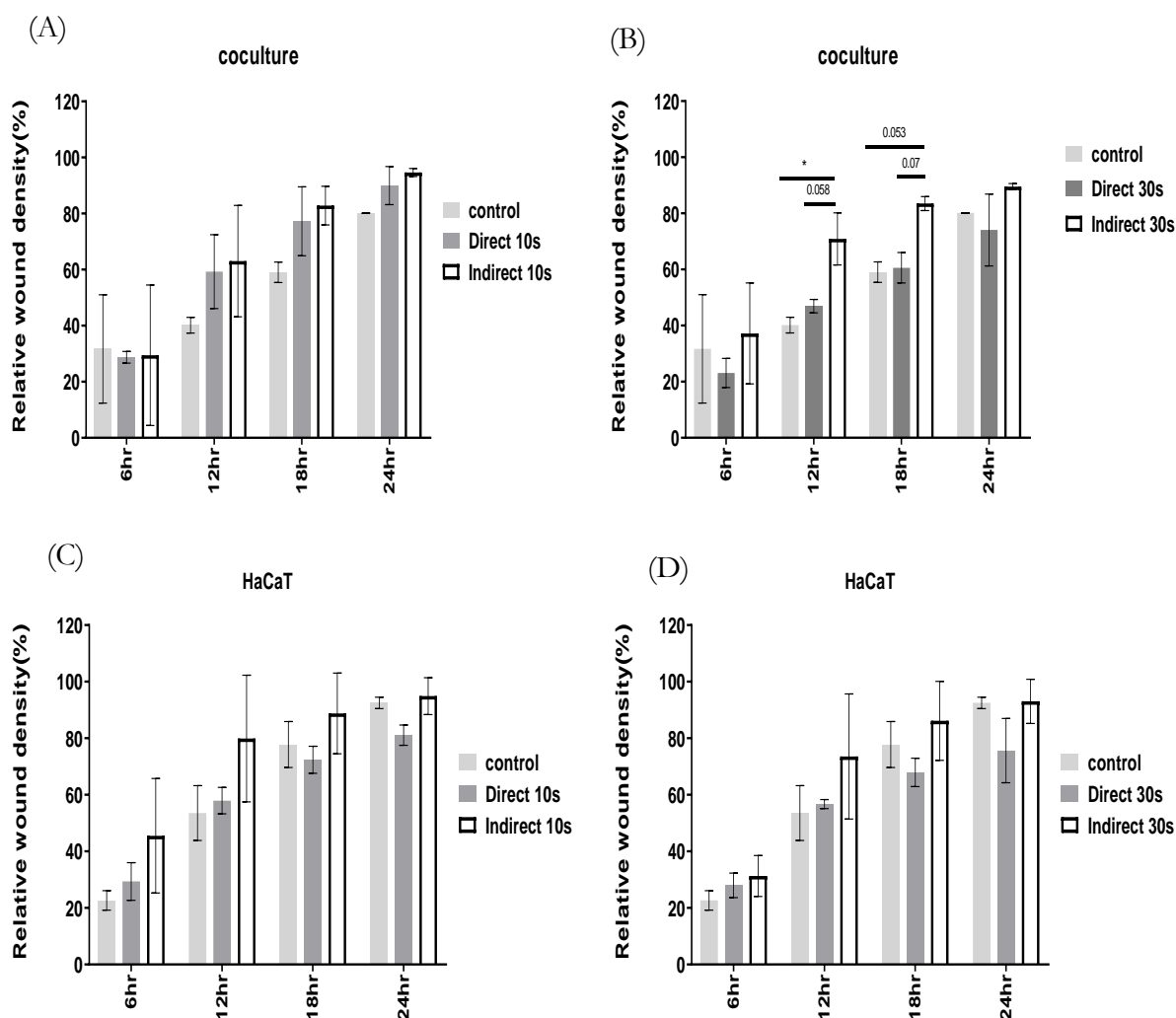
Figure 4.13 Comparison of direct and indirect CAP treatment in HaCaT cells and coculture. (A) and (B) depicts the comparison of relative wound density between direct and indirect CAP treatment in coculture at 6, 12, 18 and 24 h. (C) and (D) details the comparison of relative wound density between direct and indirect CAP treatment in HaCaT cells at 6, 12, 18 and 24 h. Dara are presented as mean ± SD from two independent experiments, each in triplicates. Statistical comparison is performed with two-way ANOVA.

4.5 CAP activates HIPPO signaling axis

We observed that cells in coculture closely mimics skin due to inclusion of both keratinocytes and fibroblasts and exhibited an improved CAP stimulation effect compared to those observed in monocultures, indicating a crosstalk between plasma treated cell types. To more thoroughly assess the paracrine signaling between the two cell types, we examined the signaling pathways involved in tissue homeostasis and regeneration. Emerging evidence suggests the activation of HIPPO signaling pathway in response to mechanicals stress, cellular stress and oxidative stress [104]. Hence, we were interested to investigate this signaling axis in response to CAP treatment in HaCaT cells and GM Fbs, as it plays an important role in cell growth, proliferation, and tissue homeostasis and is under redox control. [104]

4.5.1 CAP activates YAP-CTGF-Cyr61 signaling pathway

HaCaT and GM Fbs were incubated with untreated or 10 and 30s CAP treated medium (indirect treatment) for 3, 6, 18 and 24 hours. Quantitative PCR analysis showed that (figure 4.14), compared to early time point (3 hours), 30s CAP treatment could lead to a two-fold upregulation of YAP mRNA expression after 6 hours in GM Fbs. CTGF and Cyr61, downstream of YAP was also upregulated upon CAP treatment. In fact, 30s CAP treatment led to an about four-fold upregulation in CTGF mRNA expression at around 18 hours, which declined to near baseline by 24 hours. Cyr61 gene expression was also significantly induced starting after 6 hours, which peaked to three-fold upregulation in 18 hours and then declined to baseline by 24 hours.
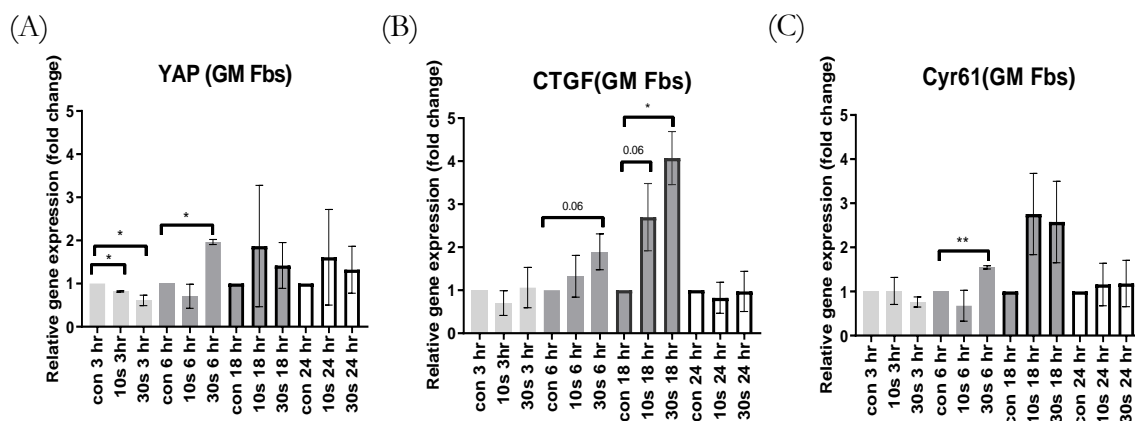
Figure 4.14 mRNA expression of HIPPO signaling effectors in GM Fbs after CAP treatment. Gene expression of YAP (A), CTGF (B) and Cyr61 (C) in GM Fbs measured 3, 6, 18, and 24 h after CAP treatment by qPCR and normalized to relative gene expression ($\Delta\Delta$Ct values on a log 2 scale). The x-axis represents CAP treatment time and incubation time after plasma treatment. Data are represented as mean ± SD of four independent experiments. Statistical analysis was performed using unpaired t-test with Welch's correction for multiple comparisons, along with normalization to the untreated control.

Figure 4.15 depicts the gene expression of YAP, CTGF and Cyr61 in HaCaT cells. In contrast to GM Fbs, a significant upregulation of YAP mRNA expression in HaCaT cells was not observed at early hours. However, both 10 and 30s CAP treatment tends to upregulate YAP gene expression after 24 hours. In case of CTGF, minimal upregulation (~1.4 -fold) was observed at 3 and 18 hours. Cyr61 gene expression was also minimally induced at 3 hours (about 1.5-fold) in HaCaT cells
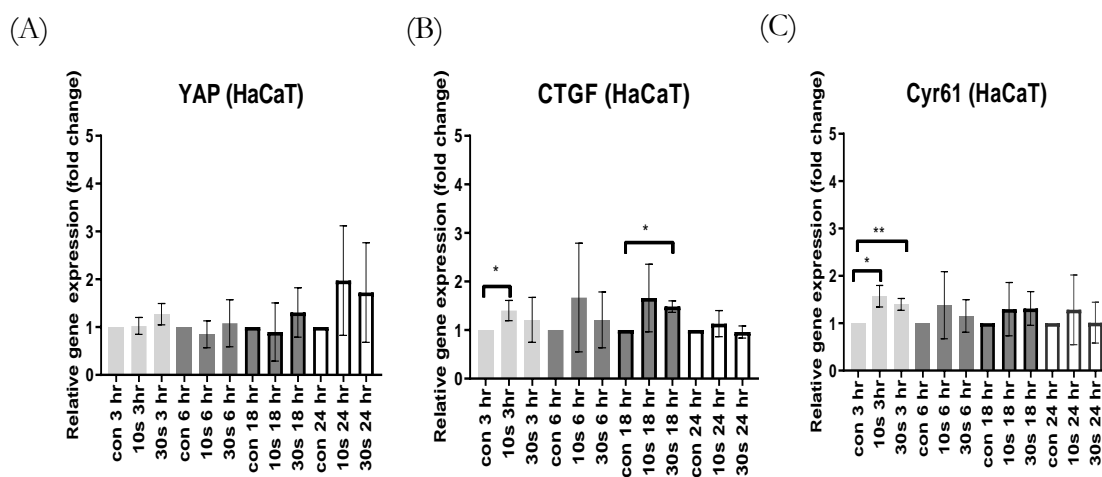
(A)   (B)   (C)

Figure 4.15 mRNA expression of HIPPO signaling effectors in HaCaT cells. Gene expression of YAP (A), CTGF (B) and Cyr61 (C) in HaCaT cells measured 3, 6, 18, and 24 h after CAP treatment by qPCR and normalized to relative gene expression ($\Delta\Delta$Ct values on a log 2 scale). The x-axis represents CAP treatment time and incubation time after plasma treatment. Data are represented as mean $\pm$ SD of three independent experiments. Statistical analysis was performed using unpaired t-test with Welch's correction for multiple comparisons, along with normalization to the untreated control.

The protein expression level of these signaling molecules were also checked after 3, 6 and 24 hours of plasma treatment (figure 4.16, 4.17). As mentioned before, unphosphorylated YAP moves to the nucleus, binds to TEAD transcription cofactors and transcribes the downstream genes namely CTGF and Cyr61. Therefore, the phosphorylation status of YAP was checked in both GM Fbs and HaCaT cells. Under serum starved conditions, as shown in figure 4.16, the ratio of phosphorylated YAP compared to total YAP was not significantly altered in GM Fbs. However, unlike the fibroblasts, there was a tendency of increased expression of phosphorylated YAP in HaCaT cells.
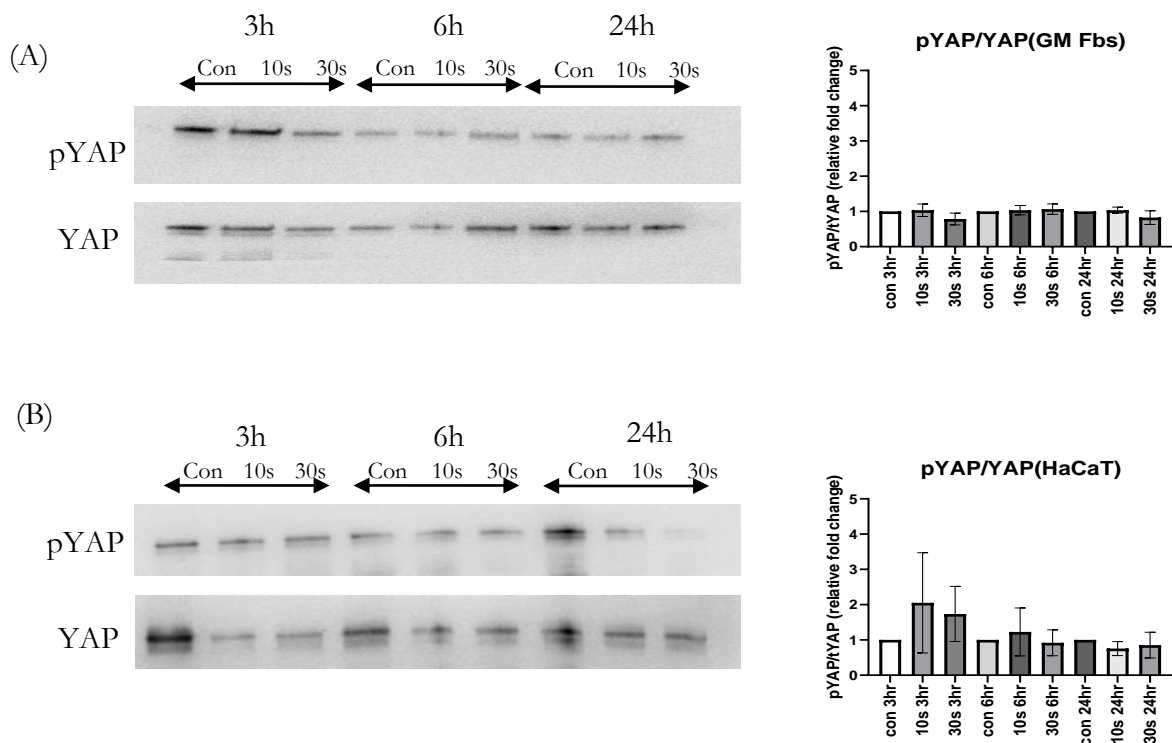
Figure 4.16 Effect of CAP on YAP protein expression. The relative phosphorylation level of YAP is shown in GM Fbs (A) and HaCaT cells (B). Quantification is performed from three independent blots. Representative blots are shown. The x-axis represents CAP treatment time and incubation time after plasma treatment. Data are represented as mean ± SD of at least three independent experiments. Statistical analysis was performed using unpaired t-test with Welch's correction for multiple comparisons, along with normalization to the untreated control.

Next, we checked the CTGF and Cyr61 protein expression in both the cell lines. In GM Fbs, we observed an increase in total cellular CTGF (~ 2-fold) in 3 hours and in total cellular Cyr61 (~3-fold) after 3 hours and (~2-fold) after 6 hours. In contrast to GM Fbs, HaCaT cells did not show any detectable range of cellular Cyr61. CTGF protein expression was also minimally increased (~1.5-fold) in HaCaT cells.

(A)

Cyr61(GM Fbs)

(B)

CTGF(GM Fbs)

CTGF(HaCaT)

(C)
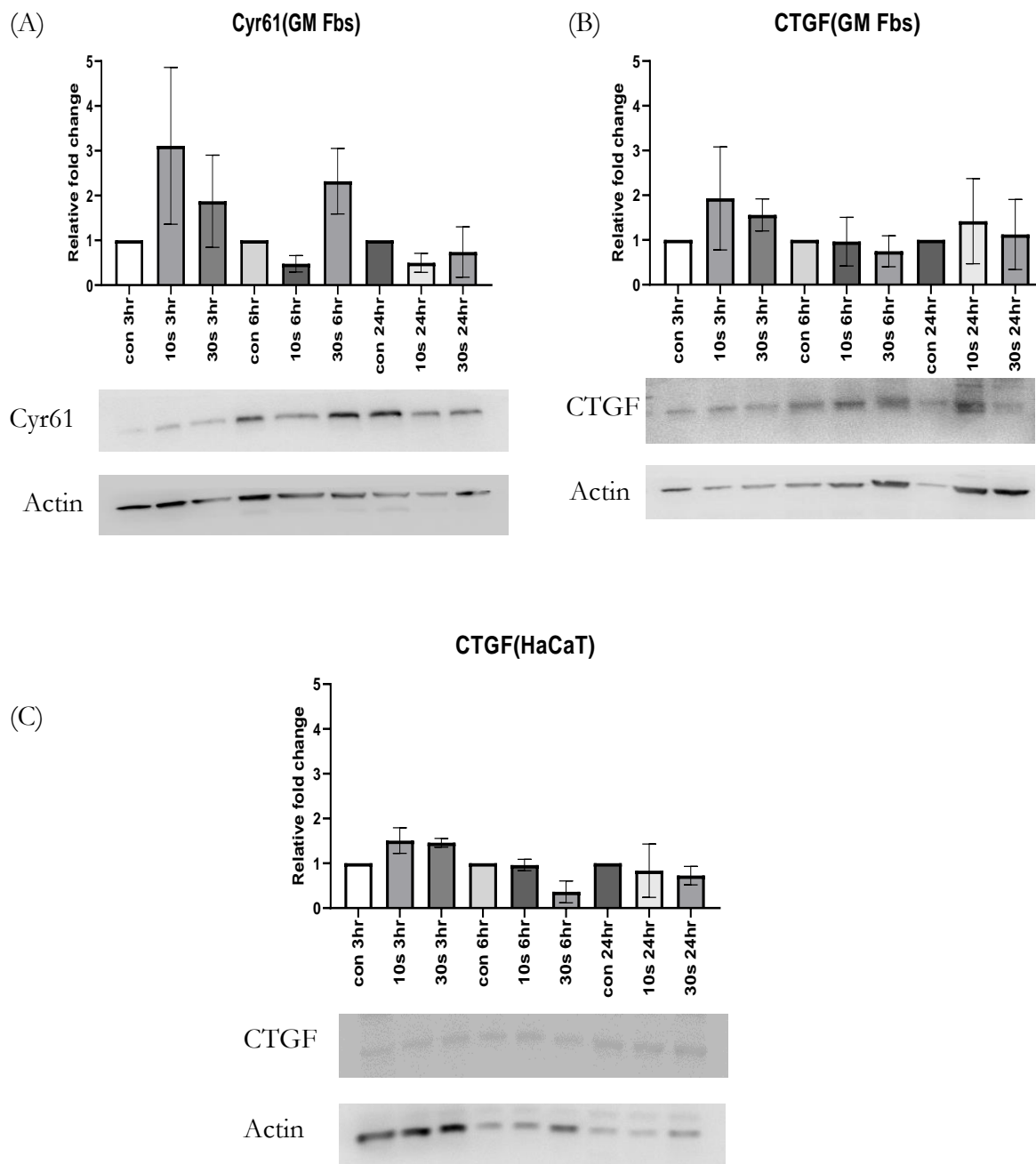
Figure 4.17 Effect of CAP on CTGF and Cyr61. CTGF and Cyr61 protein expression was enhanced after 10 and 30 s of CAP treatment in GM Fbs (A, B). CTGF expression slightly increased after 10 and 30 s of CAP treatments in HaCaT cells after approximately 3 h (C). Representative blots are shown. The *x*-axis represents CAP treatment time and incubation time after plasma treatment. Data are represented as mean ± SD of at least three independent experiments. Statistical analysis was performed using unpaired *t*-test with Welch's correction for multiple comparisons, along with normalization to the untreated control.

4.5.2 Effect of CAP on other signaling molecules in cross talk with YAP

HaCaT and GM Fbs were incubated with untreated, 10 and 30s CAP treated medium for 3, 6, 12, 18 and 24 hours. Apart from the major signaling axis, we also investigated the gene expression upon CAP treatment in functional mediators which are in cross talk with HIPPO signaling pathway (figure 4.18). We checked the gene expression of mTOR in both the cell lines. A significant upregulation of mTOR (~ 2-fold) was observed in GM Fbs after 12 hours and ~1.5-fold in HaCaT cells after 24 hours.

HIF-1α gene expression was also monitored upon CAP treatment. In GM Fbs, HIF-1α seemed to be upregulated (~1.8-2.6 fold) upon CAP treatment around 6 hours, but it was not significant. HaCaT cells, around 24 hours, also showed an upregulation of HIF-1α (~1.8-fold), but not significant. Both IGF-1 and IGF-2 gene expression was monitored in both the cell lines. CAP upregulated IGF-1 in GM Fbs around 24 hours to ~2.8-4 fold and ~2.2-fold in HaCaT cells. However, the differential expression of IGF-1 was not significant. IGF-2 upregulation was also not significant in both the cell lines.

Unlike the YAP-CTGF-Cyr61 axis, these molecules did not show a significant upregulation in their mRNA expression upon both the CAP treatments. Hence, for the following analysis of this signaling pathway, YAP, CTGF and Cyr61 were focused.

4. Results

(A)

(B)

(C)

(D)
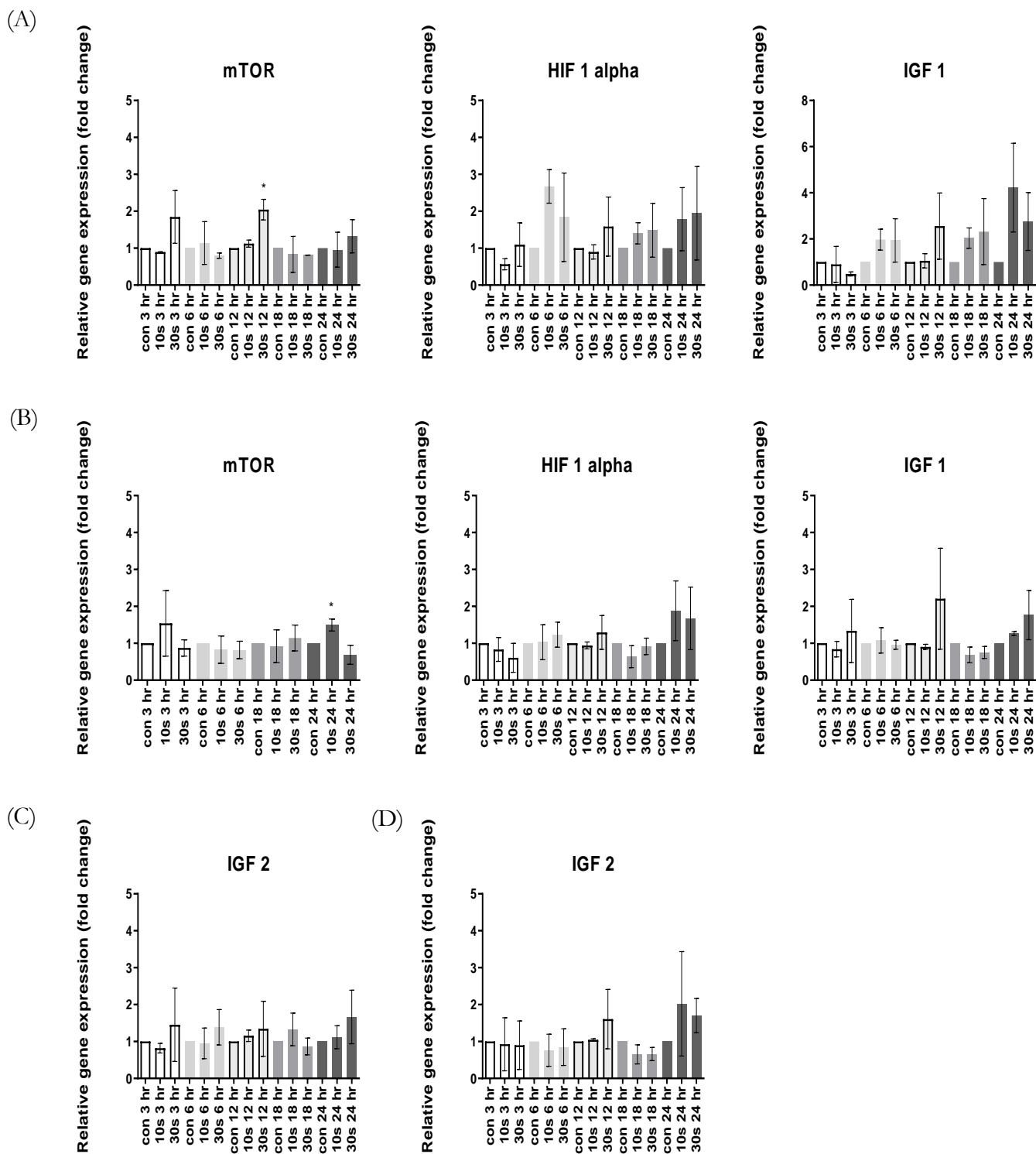
Figure 4.18 Gene expression of signaling molecules in crosstalk with YAP. Gene expression of signaling molecules in GM Fbs (A,C) and HaCaT cells (B,D) measured 3, 6, 12, 18, and 24 h after CAP treatment by qPCR and normalized to relative gene expression (ΔΔCt values on a log 2 scale). The x-axis represents CAP treatment time and incubation time after plasma treatment. Data are represented as mean ± SD of two independent experiments. Statistical analysis was performed using one-way ANOVA, along with normalization to the untreated control.

4.5.3 Effect of CAP on nuclear translocation of YAP

YAP lacks a canonical nuclear localization signal and its nuclear accumulation machinery is not well understood. The transcriptional activity is majorly dependent on nuclear YAP, thus through nucleocytoplasmic shuttling the HIPPO pathway controls its temporal activity. As we could see an upregulation of CTGF and Cyr61 gene and protein expression upon CAP treatment, we quantified the presence of total YAP in nucleus and cytoplasm after 3 hours of CAP treatment.

Immunofluorescence staining was applied to visualize the total YAP content in nucleus and cytoplasm in untreated and plasma treated HaCaT and GM Fbs. A positive nuclear staining of YAP was detected in both the cell lines in control and CAP treated samples. Nuclear and cytoplasmic YAP intensity was calculated by Image J. Upon quantification, in HaCaT cells (figure 4.19), no significant difference in the ratio of nucleus: cytoplasmic YAP was observed. In fact, in both control and plasma treated samples, nuclear staining of YAP was higher compared to cytoplasm and N/C ratio of YAP was around ~5. In GM Fbs, as observed in figure 4.20, like HaCaT cells, both control and CAP treated GM Fbs showed nuclear accumulation of YAP. But interestingly, compared to untreated GM Fbs, 10s showed a significant drop in nuclear YAP accumulation. The N/C YAP ratio in control was around ~6, compared to an N/C ratio of ~5.2 in plasma treated samples.
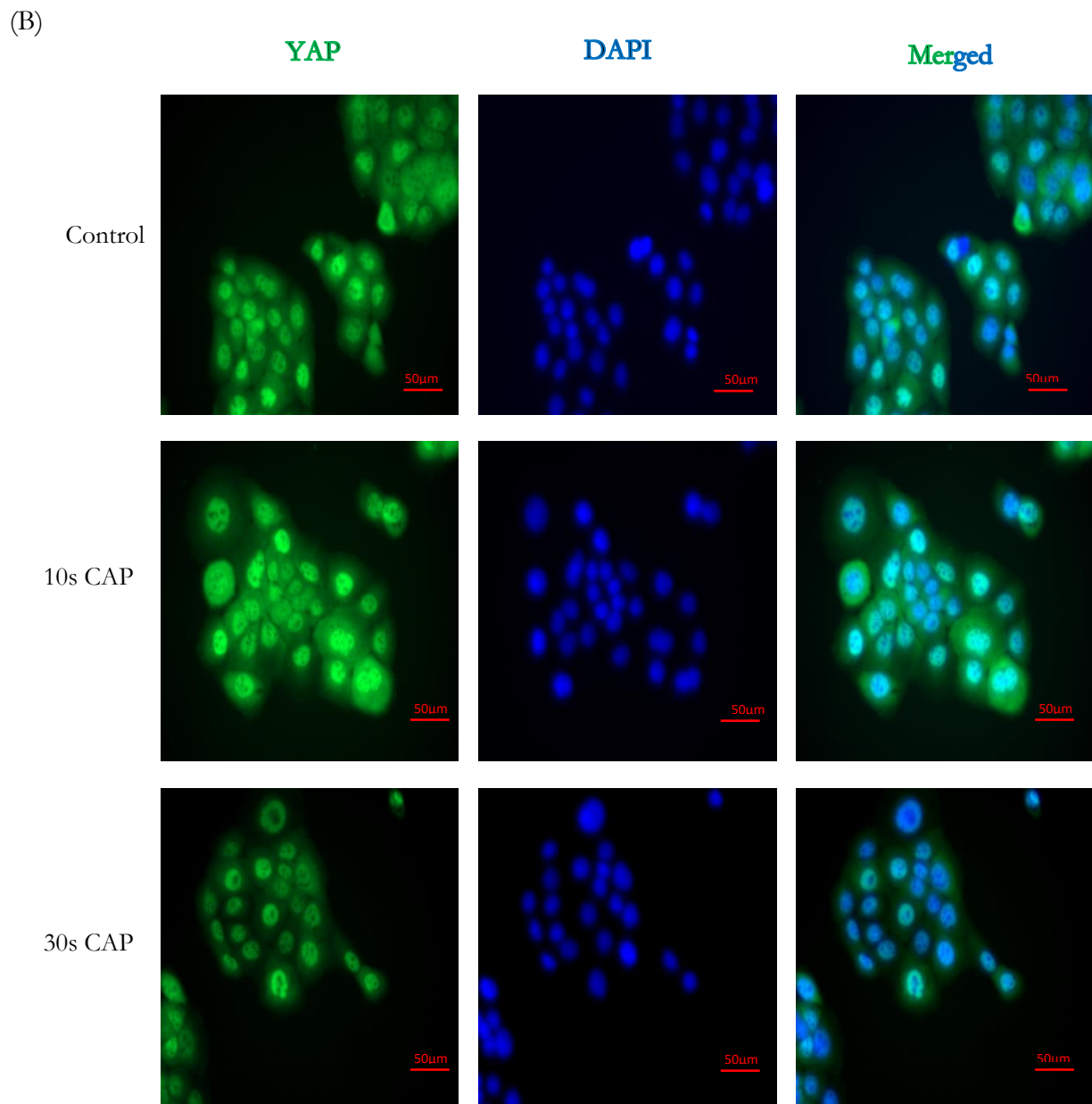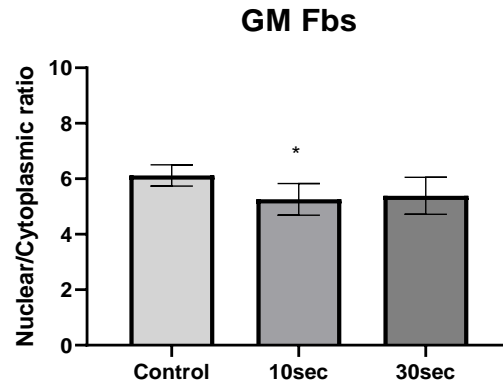
(A)

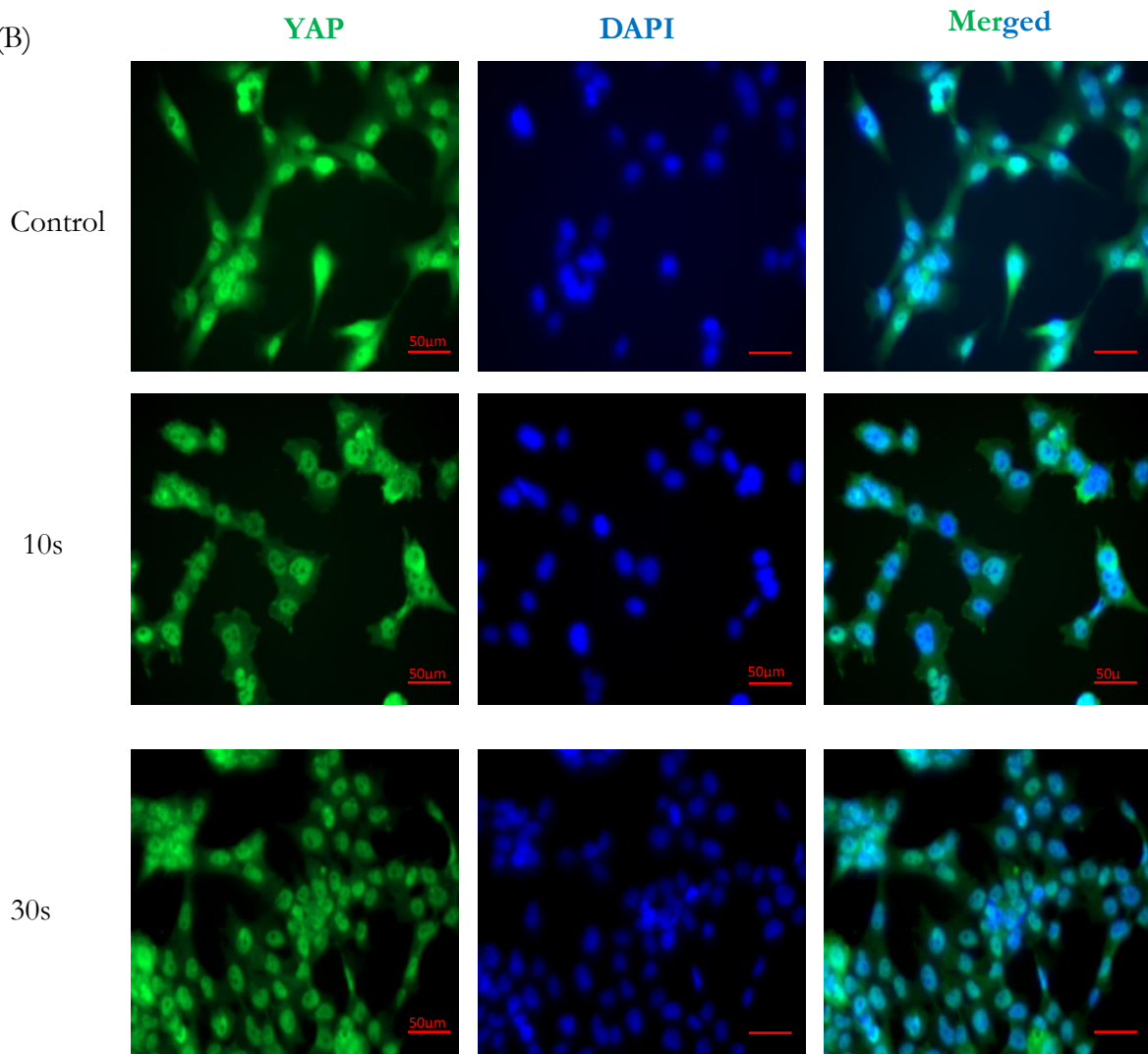

* Figure continued in the next page

(B)
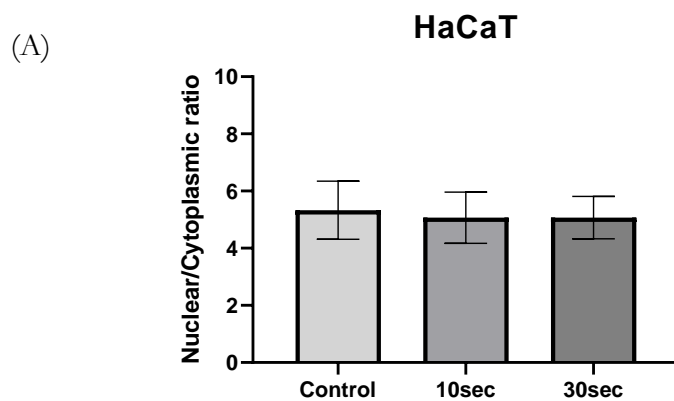
Figure 4.19 Cellular distribution of YAP in HaCaT cells. HaCaT cells were incubated with untreated and CAP treated RPMI for 3 h. (A) Details the quantification of Nuclear YAP: Cytoplasmic YAP in HaCaT cells. Representative images of untreated and CAP treated HaCaT cells are showed in (B). Immunofluorescence detection was performed with the primary anti total YAP (mouse mAB, 1:500). Nucleus was stained with DAPI. Data are presented as mean ± SD from two independent experiments, each in duplicates. At least 4 images were taken from each of the duplicates. Statistical analysis was performed with one-way ANOVA.

4. Results

(A)

(B)

Figure 4.20 Cellular distribution of YAP in GM Fbs. GM Fbs were incubated with untreated and CAP treated RPMI for 3 h. (A) Details the quantification of Nuclear YAP: Cytoplasmic YAP in GM Fbs. Representative Images of untreated and CAP treated fibroblasts are showed in (B). Immunofluorescence detection was performed with the primary anti total YAP (mouse mAB, 1:500). Nucleus was stained with DAPI. Data are presented as mean ± SD from two independent experiments, each in duplicates. At least 4 images were taken from each of the duplicates. Statistical analysis was performed with one-way ANOVA.

4.5.3 Effect of NAC on YAP-CTGF-Cyr61 signaling cascade

We have previously observed CAP mediated upregulation of HIPPO signaling cascade in GM Fbs. To exclusively conclude the role of stable CAP derived oxidants in YAP-CTGF-Cyr61 signaling cascade activation, 2.5mM NAC was incubated for 18 hours with untreated and CAP treated medium before RNA was isolated from the cells. As observed in figure 4.21, NAC alone did not have any significant impact on these HIPPO molecules in HaCaT cells. NAC in combination with 10 and 30 s CAP-treated media significantly reduced the expression of CTGF (~2.4-fold) and Cyr61 (~1.9-fold) in GM Fbs. YAP expression was slightly but not significantly reduced in GM Fbs.

Similar results were obtained in HaCaT cells that revealed that YAP expression remained unaltered upon treatment with NAC alone or in combination with plasma. CTGF expression was also reduced upon NAC treatment in HaCaT cells (but no significance). Cyr61 mRNA expression in HaCaT cells were significantly reduced upon NAC treatment in combination with both 10 and 30s CAP treatment. This study further signifies that, stable ROS produced from CAP significantly activates the YAP-CTGF-Cyr61 axis. In presence of ROS quencher NAC, this CAP mediated signaling cascade is terminated.
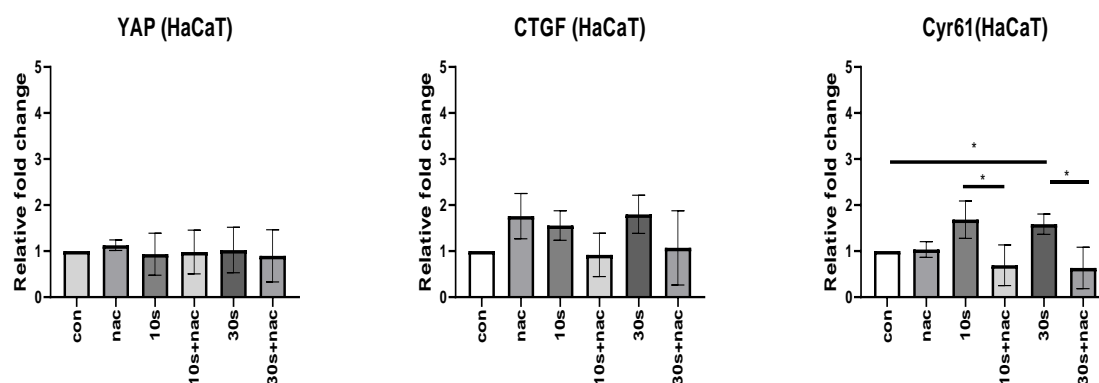
(A)
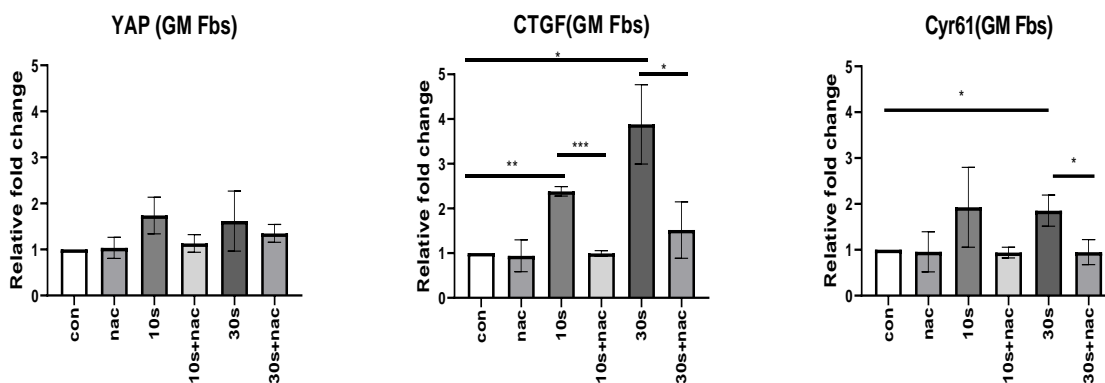
(B)

Figure 4.21 Effect of NAC on the YAP-CTGF-Cyr61 signaling cascade. Gene expression of YAP, CTGF, and Cyr61 in GM Fbs (A) and HaCaT cells (B) measured 18 h after CAP treatment by qPCR and normalized to relative gene expression ($\Delta\Delta$Ct values on a log 2 scale). Data are presented as mean $\pm$ SD from at least three independent experiments, and statistical analysis was performed using unpaired t-test with Welch's correction.

4.5.4 CAP Promotes Migration in coculture through Secreted CTGF and Cyr61

In our coculture migration experiments (figure 4.8), we observed significantly higher acceleration in cell migration compared to HaCaT cells alone upon CAP treatment. Therefore, we hypothesized that CAP not only influences the keratinocytes and fibroblasts alone, but also regulates their interaction in a coculture. We assumed that the major signaling molecules activating this paracrine signaling are CTGF and Cyr61.

Therefore, we first analyzed the GM Fb conditioned medium (collected 18 hours after CAP treatment) by ELISA and we observed an increase in secreted CTGF and Cyr61 upon CAP treatment (figure 4.22). Next, we performed a cell migration assay with recombinant CTGF and Cyr61. HaCaT monoculture was treated with 10 and 50 ng/ml of recombinant CTGF and 100 ng and 1μg/ml of Cyr61 (Peprotech GmbH). Treatment with both 10 and 50 ng/ml CTGF significantly accelerated cell migration (figure 4.23 a-b). Treatment with either 100 ng/ml or 1 μg/ml Cyr61 also accelerated cell migration at early time point (figure 4.23 c-d).

(A)

(B)
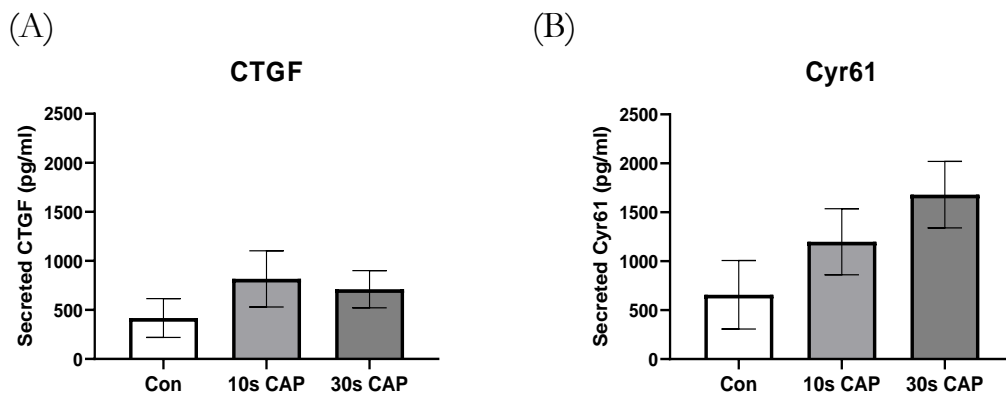
Figure 4.22 CAP enhances secreted CTGF and Cyr61 expression from GM Fbs. Secreted CTGF (A) and Cyr61 (B) (pg/ml) was analyzed by ELISA. Data are presented as mean ± SD from two independent experiments, and statistical analysis was performed using one-way ANOVA.
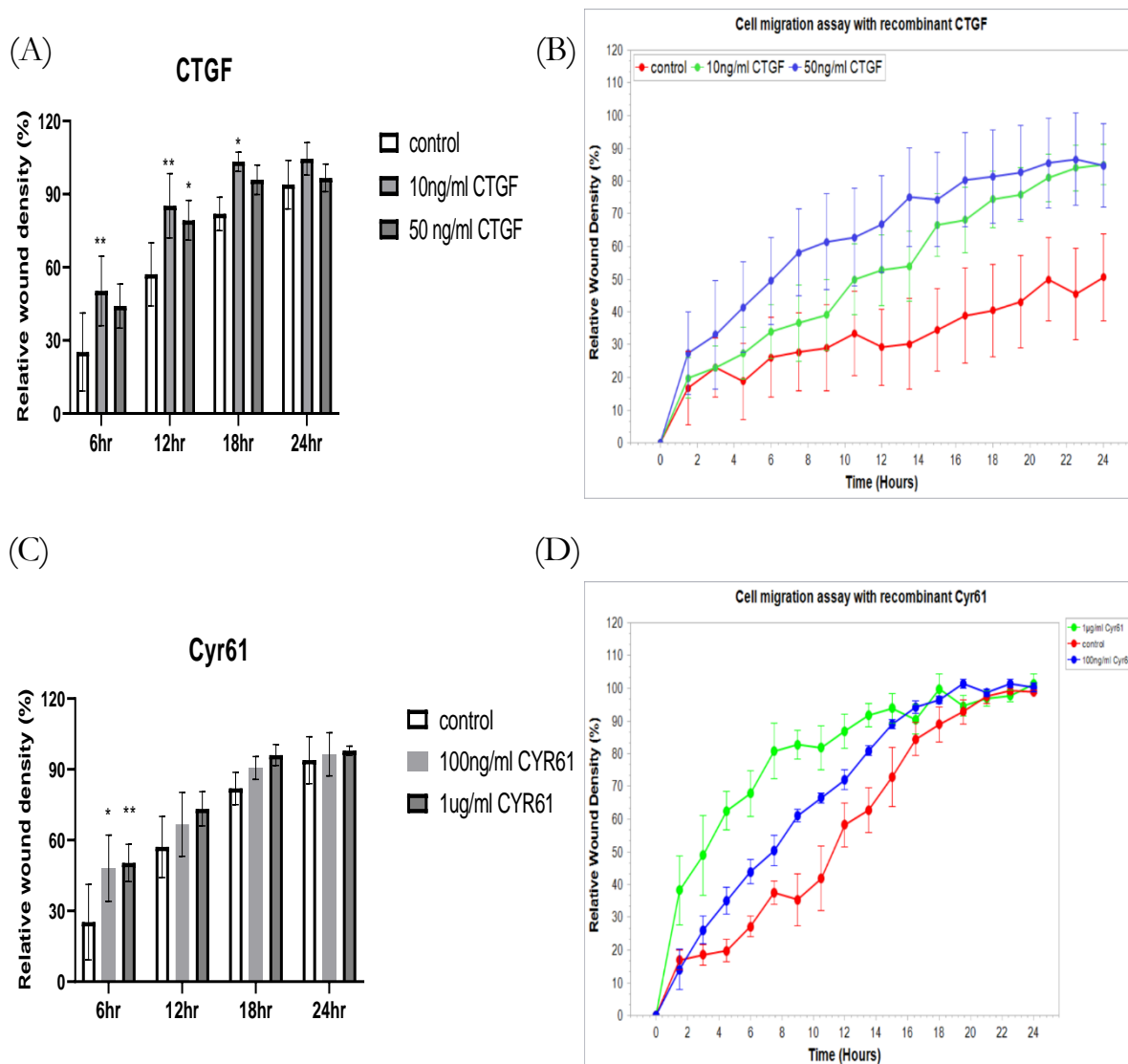
Figure 4.23 Cell migration of HaCaT monoculture in presence of recombinant CTGF and Cyr61. Relative wound density in HaCaT cells was monitored after treatment with 10 and 50 ng/ml CTGF and 100 ng/ml and 1 μg/ml Cyr61. (A) Details the summation of relative wound density upon treatment with recombinant 10 and 50 ng/ml CTGF. (B) Details of a representative time course analysis of CTGF mediated wound healing in HaCaT cells. (C) Depicts the summation of relative wound density upon treatment with recombinant 100 ng/ml and 1μg/ml Cyr61. (B) Details a representative time course analysis of Cyr61 mediated wound healing in HaCaT cells. Data are presented as mean ± SD from three independent experiments, and statistical analysis was performed using two-way ANOVA.

As we observed that recombinant CTGF and Cyr61 have the potential to stimulate cell migration of HaCaT monoculture, we assumed that the secreted CTGF and Cyr61 in GM Fbs CM would accelerate HaCaT wound healing. Therefore, we performed a cell migration assay to determine the migratory behavior of HaCaT cells grown in media conditioned from untreated or CAP-treated GM Fbs (figure 4.24). As expected, conditioned medium harvested from 10 and 30s CAP-treated GM Fbs at 18 hours significantly accelerated

4. Results

HaCaT cell migration compared to conditioned medium from untreated GM Fbs and normal medium (control).
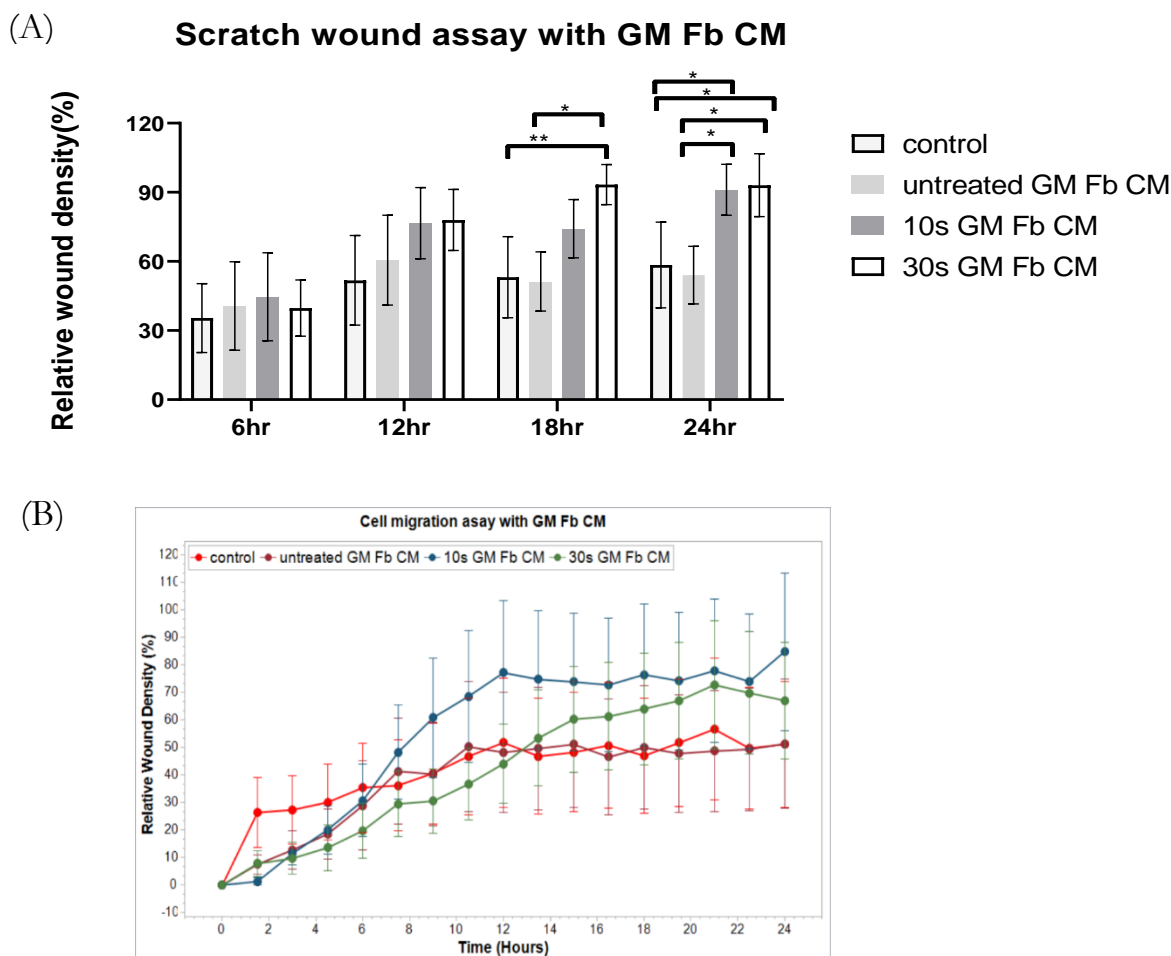
(A)

(B)

Figure 4.24 Effect of CAP on paracrine signaling between keratinocytes and fibroblasts. HaCaT cells were incubated with conditioned media harvested from untreated or 10 and 30 s CAP-treated GM Fbs. (A) Details the summation of relative wound density of HaCaT cells upon treatment with untreated and CAP treated GM Fb CM. (B) Details a representative time course analysis of the same. Data are presented as mean ± SD from three independent experiments, and statistical analysis was performed using two-way ANOVA.

4.6 Influence of CAP on regenerative signaling molecules

Our study validated the activation of a regenerative signaling axis in dermal cells and thus indicated the activation of a paracrine signaling pathway upon CAP treatment. We already observed the activation of YAP-CTGF-Cyr61 axis in GM Fbs, which in turn stimulates a reciprocal communication with HaCaT cells resulting in improved wound healing of keratinocytes, cocultured with the fibroblasts. To gain further insights on the regenerative

signaling in GM Fbs, RT^2 PCR profiler array was performed 6 hours after 30 and 60s of CAP treatment. 84 genes from HIPPO signaling axis and 84 genes from extracellular matrix and adhesion molecules were investigated through the array.

4.6.1 CAP activates HIPPO signaling molecules in GM Fbs

GM Fbs were treated with untreated, 30s and 60s of CAP treatment after making scratches to figure out the differential gene expression upon CAP treatment in a wound healing set up. 84 genes of HIPPO signaling pathway was analyzed by RT^2 PCR array. These genes belong to different subgroups of biological process including metabolic process, biological adhesion, cellular component organization, biological regulation, signaling etc. The PANTHER classification of these genes according to biological process are listed in figure 4.25.
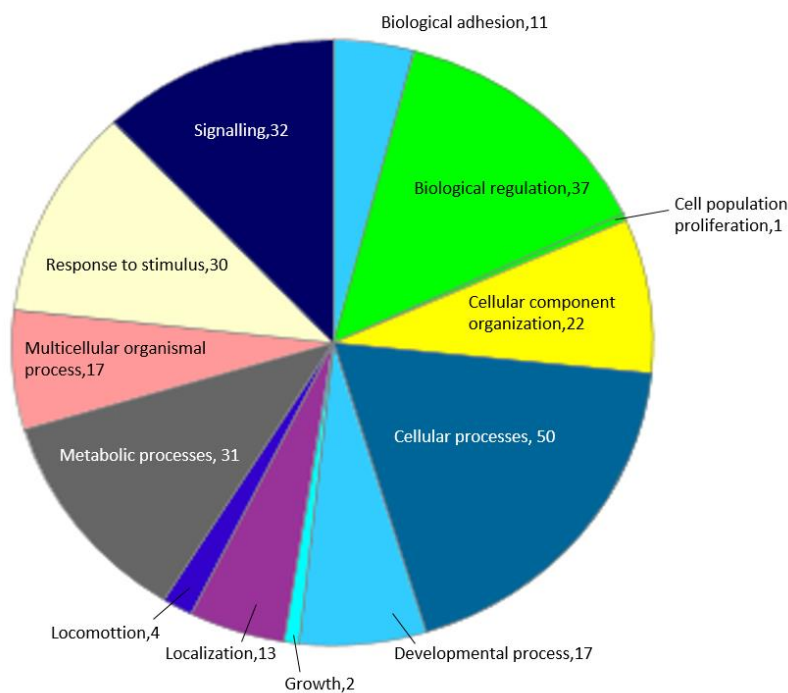
Figure 4.25 PANTHER biological process classification of HIPPO genes analyzed by RT^2 PCR array

Table 4.1 lists the 59 genes upregulated after plasma treatment.

4. Results

Table 4.1 List of HIPPO signaling molecules which showed a significantly changed gene expression after CAP treatment compared to untreated control. >2 fold change was termed as upregulation. <-2 fold was termed as down regulation.

Short gene name	Gene name	Treatment time	Fold regulation	p value
ACTG1	Actin, gamma 1	60s	2.19	0.517911
AMOT	Angiomotin	60s	2.19	0.598629
AMOTL1	Angiomotin like 1	60s	4.16	0.105547
AMOTL2	Angiomotin like 2	60s	3.90	0.090454
CASP3	Caspase 3	60s	3.37	0.061797
CCNE1	Cyclin E1	60s	3.13	0.067478
CCNE2	Cyclin E2	60s	2.83	0.048263
DCHS1	Dachsous 1 (Drosophila)	60s	13.01	0.339051
		30s	3.93	0.435280
DCHS2	Dachsous 2 (Drosophila)	60s	3.80	0.181995
DIAPH2	Diaphanous homolog 2	60s	2.01	0.229300
DLG1	Discs, large homolog 1	60s	2.17	0.279271
DVL2	Dishevelled, dsh homolog 2	60s	2.61	0.112809
FAT1	FAT tumor suppressor homolog 1	60s	3.39	0.047915
FAT2	FAT tumor suppressor homolog 2	60s	3.84	0.201613
		30s	2.03	0.752296
FAT3	FAT tumor suppressor homolog 3	60s	4.80	0.067670
FAT4	FAT tumor suppressor homolog 4)	60s	2.31	0.288413
FJX1	Four jointed box 1 (Drosophila)	60s	5.95	0.085925
		30s	2.02	0.860189
GPC5	Glypican 5	60s	2.04	0.383451
HIPK2	Homeodomain interacting protein kinase 2	60s	3.80	0.112353
LATS1	Large tumor suppressor, homolog 1	60s	4.76	0.030073
LATS2	Large tumor suppressor, homolog 2	60s	4.25	0.063708
LIMD1	LIM domains containing 1	60s	2.84	0.292172
LIX1L	Lix1 homolog (mouse)-like	60s	2.78	0.315281

* Table continued in the next page

4. Results

| LLGL1	Lethal giant larvae homolog 1	60s	2.72	0.251759
LLGL2	Lethal giant larvae homolog 2	60s	2.45	0.220092
LPP	LIM domain containing preferred translocation partner in lipoma	60s	3.13	0.065169
MOB1B	MOB1, Mps One Binder kinase activator-like 1A (yeast)	60s	3.88	0.137801
MOB1A	MOB1, Mps One Binder kinase activator-like 1B (yeast)	60s	3.05	0.100418
MPP5	Membrane protein, palmitoylated 5	60s	3.10	0.125213
NF2	Neurofibromin 2 (merlin)	60s	4.03	0.031044
POTEF	POTE ankyrin domain family, member F	60s	2.28	0.108282
PPP2CB	Protein phosphatase 2, catalytic subunit, beta isozyme	60s	2.43	0.090477
PPP2R1A	Protein phosphatase 2, regulatory subunit A, alpha	60s	2.06	0.282850
PPP2R2D	Protein phosphatase 2, regulatory subunit B, delta	60s	4.66	0.053238
PRKCI	Protein kinase C, iota	60s	2.85	0.206932
PRKCZ	Protein kinase C, zeta	60s	2.17	0.323039
PTPN14	Protein tyrosine phosphatase, non-receptor type 14	60s	2.44	0.474564
RASSF2	Ras association (RalGDS/AF-6) domain family member 2	60s	2.29	0.216716
SCRIB	Scribbled homolog (Drosophila)	60s	4.79	0.083976
SMAD1	SMAD family member 1	60s	2.74	0.163789
STK3	Serine/threonine kinase 3	60s	2.73	0.370386
STK4	Serine/threonine kinase 4	60s	3.89	0.173296
TAOK1	TAO kinase 1	60s	2.48	0.147607
TAOK2	TAO kinase 2	60s	3.67	0.128899
TEAD1	TEA domain family member 1	60s	3.06	0.125905
TEAD2	TEA domain family member 2	60s	2.22	0.198271
TEAD3	TEA domain family member 3	60s	2.14	0.144745

* Table continued in the next page

TEAD4	TEA domain family member 4	60s	2.17	0.063983
TJP1	Tight junction protein 1	60s	3.15	0.106808
TJP2	Tight junction protein 2	60s	2.77	0.112749
TSHZ3	Teashirt zinc finger homeobox 3	60s	2.31	0.191378
WNT1	Wingless-type MMTV integration site family, member 1	60s	2.53	0.192024
WTIP	Wilms tumor 1 interacting protein	60s	3.85	0.058564
WWC1	WW and C2 domain containing 1	60s	3.78	0.051908
WWTR1	WW domain containing transcription regulator 1	60s	3.19	0.195357
YAP1	Yes-associated protein 1	60s	4.35	0.077360
YWHAE	Tyrosine 3-monooxygenase/tryptophan 5-monooxygenase activation protein, epsilon polypeptide	60s	2.83	0.148402
YWHAZ	Tyrosine 3 monooxygenase/tryptophan 5-monooxygenase activation protein, zeta polypeptide	60s	2.67	0.183889
ZDHHC18	Zinc finger, DHHC-type containing 18	60s	4.14	0.147844

30s CAP treatment resulted in upregulation of 3 genes and 60s treatment could upregulate 59 genes compared to untreated control, 6 hours after treatment. As shown in table 4.1, both 30s and 60s CAP treatment induced FAT2 gene, transcribing cadherin family protein to 2.03-fold and 3.84-fold respectively. Another cadherin member gene transcribing DCHS1 was also upregulated by both 30 and 60s to 3.93 and 13.01-fold respectively, 6 hours after treatment. Cyclin family member genes Cyclin E1 and Cyclin E2 were also significantly upregulated by 60s of CAP treatment. LATS1 and LATS2 genes transcribing STK protein kinases, directly upstream of YAP transcription factor was also significantly upregulated > 4-fold within 6 hours of 60s treatment. Another cell adhesion and cell motility gene transcribing LIM1 was also significantly upregulated by CAP treatment. NF2, another gene involved in cytoskeletal dynamics was also upregulated >4-fold by 60s CAP treatment. Protein phosphatase family member genes PPP2CB, PPP2R1A and PPP2R1D were also upregulated (>2-fold) by 60s treatment. All the TEAD family member genes (1, 2, 3 and 4) were upregulated (>2-fold) within 6 hours of CAP treatment. Another transcriptional corepressor WTIP1 and transcriptional coactivator WWC1 were also significantly

4. Results

upregulated to more than 3-fold by 60s CAP treatment. YAP as previously shown before, was also upregulated >4-fold by 60s CAP treatment after 6 hours. Gene ontology analysis was carried out by DAVID. As demonstrated in figure 4.26, the functional annotation of genes showing significant enrichment ($p<0.05$) compared to control were classified according to biological process, molecular function and cellular components.

(A)

GOTERM_MF_FAT (Gene ontology)
Top 5 terms of DAVID functional annotation chart
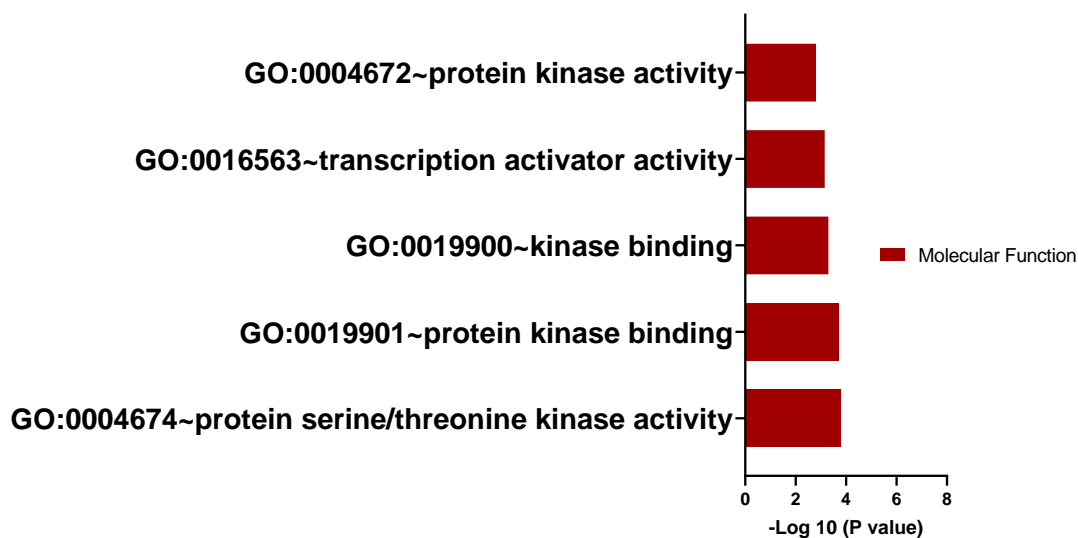
(B)

GOTERM_CC_FAT (Gene ontology)
Top 5 terms of DAVID functional annotation chart

* Figure continued in the next page

(C)

GOTERM_BP_FAT
(Gene ontology)
Top 5 terms of DAVID functional
annotation chart
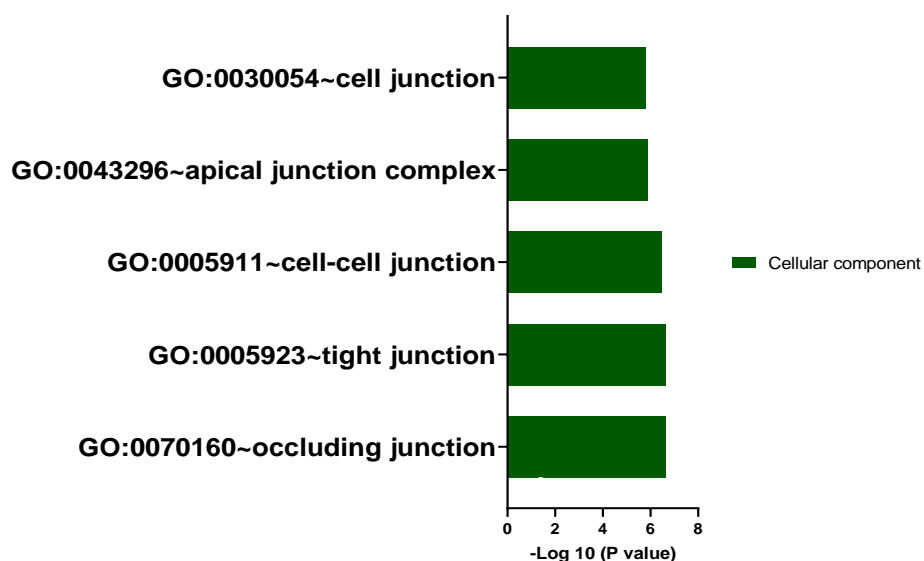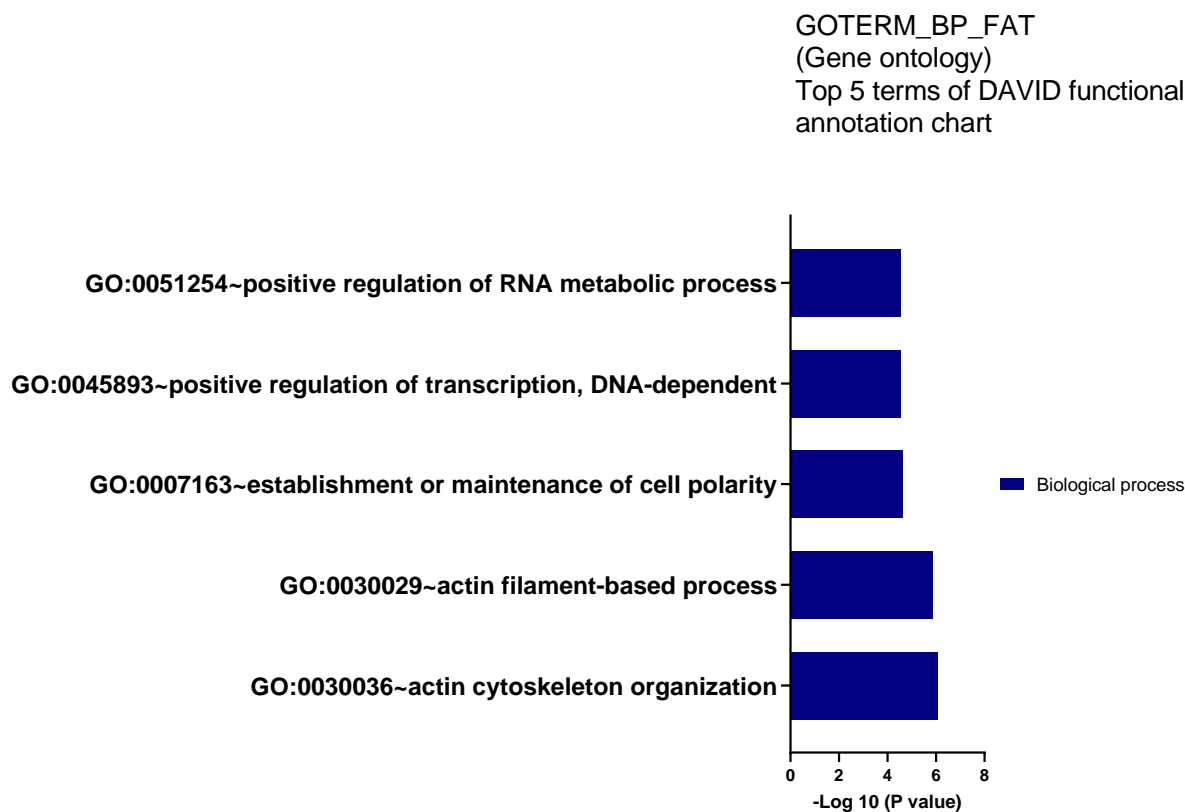
Figure 4.26 Gene ontology analysis of significantly upregulated genes of HIPPO signaling pathway. (A) Defines the MF classification, (B) defines the CC classification and (C) defines the BP classification. Top 5 terms of all the category have been provided here.

4.6.2 CAP activates Extracellular matrix (ECM) and adhesion molecules

GM Fbs were treated with untreated, 30s and 60s of CAP-treated medium after making scratches to figure out the differential gene expression upon CAP treatment in a wound healing set up. 84 genes of ECM and adhesion pathway were analyzed by RT^2 PCR array. These genes belong to different subgroups of biological process including metabolic process, biological adhesion, cellular component organization, biological regulation, signaling etc. The PANTHER classification of these genes according to biological process are listed in figure 4.27.

4. Results
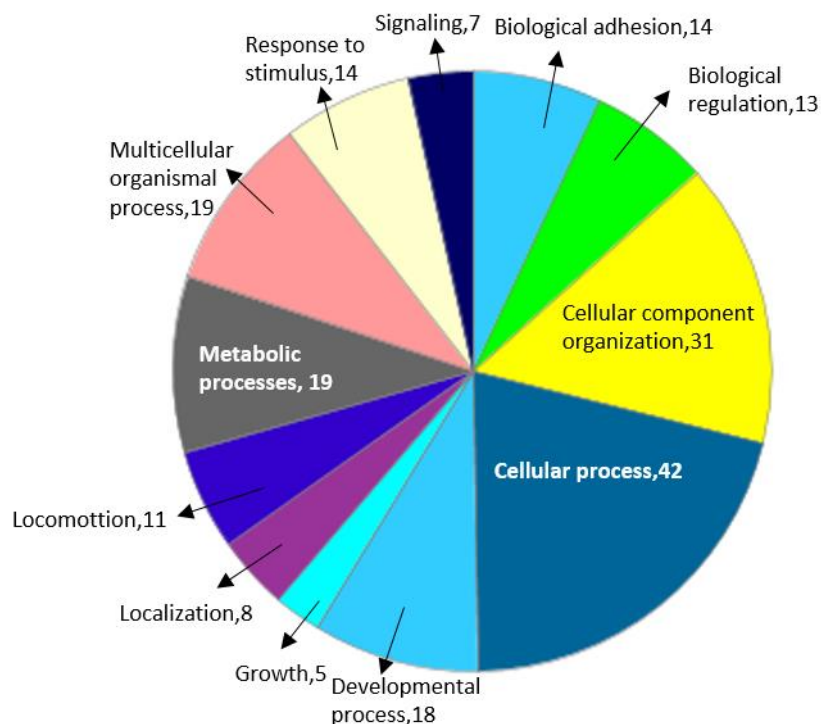
Figure 4.27 PANTHER Biological process classification of ECM and adhesion molecules, analyzed by RT^2 PCR array

Table 4.2 lists all the 34 differentially regulated genes upon plasma treatment

Table 4.2 List of Extracellular matrix and adhesion molecules, which showed a significantly changed gene expression upon CAP treatment compared to untreated control. >2 fold change was termed as upregulation. <-2 fold was termed as down regulation.

Short gene name	Gene name	Treatment time	Fold Regulation	p Value
ADAMTS1	ADAM metallopeptidase with thrombospondin type 1 motif, 1	60s	3.18	0.000657
ADAMTS13	ADAM metallopeptidase with thrombospondin type 1 motif, 13	60s	2.08	0.000381
CD44	CD44 molecule (Indian	60s	2.33	0.004781

* Table continued in the next page

4. Results

	blood group)			
CLEC3B	C-type lectin domain family 3, member B	60s	2.67	0.473928
COL12A1	Collagen, type XII, alpha 1	60s	2.06	0.007246
COL15A1	Collagen, type XV, alpha 1	60s	2.54	0.017258
COL4A2	Collagen, type IV, alpha 2	60s	2.53	0.000601
COL5A1	Collagen, type V, alpha 1	60s	2.10	0.020984
COL6A1	Collagen, type VI, alpha 1	60s	2.37	0.042276
COL6A2	Collagen, type VI, alpha 2	60s	2.93	0.005369
COL7A1	Collagen, type VII, alpha 1	60s	4.35	0.002748
COL8A1	Collagen, type VIII, alpha 1	60s	2.71	0.248261
CTNND2	Catenin (cadherin-associated protein), delta 2 (neural plakophilin-related arm-repeat protein)	60s	3.16	0.027769
ITGA3	Integrin, alpha 3 (antigen CD49C, alpha 3 subunit of VLA-3 receptor)	60s	2.19	0.098243
ITGB2	Integrin, beta 2 (complement component 3 receptor 3 and 4 subunit)	60s	2.03	0.017578
ITGB4	Integrin, beta 4	60s	2.44	0.006163
MMP13	Matrix metallopeptidase 13 (collagenase 3)	60s	2.10	0.000847
MMP14	Matrix metallopeptidase 14 (membrane-inserted)	60s	4.64	0.014415
MMP3	Matrix metallopeptidase 3 (stromelysin 1, progelatinase)	60s	3.20	0.010258
		30s	2.0	0.156489
THBS1	Thrombospondin 1	60s	2.95	0.000895
TIMP2	TIMP metallopeptidase inhibitor 2	60s	2.32	0.054272
VCA N	Versican	60s	3.84	0.050823
VTN	Vitronectin	60s	2.07	0.016908

* Table continued in the next page

76

ADAMTS8	ADAM metallopeptidase with thrombospondin type 1 motif, 8	60s	-4.88	0.290210
CDH1	Cadherin 1, type 1, E-cadherin (epithelial)	60s	-2.49	0.073696
ECM1	Extracellular matrix protein 1	60s	-3.31	0.000353
ITGAM	Integrin, alpha M (complement component 3 receptor 3 subunit)	60s	-2.43	0.338333
LAMB1	Laminin, beta 1	60s	-2.21	0.000980
MMP12	Matrix metallopeptidase 12 (macrophage elastase)	60s	-776.57	0.147875
MMP8	Matrix metallopeptidase 8 (neutrophil collagenase)	60s	-2.69	0.245800
PECAM1	Platelet/endothelial cell adhesion molecule	60s	-2.31	0.385806
VCAM1	Vascular cell adhesion molecule 1	60s	-2.47	0.195074

30s CAP treatment increased Matrix Metallo Proteinases 3 (MMP3) expression and 60s CAP treatment resulted in differential regulation of 34 genes. 60s CAP treatment significantly increased the expression of genes transcribing collagen moieties including COL12, COL15, COL4, COL5, COL6 and COL7. ADAMTS, a family of multidomain extracellular protease enzymes, showed differential regulation upon CAP treatment. ADAMTS 1 and 13 were significantly upregulated upon 60s CAP treatment in 6 hours, whereas ADAMTS8 was downregulated. Integrin family genes ITGB 2 and 4 were also significantly upregulated upon 60s CAP treatment. MMPs showed a differential regulation upon 60s CAP treatment. MMP 3 and 14 were significantly upregulated whereas MMP8 and MMP12 were downregulated. Several genes transcribing cell adhesion molecules like CDH1, VCAM1 and PECAM1 were also downregulated. Genes transcribing extracellular matrix proteins like ECM1 and LAMB1 were significantly downregulated upon CAP treatment. Gene ontology analysis was carried out by DAVID. The functional annotation of upregulated and downregulated genes compared to control were classified according to biological process, molecular function and cellular components (figure 4.28, 4.29).

4. Results

GOTERM_MF_FAT (Gene ontology)
Top 5 terms of DAVID functional annotation chart

(B)

GOTERM_CC_FAT (Gene ontology)
Top 5 terms of DAVID functional annotation chart
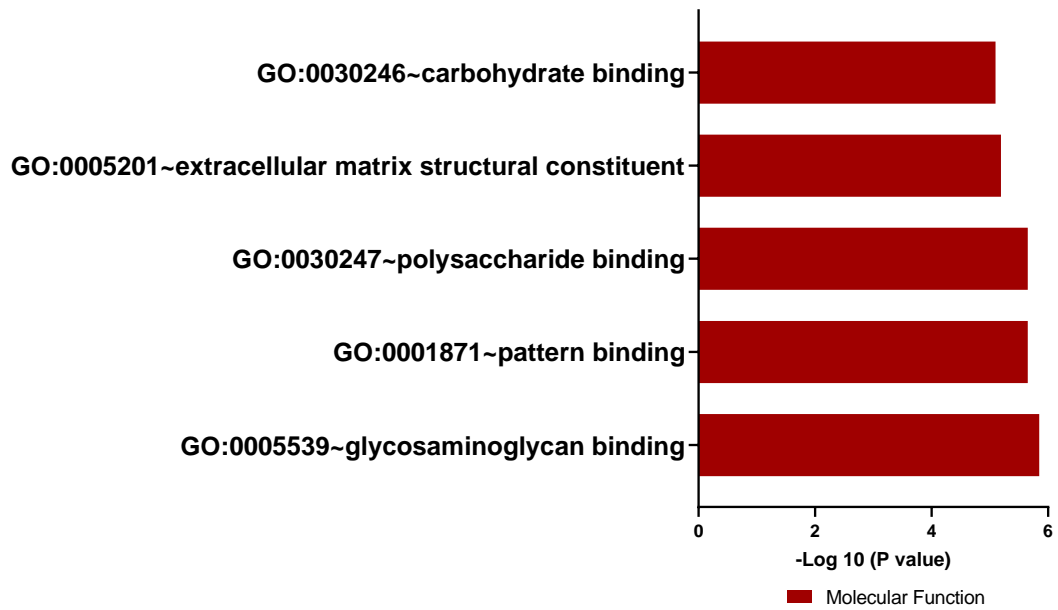
* Figure continued in the next page

4. Results

GOTERM_BP_FAT (Gene ontology)
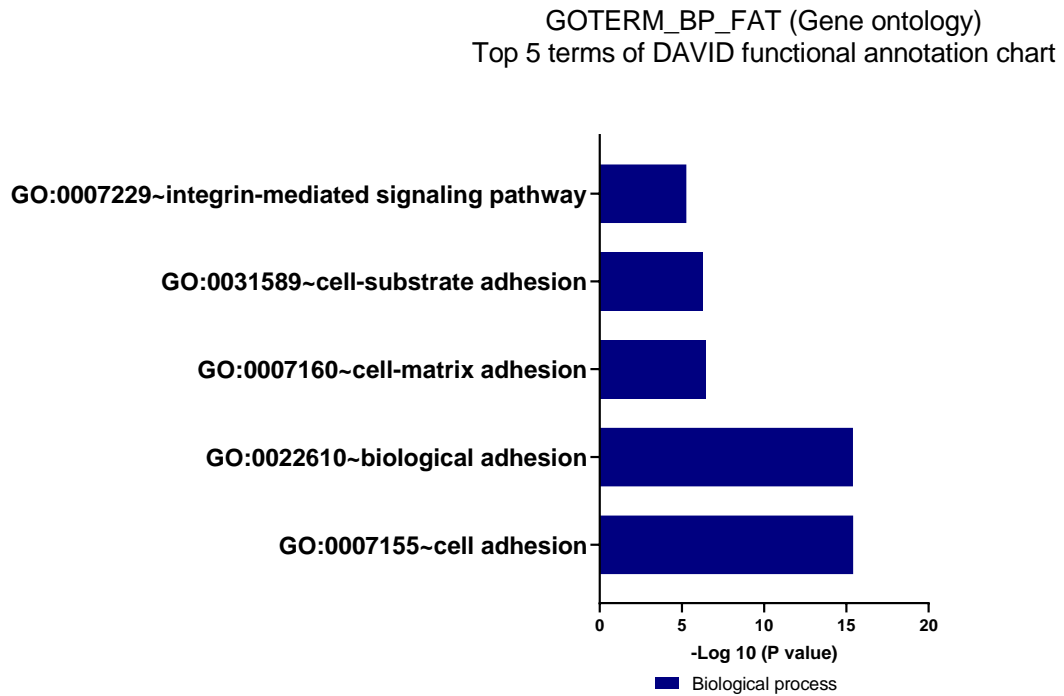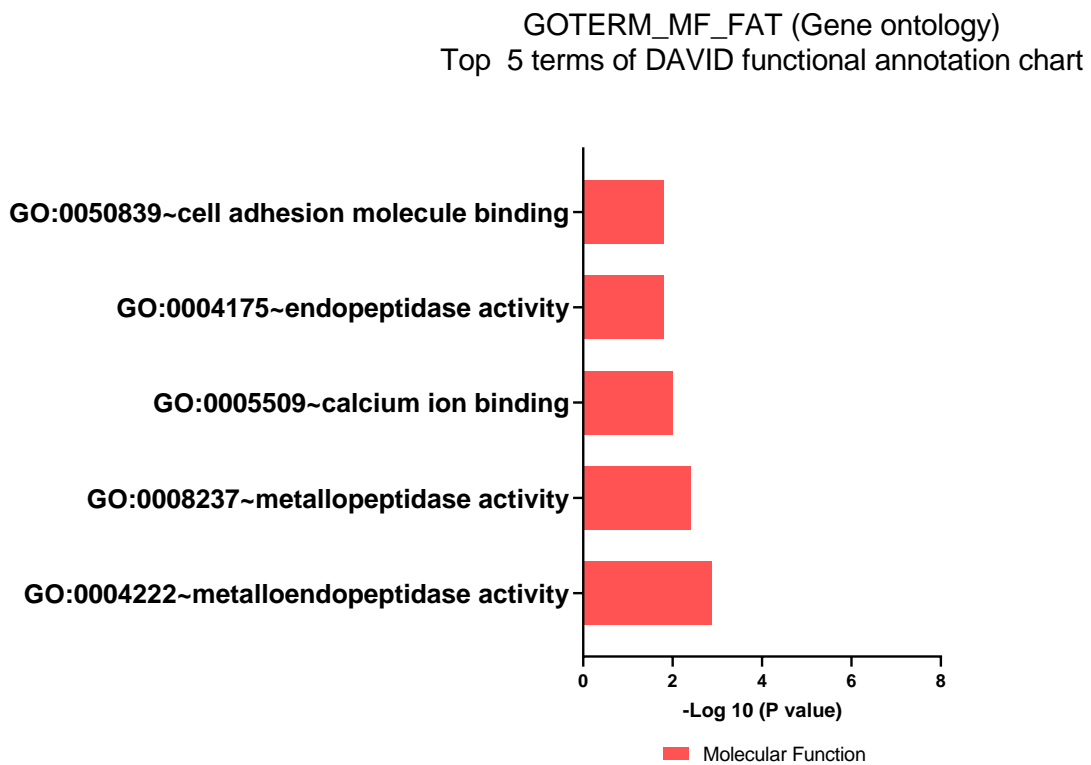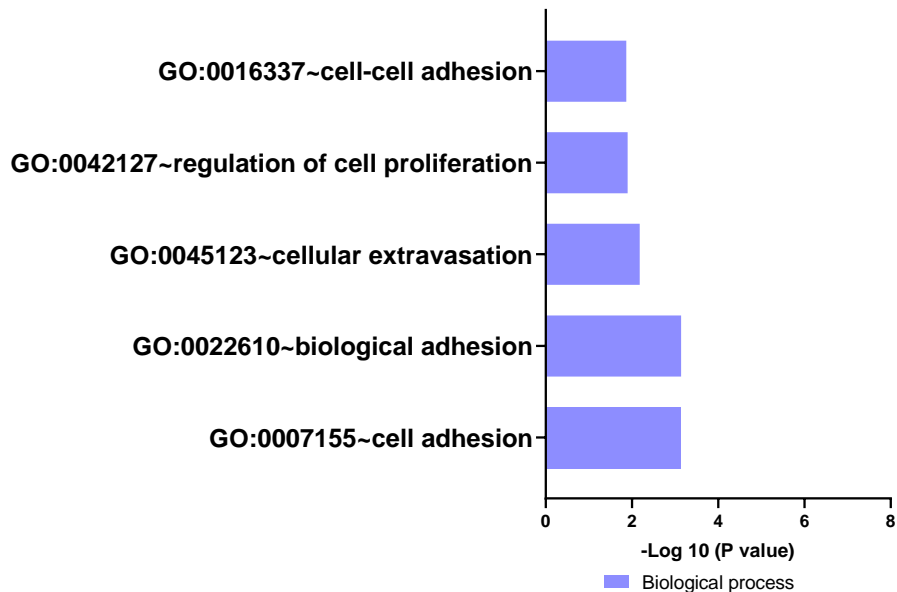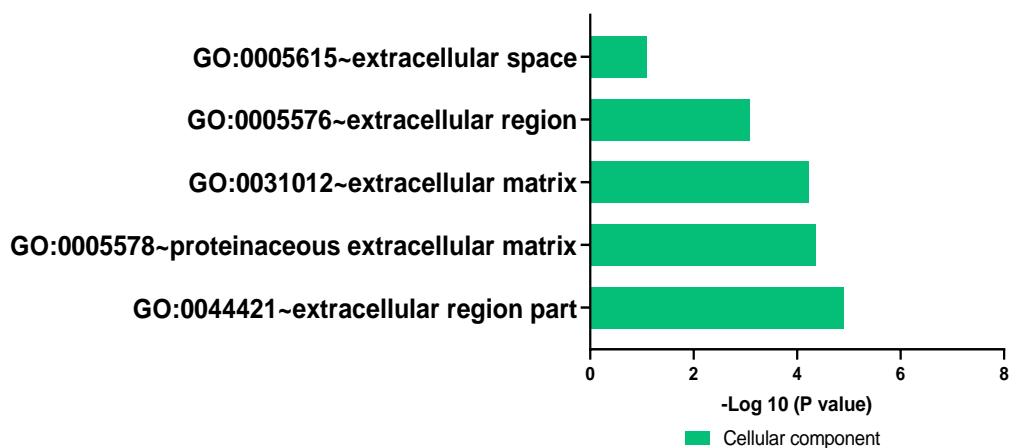Top 5 terms of DAVID functional annotation chart
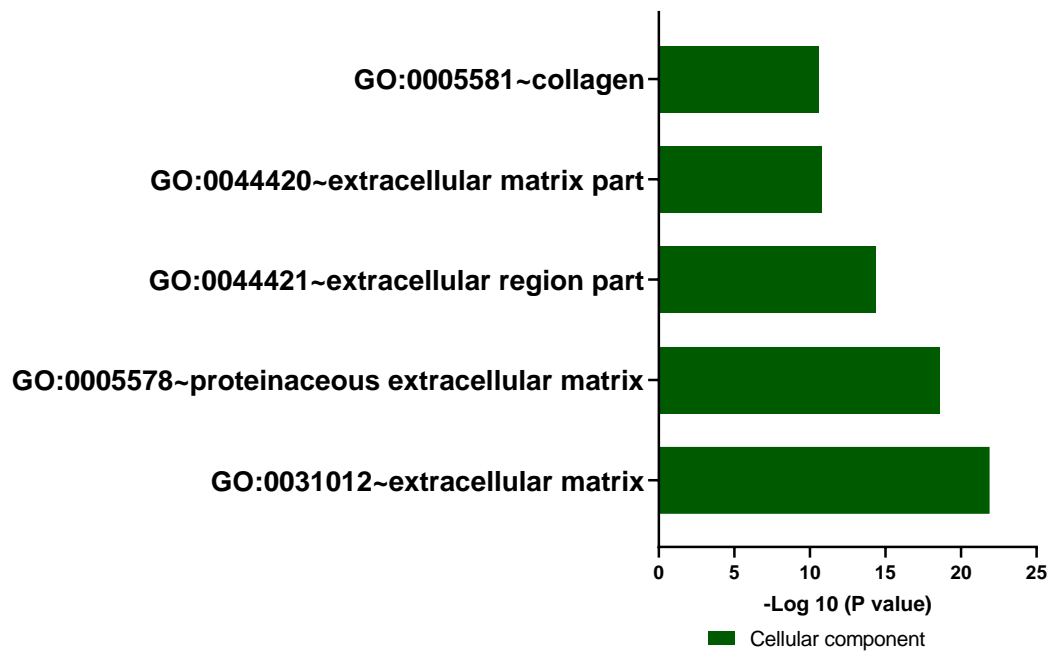
Figure 4.28 Gene ontology analysis of significantly upregulated genes of ECM and adhesion array. (A) Defines the MF classification, (B) defines the CC classification and (C) defines the BP classification. Top 5 terms of all the category have been provided here.

(A)

GOTERM_MF_FAT (Gene ontology)
Top 5 terms of DAVID functional annotation chart

* Figure continued in the next page

4. Results

(B)

GOTERM_BP_FAT (Gene ontology)
Top 5 terms of DAVID functional annotation chart

(C)

GOTERM_CC_FAT (Gene ontology)
Top 5 terms of DAVID functional annotation chart

Figure 4.29 Gene ontology analysis of significantly downregulated genes of ECM and adhesion array. (A) Defines the MF classification, (B) defines the CC classification and (C) defines the BP classification. Top 5 terms of all the category have been provided here.

5. Discussion

The aim of this study was to examine the stimulatory effect of CAP on cell migratory behaviors and molecular signaling resulting in wound healing. For this, we performed cell migration experiments accompanied with gene and protein expression studies focusing on the HIPPO signaling pathway. The results show for the first time the activation of this pathway in dermal fibroblasts and paracrine regenerative signaling between keratinocytes and fibroblasts upon CAP treatment. The effect of CAP on cell migration of monoculture and coculture was also studied separately. This study also aimed to generate a regenerative signaling molecule map upon CAP treatment in a wound healing set up.

5.1 Effect of CAP on cell migration and extracellular matrix molecules

There are compelling evidences in previous studies that H_2O_2 is one of the stable oxidants produced by CAP. Wende et al. have previously shown that feed gas composition is an important contributor of plasma generated chemical entities [180]. H_2O_2 is an important second messenger generated by CAP which triggers the release of growth factors during the wound healing process and has been shown to increase keratinocyte viability and migration in wound models [181]. Therefore, the first focus of the thesis was to quantify H_2O_2 in RPMI. kINPen is primarily an argon plasma jet which in contact with ambient air and cell culture medium generate radical and non-radical species [151]. We quantified the H_2O_2 concentration in 5 ml RPMI medium after 10, 30 and 60s of plasma treatment with kINPen MED, and we observed a time dependent increase of H_2O_2 production (figure 4.1) as shown in previous studies.

The epidermal layer functions as a barrier to the outside of the skin, and upon damage, newly divided keratinocytes cover damaged skin by migrating across the dermis. Here, we optimized monocultures of HaCaT and GM Fbs and an *in vitro* coculture model that incorporated both keratinocytes and fibroblasts at a ratio of 2:1. Unlike in single cell studies, the coculture model for migration studies provides the opportunity to monitor the influence of the two cell types on each other after CAP treatment. We investigated the cell migration rate in a scratch wound assay. There are a few limitations of manual in vitro scratch assay. For example, manual scratch with pipettes could yield in higher variability in initial wound size and shape. Removed cells could also accumulate at the edge of wound sites [182]. In

contrast, we executed scratches with the Essen Bioscience wound maker, as described in the methods section. With its identical 96 pins, the variability in wound size was reduced and higher reproducibility was achieved in experimental replicates. Upon a standardized scratch formation, monocultures and coculture were incubated with untreated and plasma-treated medium until 24 hours followed by a computerized analysis.

CAP did not significantly increase the cell migration rate in keratinocytes and fibroblasts (figure 4.6, 4.7). Previously Loo et al. has described that H_2O_2, one of the long-living molecule produced by CAP, could stimulate migration of keratinocytes in a scratch wound model [183]. In our studies, for HaCaT cells, even though a tendency of increased migration rate for 10 and 30s starting from around 18 hours was observed, the difference was not significant. In the scratch wound model, GM Fbs did not migrate collectively, but rather they migrated as single cells. Depletion of NF2 reduces the collective motility in epithelial cells, but increases the individual cell motility [184]. CAP mediated upregulation of NF2 probably supports single cell motility in fibroblast monolayer. The cellular adhesion receptor CD44 was also upregulated upon cold plasma treatment. CD44 is important for facilitating an organized directional migration in response to injury. Cold plasma-mediated directional single cell migration, as observed in fibroblasts, could therefore be credited to CAP mediated induction of NF2 and CD44.

For GM Fbs in monoculture, we observed a decrease in cell migration with 30s treatment but an increase with 10s CAP treatment. This could be due to the differential sensitivity of keratinocytes and fibroblasts towards H_2O_2 [185]. However, we observed that keratinocytes cocultured with fibroblasts showed an improved cell migration (figure 4.8). Therefore, each cell type might display a specific treatment window for CAP treatment, where under optimal conditions, a stimulation of cell activities is possible.

Coculture mimics real skin more closely due to the inclusion of both keratinocytes and fibroblasts. As CAP treatment showed a better stimulation effect on keratinocyte migration in coculture, the cross talk between these two different cell types and the influence of CAP on these cells come into focus. Many growth factors and cytokines are released from fibroblasts after injury, and this could provide an explanation for the acceleration of coculture in wound closure [186, 187]. In a previous study by Seo et al. [188], HaCaT cell motility increased when HaCaT cells and fibroblasts were cultured together. This was mainly attributed to a synergistic effect where HaCaT cells showed an increased expression of TGF-ß and fibroblasts showed an increased expression of Cyr61 [189]. Keratinocytes in direct contact with fibroblasts also showed enhanced migratory rate due to HB-EGF produced by IL-1 and TGF ß stimulated fibroblasts [187]. Therefore, these and numerous other recent studies, have emphasized the importance of synergistic interaction between keratinocytes and fibroblasts. Hence, a better stimulation effect on cell migration upon CAP treatment is justified compared to monocultures.

Dynamic interactions between the secreted factor and extracellular matrix components are essential for wound healing. Fibroblasts, as one of the key players in wound healing, remodel ECM molecules, and support re-epithelialization via cell migration and motility [176]. In GM Fbs, we observed an increase in collagen molecules (specifically COL4, COL5, COL6, COL7, COL 15 and COL12) after CAP treatment (table 4.2). COL7 is secreted by dermal fibroblasts and is crucial for wound re-epithelialization. COL7A1 has been found to directly regulate keratinocyte cell migration [190]. Therefore, the increase in COL7A1 in dermal fibroblasts may also attribute to the increased migration in co culture. Cold plasma also significantly upregulated MMP 13, MMP 14, TIMP-2, MMP 3 molecules in dermal fibroblasts (table 4.2), which are known for their impact on remodeling of dermal tissue. However, metalloproteinase like MMP 8, MMP 9 were downregulated indicating a possible reduction of elevated level of these proteins, as often observed in chronic wounds. MMP 13 are expressed in leading edges of migratory epithelial cells in a cutaneous wound healing mice model and plays an important role in keratinocyte migration, angiogenesis and contraction in wound healing [191]. MMP 13 is activated by MMP 3, MMP 14 and MMP 2 molecules [192, 193]. Upregulation and activation of MMPs in GM Fbs could therefore have a synergistic effect on keratinocyte migration in coculture. Tight junctional proteins are also important for directional migration of epithelial cells, endothelial chemotaxis and barrier integrity [194]. TJP 1 was shown to regulate the cell migration, barrier formation and angiogenesis in human dermal microvascular endothelial cells (HDMEC) [194] . TJP-1 is also present at the leading edge of migrating fibroblasts in the corneal fibroblast scrape wound model. An upregulation of TJP-1 and TJP-2 expression in GM Fbs observed after 60s CAP treatment (table 4.1), hence supports the accelerated healing in coculture. In line with our observation, Schmidt et al. also showed that periodic exposure of CAP on keratinocytes could significantly upregulate TJP-1 up to 6 weeks [195]. CAP exerts its effect separately on dermal fibroblasts and keratinocytes and also influences their synergistic interaction and crosstalk in coculture by differentially regulating these matrix molecules.

Integrins are cell adhesion molecules and are responsible for proliferation, migration, differentiation and gene expression [196]. In our real time PCR experiments (table 4.2), we observed an upregulation of integrins namely ITGA3, ITGB2 and ITGB4. The adhesive nature of integrin allows them to bind with extracellular matrix proteins like laminin, collagen, vitronectin, fibronectin etc. [196] which were also differentially expressed upon cold plasma treatment in fibroblasts. Most of the laminin chains (LAMA3, LAMC1 etc.) remained unaltered (supplementary data, table 4), however, several collagen moieties (COL4, COL7 etc.) and vitronectin were significantly upregulated upon plasma treatment, which in patients would be a good indicator for a wound healing supported by the formation of new connective tissue. Several other adhesion molecules like Cadherin 1, catenin, PECAM1, VCAM1 were also differentially regulated upon 60s CAP treatment in GM Fbs. Together, these results suggest that, CAP could influence genes coding for proteins related to transmembrane molecules, cell-cell adhesion, cell-matrix adhesion, and a number of other ECM molecules which ultimately contribute to accelerated healing in coculture.

We also compared the effect of direct and indirect CAP treatment on cell migration in HaCaT alone and cocultured with fibroblasts (figure 4.13). We could observe that, compared to direct treatment, both 10s and 30s indirect CAP treatment accelerated cell migration in HaCaT mono and coculture. This can be attributed to the composition of direct and indirect CAP treatment. Direct CAP treatment exerts the effect of UV rays, electrical field, several other short and long lived reactive species such as $\bullet$NO, $\bullet$OH, $O_2\bullet$-/$\bullet$OOH, as well as non-radical chemical compounds, such as singlet oxygen $^1O_2$ [197] which could impose a direct oxidative stress on HaCaT cells and in coculture. Whereas indirect plasma treatment would primarily exert the effect of stable long-lived reactive species such as H_2O_2, NO_2^-, and NO_3^-, produced upon interaction of CAP with the medium.

In HaCaT cells, as observed in figure 4.12, both 10 and 30s direct CAP treatment exposed a negative effect on cell migration. Cell migration was stunted when co culture was treated with 30s direct CAP treatment, however 10s direct CAP treatment induced cell migration, though the differences were not statistically significant. With increase in plasma treatment time the intracellular ROS generation also increases in HaCaT cells [198]. We also observed a treatment time-dependent increase of intracellular ROS production both in HaCaT and fibroblasts (figure 4.2), even though compared to positive control, 100 µM H_2O_2, the fold change was insignificant. So, essentially it is a balance between the cumulative redox species posed to cells which determines CAP mediated effect on cell migration. Persistent short- and long-lived reactive species, as found in longer direct treatments generate an imbalance where the free reactive species are higher than the body's antioxidant system and therefore delays cell migration. Thus, 30s direct CAP treatment probably imparts an oxidative stress which is not evident upon 10s plasma treatment. Hence, we observe a delayed cell migration rate with longer plasma treatment time.

5.2 NAC abrogates CAP mediated cell migration

NAC is a thiol, mucolytic agent and a precursor of L- cysteine and reduced glutathione (GSH) and acts as a free radical scavenger of OH, H_2O_2 and O_2^-. NAC directly reacts with the radical species and scavenges them. However, NAC is a poor scavenger and the antioxidant and cytoprotective effect of NAC has been investigated by Ezerina et al [199]. In their study they showed that cysteine is desulfurated to generate hydrogen sulfide, which in turn is oxidized to sulfane sulfur species, predominantly within mitochondria. These sulfane sulfur species are the actual mediators of the immediate antioxidative and cytoprotective effects provided by NAC [199]. The in vivo antioxidant activity of NAC is attributed to its ability to replenish depleted GSH pools [200]. Recently, another mechanism of NAC antioxidant activity has been considered. NAC has the ability to disrupt thiolated proteins, the free thiol groups have better antioxidant effect than NAC and boosts GSH synthesis thus exerting the indirect antioxidant effect of NAC [200].

After making scratches, HaCaT cells in monoculture and cocultured with GM Fbs were incubated with untreated and CAP treated medium in combination with NAC. NAC could abrogate CAP stimulated cell migration in all three settings. We observed that NAC significantly reduced the cell migration rate in both monoculture and coculture of keratinocytes (figure 4.10, 4.11). NAC can exclusively disrupt cell migration in keratinocytes [201], fibroblast [202] as well as in coculture. Similar to our results, Loo et al. found that in a coculture model, where H_2O_2 could improve re-epithelialization of keratinocytes, 5 mM NAC could prevent it [185]. The delay in the cell migration rate that we observed upon NAC treatment could be partially accredited to its effect on signaling molecules. NAC could significantly reduce H_2O_2 induced collagen production in oral mucosal cells [203]. In a model of tissue fibrosis, it was observed that NAC abrogated TGF-ß signaling in fibroblasts [204]. NAC treatment suppressed p38 phosphorylation and IL-6 production in HaCaT cells [205]. NAC could also significantly downregulate the production of VEGF in basal human keratinocytes [206]. Therefore, the exact mechanism on how and why NAC suppresses cell migration in HaCaT cells and in coculture is not self-explanatory. But, NAC probably suppresses growth factors, extracellular matrix molecules, interleukins and MAP kinases which can abrogate CAP-mediated cell migration in HaCaT cells and in coculture.

In summary, it could be shown that short-term CAP treatment could accelerate cell migration in coculture and has an impact on the synergistic interactions between keratinocytes and fibroblasts. It effects on extracellular matrix molecules, cell adhesion molecules which possibly show a cumulative positive effect on keratinocyte cell migration. NAC could disrupt this CAP mediated cell migration, indicating that CAP-generated reactive species trigger stimulation of cellular motility.

5.3 Effect of CAP on metabolic activity

In this work, cellular viability/metabolic activity of monocultures HaCaT, GM Fbs and coculture was investigated after 10, 30 and 60s CAP treatment. Cell viability was determined by the Alamar Blue assay, and as shown in figure 4.3, we observed a significant decrease in cell viability in all three different cell set ups 3 hours after a 60s CAP treatment. In fact, 24 hours after treatment, GM Fbs showed a further significant drop in metabolic activity after both 30 and 60s treatment. Previous studies have already pointed out that high amounts of ROS/RNS species can affect human cells and lead to cell death and reduction in cell viability and proliferation [207]. This results are in accord with the previous observations where Schmidt et al. have shown that 24 hours after 180s long-term CAP treatment in HaCaT cells, dead cells percentage increased to almost 1.5-fold [208]. Longer than 25s CAP treatment could also significantly decrease cell viability in L929 murine fibroblasts. However, a treatment time of 5-15 s could improve cell viability in L929 cells [209]. Consequently, the difference in cell viability in different cell types could be attributed

to the difference in plasma source, scarcity of standardized conditions, plasma treatment time, plasma treatment distance and type of the cell. It was quite apparent from our data and previous literature that, short term CAP treatment (like 10s) was not harmful for the cells and there was no significant reduction in metabolic activity in all the three cell types even after 24 hours. However, a longer treatment time like 60s could immediately decrease the metabolic activity within 3 hours. Even though HaCaT cells could restore the metabolic activity 24 hour after treatment, GM Fbs could not restore the metabolic activity when cultured as monocultured cells. In fact, it resulted in a drop of approximately 50% in metabolic activity after long term CAP treatment. Coculture of keratinocytes and fibroblasts was comparatively resistant towards the plasma treatment, and like HaCaT cells, these cells could restore the cell viability 24 hours after all the treatment types.

NAC, the well-known scavenger of redox species was tested for its capability to restore the metabolic activity in all the cell types. In LPS induced RAW 264.7 macrophages, NAC significantly reduced cell death and counteracted the effect of oxidative stress inducing agent and improved cell viability [210]. Even in human primary gingival fibroblasts, high NAC concentration (5-10 mM) could significantly reduce cell death[211]. In accordance with the previous literature, NAC significantly restored the metabolic activity in both monocultures of fibroblasts and keratinocytes and in their coculture. In our studies, NAC alone did not significantly increase metabolic activity in HaCaT and coculture, but in GM Fbs, NAC alone could significantly improve metabolic activity 3 hours after treatment. As a positive control 60 µM H_2O_2 was used in this metabolic activity experiment (figure 4.4). 60 µM H_2O_2 decreased cell viability in both the monoculture and coculture 3 hours after treatment. But, when the cells were treated with H_2O_2 in combination with NAC, metabolic activity was restored. 24 hours after plasma treatment, metabolic activity was reduced in all the three cell set ups, but NAC significantly counteracted the effects of CAP treatment and restored the metabolic activity in all the three experimental set ups. This protective effect of NAC could be attributed to its direct scavenging properties or de novo synthesis of intracellular GSH pool with NAC as a precursor. Apart from 2.5 mM NAC, metabolic activity was also tested with 5mM NAC, and the results were identical to 2.5 mM NAC treatment (data not shown).

In summary, it could be shown that shorter CAP treatment did not have a significant effect on the metabolic activity. However, longer CAP treatment (60s) could significantly reduce the metabolic activity, which could be restored when cells were treated in combination with 2.5mM NAC.

5.4 Effect of CAP on HIPPO signaling pathway and paracrine signaling

CAP showed a better stimulation effect on cell migration in coculture compared to HaCaT monoculture. This indicates a signaling cross talk between keratinocytes and fibroblasts in coculture which is under CAP influence. To more thoroughly assess the signaling axis, we investigated signaling pathways involved in tissue homeostasis and regeneration. In this context, we investigated HIPPO signaling pathway in both the cell types which play a pivotal role in tissue homeostasis and regeneration.

5.4.1 CAP modulated activation of YAP-CTGF-Cyr61

YAP is a multifunctional adapter protein that possesses one coactivator domain. It is the major nuclear executer of the HIPPO signaling pathway [212]. While the upstream signaling kinases of HIPPO pathway are inactivated, YAP moves to nucleus, binds to gene enhancer elements in complex with a TEAD TF, interacting with chromatin remodeling factors and modulating RNA polymerase II to drive or repress the expression of target genes, which prominently include cell migration regulators [213].

YAP is highly expressed and predominantly nuclear in the early embryonic epidermal progenitors, and is essential for the proliferative capacity of progenitors and the development of the epidermis [214]. Deletion of YAP leads to a reduction of cell growth, inhibition of keratinocyte differentiation, and delay in wound healing [88]. Therefore, the role of YAP in wound healing is of utmost importance. In our study, we found an upregulated mRNA expression of YAP in GM Fbs upon CAP treatment. From our gene expression data, we also observed an upregulation of WWC1 in GM Fbs (table 4.1), an upstream regulator of YAP. WWC1 stimulates the phosphorylation of LATS1/2 on their hydrophobic motif. Its overexpression stimulates the phosphorylation of YAP and deletion reduces the phosphorylation [215]. In GM Fbs, we could observe that both LATS1/2 were upregulated upon CAP treatment (table 4.1). LATS1/2 can phosphorylate YAP/TAZ leading to its inactivation and cytoplasmic sequestration. Upon phosphorylation by upstream LATS kinases, YAP is associated with 14-3-3 protein and sequestered in the cytoplasm. But recent studies show that LATS-dependent phosphorylated YAP can be retained in the nucleus and is not necessarily exported to the cytoplasm [216]. However, in our settings, we did not observe any significant change in YAP phosphorylation in fibroblasts upon plasma treatment. We also quantified the nuclear-cytoplasmic distribution of YAP with immunofluorescence, as this distribution is a key determinant of its activity and is a major target of their regulation. Both untreated and 30s plasma treatment showed comparable cellular distribution of YAP. A minimal significant decrease in nuclear distribution of YAP upon 10s plasma treatment in GM Fbs was observed further indicating that YAP molecules are dynamic. Several studies describe that YAP molecules are not static, rather they

dynamically shuttle between cytoplasm and nucleus [217-220]. This might explain why we observe the equivalent distribution of YAP in control and plasma treated cells.

Reactive species play an important role in YAP target gene CTGF and Cyr61 induction. H_2O_2 and hydroxyl radicals induced CTGF expression in human lens epithelial cells [221]. CTGF was also upregulated in retinal pigment epithelial cells upon redox stimulation [222]. As observed in these studies, incubation with CAP generated reactive species stimulated the mRNA expression of CTGF in GM Fbs compared to control (figure 4.14). Protein expression of CTGF was also upregulated in GM Fbs (figure 4.17). CTGF promotes cell migration and adhesion by binding to integrin receptors on cell surface. Upregulation of integrin like ITGB4, ITGB2 and ITGA3 upon plasma treatment (table 4.2) could possibly link towards the CTGF- integrin signaling. Integrin activation leads to ERK and p38 phosphorylation, activation of F actin and Paxillin resulting in actin reorganization [223]. Integrin activation can also potentiate focal adhesion formation and cellular migration by stimulating FAK [99]. Even though we have not tested the expression of FAK, a possible crosstalk of CTGF-integrin FAK signaling could be ventured based on these results.

Cyr61 is also expressed in dermal fibroblasts during cutaneous wound healing. Upon CAP treatment, Cyr61 was induced at protein and gene level in GM Fbs. Similar to CTGF, Cyr61 also binds with the integrin receptors and mediates adhesion of dermal fibroblasts, VSMCs and platelets [97]. Cyr61 also binds to vitronectin with high affinity [224], which was also upregulated in our results (table 4.2). Several cell adhesion molecules like VCAM1, VTN, cadherins were differentially regulated (table 4.2). This indicate that Cyr61 might upregulate cell adhesion molecules. Cyr61 enhances endothelial cell adhesion, migration, proliferation and microtubule formation, by directly binding to $\alpha v \beta 3$ receptor [97]. Even though we observed an increased expression of Cyr61 in our data (figure 4.16, 4.17), gene expression of ITGB3 or ITGA5 remained unaltered in fibroblasts (supplementary data, table 4).

In HaCaT cells, we found an increase in YAP mRNA expression, though not significant. Interestingly, nuclear YAP is identified in basal cells throughout the wound healing zones of regenerative epidermis and is present is the leading edges of the wound where keratinocytes migrate as a sheet [213]. We further checked the phosphorylation status of YAP in HaCaT cells compared to total YAP. We found an increase in phosphorylated YAP compared to total YAP in HaCaT cells. In accordance with the canonical model, phosphorylated YAP is retained in the cytoplasm, probably which is why we observed that, YAP target genes, CTGF and Cyr61 are minimally transcribed in HaCaT cells. In HaCaT cells CTGF protein expression was slightly increased and Cyr61 was not detected. This is similar to previous study where Seo et al. showed that Cyr61 is not detected in keratinocytes, but was present in fibroblast and coculture [189]. Thus, our results clearly indicate a paracrine signaling based on the HIPPO mediated signaling molecules which is initiated from the fibroblasts upon CAP treatment, finally leading to an improvement in wound regeneration.

Previous studies have indicated the inhibitory effect of NAC on CTGF and Cyr61. Pre-incubation with 1 and 2 mM NAC significantly attenuated CTGF expression in GO orbital fibroblasts [225]. In human gingival fibroblasts and human dermal fibroblasts NAC could significantly impair the ability of TGF-ß1 to induce CTGF protein expression [226]. Upregulation of rapamycin induced CTGF was also completely blocked with 5mM NAC pretreatment in hepatic progenitor cells [227]. In good accordance with these findings, we detected a significant drop in CTGF mRNA expression in GM Fbs and HaCaT cells further pointing to a redox species mediated signaling triggered by CAP. NAC also reduced ROS mediated induction of Cyr61 and loss of intracellular type I collagen in human dermal fibroblasts [228]. In line with this study, we also detected a significant reduction of Cyr61 mRNA expression in both HaCaT and GM Fbs incubated with CAP treated medium in combination with NAC. This clearly shows the importance of a well-balanced ROS signaling in cells involved in wound healing – regulating the activity of the HIPPO pathway. Applying cold plasma at short-term treatment triggers keratinocytes slightly and a more pronounced activation could be found in fibroblasts. These CAP effects were even enhanced when cells were in coculture – implicating a paracrine effect between fibroblasts and keratinocytes triggered by a CAP activation of the HIPPO pathway.

5.4.2 Effect of CAP on paracrine signaling between keratinocytes and fibroblasts

As stated before, our coculture experiments clearly displayed the advantage of this 1:2 mixture of fibroblasts and keratinocytes in comparison to monocultures of those cells. This was reflected in higher survival rates, but also in an increased cell migration. An increasing number of studies are focusing on the paracrine signaling and interaction between keratinocytes and fibroblasts in the context of wound repair. To test our hypothesis that CAP-induced stimulatory effects in coculture are a result of paracrine crosstalk, we monitored the cell migration of HaCaT cells that were incubated with conditioned media harvested from CAP-treated GM Fbs (GM-Fb-CM) collected after 18 hours of CAP treatment.

Conditioned media acquired from GM Fbs stimulated cell migration to a greater extent compared to conditioned media from untreated fibroblasts or no conditioned media at all. This phenomenon supports our hypothesis that CAP induces paracrine signaling between these two cell types by releasing paracrine effectors and hence promoting keratinocyte migration. We hypothesized that both CTGF and Cyr61 are involved in paracrine signaling, as both of these molecules are secreted and are actively involved in wound healing cascade. Both CTGF and Cyr61 are transcriptionally activated by serum, platelet derived growth factor, TGF-ß1 and basic fibroblast growth factor [97]. CTGF is actually involved in early wound healing and repair. Topical application of CTGF also could accelerate diabetic wound closure rate compared to vehicle treated control wounds [95]. Loss of CTGF impairs efficient re-epithelialization. This is especially evident from the expression pattern of this

protein in acute and chronic wound. Significantly reduced levels of CTGF was found in chronic wounds compared to acute wounds, which further suggests the role of CTGF in therapeutic wound healing [229]. Like CTGF, Cyr61 is also strongly expressed in dermal fibroblasts of the granulation tissue during wound healing, coincident with wound contraction and ECM remodeling [97]. Both CTGF and Cyr61 can regulate the production of angiogenic molecules (VEGF, bFGF) , MMPs and TIMPs which affect the integrity of ECM [91]. In accord with our hypothesis and existing literature, we demonstrated an increase in secreted CTGF and Cyr61 upon CAP treatment (figure 4.22). The increased secretion of CTGF and Cyr61 by CAP treated Fbs confirms that through their paracrine action they directly participate in wound healing of HaCaT cells.

We further tested our hypothesis by incubating HaCaT cells with recombinant human CTGF and Cyr61. Both recombinant CTGF and Cyr61 could significantly induce HaCaT cell migration (figure 4.23). The role of recombinant CTGF has been studied before by Seher et al [230]. They showed that human recombinant CTGF induces an inflammatory and wound healing response in primary tendon fibroblasts. Human recombinant CTGF could upregulate the transcription of several cytokines (IL-6, IL-8, CXCL1, and CXCL2) in human fibroblasts [231]. Exogenous addition of CTGF could also accelerate keratinocyte cell migration in a scratch wound model by phosphorylating ERK [232], which supports our cell migration studies (figure 4.23 a). In a coculture with both HaCaT cells and fibroblasts, secretion of Cyr61 from fibroblasts could significantly accelerate HaCaT cell migration, even when Cyr61 was not detected in HaCaT cells [233]. Combining these results, it is evident that, CTGF and Cyr61 secreted from CAP treated fibroblasts act as paracrine effectors in wound healing. These results confirm our hypothesis that CAP promotes a beneficial interaction between keratinocytes and fibroblasts that ultimately contributes to wound healing.

Here, for the first time, we demonstrated that CAP can stimulate a regenerative signaling pathway in dermal cells-namely the HIPPO pathway. We observed that the cold plasma-mediated effect on skin repair is mainly due to the activation of fibroblasts that when stimulated by CAP causes a paracrine stimulation of keratinocytes by releasing extracellular proteins as indicated by our coculture and migration experiments with conditioned media. Together, these results confirm the role of the HIPPO pathway in plasma-mediated wound healing that is dominantly triggered by long-living ROS that are generated by cold plasma. It also confirmed the negative effects of antioxidants on ROS mediated signaling in wound healing.

5. Discussion

An overview of the impact of CAP treatment on the cellular redox signaling based on this data is provided in figure 5.1.
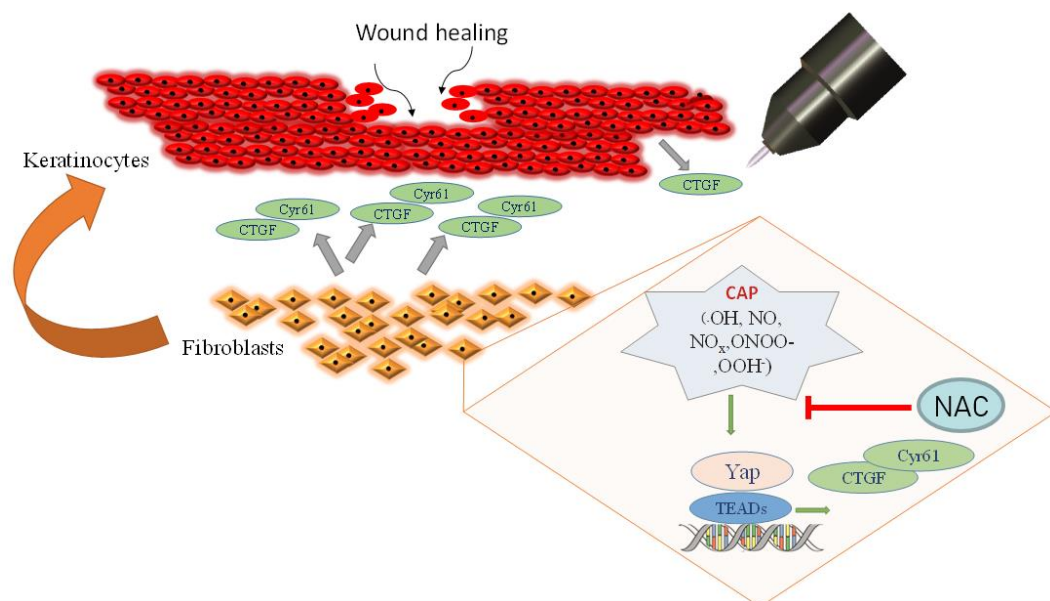
Figure 5.1 Schematic of keratinocyte activation by CAP modulated fibroblasts. The primary event in this scheme is the generation of reactive species in response to CAP treatment. These reactive species function as secondary messengers and stimulate the production of HIPPO signaling effectors such as CTGF in HaCaT and CTGF and Cyr61 by dermal fibroblasts in the vicinity. These extracellular matrix proteins and signaling molecules that are released from fibroblasts in turn activate keratinocytes, accelerate migration, and promote wound healing. This figure is adapted from [212].

In conclusion, this study provides the mechanistic insight on how CAP regulates a regenerative signaling pathway (HIPPO) and paracrine interactions between keratinocytes and fibroblasts. A detailed expression profile of extracellular matrix and adhesion molecules reveals that CAP regulates several ECM and adhesion molecules which promote re-epithelialization, immune cell infiltration, and granular tissue maturation ultimately leading to wound healing. Overall, this study contributes to a better understanding on the effect of CAP on re-epithelialization and regeneration which promote wound healing, based on the regenerative modulation of cells by HIPPO signaling.

6. Outlook

CAP treatment results into a complex cross talk between redox signaling pathways in mammalian cells via the impact of short- and long-lived reactive species. Here in this study, for the first time, we provided a mechanistic insight on how CAP activate HIPPO signaling in dermal fibroblasts. Although keratinocytes produced small amounts of CTGF, it is predominantly the secretion of CTGF and Cyr61 from dermal fibroblasts which influences the activation of keratinocytes through paracrine signaling and improves cell migration. During the course of this investigation, we could pinpoint to several molecules that are important in CAP-mediated wound healing.

Our RT-PCR data revealed an upregulation of HIF-1α in GM Fbs and HaCaT cells. Previous studies have already demonstrated a functional link between YAP and HIF-1α. [86]. Even though we observed an increase in HIF-1α in both GM Fbs and HaCaT cells, we did not check the stability of this protein upon knockdown of YAP. CAP could also induce heme oxygenase-1 (HMOX-1), a downstream target of HIF-1α, in both keratinocytes and fibroblasts [178, 234]. Thus, a possible signaling of YAP-HIF-1α- HMOX-1 should be further explored.

Several metalloproteinase (ADAMTS, MMPs), cell adhesion molecules (integrin, cadherin), extracellular matrix molecules were differentially expressed upon cold plasma treatment (table 4.2). In order to validate these observations, the protein profiles should be examined and the role of these factors in immune cell infiltration, granular tissue maturation and re-epithelialization should be further explored. HIPPO signaling effectors were investigated by RT^2 PCR array and we observed differential regulation of 59 genes (FAT family, LATS family, TEAD family, Cyclins etc.) upon cold plasma treatment (table 4.1). Thus changes in the protein level of these genes should be investigated as HIPPO signaling seems to be the major CAP activated pathway, involved in re-epithelialization and wound healing. Initial results already point to several signaling pathway that can be explored in future. For example, FAT1 and FJX1 were upregulated in our RT-PCR data. FAT1 is an upstream regulator of HIF-1α [235] and FJX1 is responsible for its stabilization [236]. These molecules might be involved in the signaling process. Overall, HIF-1α seems to be another CAP-induced major regulator that needs to be studied in future in context of wound healing.

This study was performed in selected cell lines, however various other cell types are involved in wound healing. Thus an animal model mimicking either an acute or a chronic wound should be employed to study the complex interaction of various cell types in respect to their reaction to plasma treatment.

7. Summary

Reactive species play an essential role in orchestrating wound healing responses. They act as secondary messengers and drive redox-signaling pathways that are involved in the hemostatic, inflammatory, proliferative and remodeling phases of wound healing. Cold plasma produces a profusion of short- and long-lived redox species that promotes wound healing, however, until today, the knowledge of CAP mediated wound healing remained scarce. In this thesis, CAP mediated wound healing mechanism and their effect on extracellular matrix and adhesion molecules have been investigated. To this end, a keratinocyte cell line (HaCaT), skin fibroblast cell line (GM Fbs) and an *in vitro* coculture model including both HaCaT and GM Fbs at a 2:1 ratio, were employed to investigate the cross talk between these two skin cell types.

We examined the impact of CAP on extracellular matrix proteins and cell adhesion molecules in GM Fbs and observed a significant impact of cold plasma treatment on the expression level of collagen moieties, cell adhesion molecule like integrin, cadherin, versican, MMPs as well as extracellular matrix proteins.

Moreover, scratch assays with monocultures of HaCaT, GM Fbs and coculture of these two cell types were performed. We detected that, CAP accelerated the migratory capability of HaCaT cells cocultured with fibroblasts. In fact, compared to HaCaT monoculture, a significant acceleration on cell migration was observed in coculture upon CAP treatment. NAC, a potent antioxidant could abrogate this CAP-stimulated cell migration in coculture, further pointing towards the importance of well-orchestrated reactive species in wound healing. To better understand this CAP-mediated effect on cell migration, we examined the signaling pathways involved in tissue homeostasis and regeneration. We checked the HIPPO signaling pathway and observed an upregulation of several signaling molecules at transcriptional level in GM Fbs upon CAP treatment.

YAP is the central nuclear executer of HIPPO signaling pathway. YAP was upregulated in both HaCaT cells and GM Fbs. The major downstream effectors of the HIPPO signaling pathway (CTGF and Cyr61) were also upregulated in dermal fibroblasts at both transcriptional and protein level. However, administration of antioxidant NAC inhibited CAP-mediated wound healing and abrogated the gene expression of the HIPPO downstream effectors. These results confirm that the upregulation of YAP-CTGF-CYR61 axis is due to CAP-generated redox species. In HaCaT cells, both CTGF and Cyr61 was minimally transcribed. Even though CTGF was rarely detected in HaCaT cells on the protein level,

Cyr61 remained undetected. This again shows the importance of the cross talk between fibroblasts and keratinocytes.

The coculture with the inclusion of fibroblasts showed an accelerated migration rate, compared to HaCaT monoculture which specifies a cross talk between these two cell types. Thus, monoculture of HaCaT cells were incubated with CAP-treated and untreated fibroblast conditioned medium. Interestingly, we observed that HaCaT cells exhibited an improved cell migration rate when incubated with CAP-treated fibroblast-conditioned media compared to that observed after incubation with untreated media. Upon investigation, an induction of CTGF and Cyr61 secretion was observed upon CAP treatment in the fibroblast-conditioned media. Furthermore, exposure to recombinant CTGF and Cyr61 could also significantly improve HaCaT cell migration which confirms that CAP mediated accelerated cell migration is due to activation of YAP-CTGF-Cyr61 axis.

In conclusion, this study revealed a completely new mechanical insight of CAP mediated wound healing. Along with several other ECM molecules, CAP activates a regenerative signaling pathway i.e., HIPPO signaling pathway in dermal fibroblasts at the onset of wound healing. Dermal fibroblasts drive a paracrine interaction by secreting CTGF and Cyr61 in close vicinity of wound, resulting in accelerated keratinocyte migration and wound healing in coculture.

8. Zusammenfassung

Reaktive Spezies spielen eine wesentliche Rolle bei der Orchestrierung von Wundheilungsreaktionen. Sie wirken als sekundäre Botenstoffe und steuern Redox-Signalwege, die an den hämostatischen, entzündlichen, proliferativen und transformativen Phasen der Wundheilung beteiligt sind. Kaltes Plasma erzeugt eine Fülle von kurz- und langlebigen Redoxspezies, die die Wundheilung fördern. Das Wissen über die CAP-vermittelte Wundheilung ist jedoch noch rar. In dieser Arbeit untersuchten wir den CAP-vermittelten Wundheilungsmechanismus und seine Wirkung auf extrazelluläre Matrix- und Adhäsionsmoleküle. Zu diesem Zweck haben wir die Keratinozyten-Zelllinie (HaCaT), die Hautfibroblasten-Zelllinie (GM00637 Fbs) und ein In-vitro-Kokulturmodell ausgewählt, das sowohl HaCaT als auch GM Fbs im Verhältnis 2:1 um den cross-talk zwischen den beiden Zelltypen zu untersuchen.

Im Rahmen der vorliegenden Doktorarbeit wurde der Einfluss von CAP auf extrazelluläre Matrixproteine und Zelladhäsionsmoleküle in GM Fbs untersucht. Dabei konnten unterschiedliche Genexpressionsniveaus mehrerer Kollagene, Zelladhäsionsmoleküle wie Integrin, Cadherin, Versican, sowie MMPs und extrazelluläre Matrixproteine nach der Behandlung mit kaltem Plasma beobachtet werden.

Darüber hinaus wurden Scratch-Assays mit Monokulturen von HaCaT, GM Fbs und Kokultur dieser beiden Zelltypen durchgeführt. Dabei wurde festgestellt, dass CAP die Migrationsfähigkeit von mit Fibroblasten kokultivierten HaCaT-Zellen beschleunigt. Tatsächlich wurde im Vergleich zur HaCaT-Monokultur eine signifikante Beschleunigung der Zellmigration in der Kokultur nach CAP-Behandlung beobachtet. NAC, ein starkes Antioxidans, könnte diese CAP-stimulierte Zellmigration in der Kokultur aufheben, was die Bedeutung einer gut ausbalancierten Steuerung der reaktiven Spezies für die Wundheilung weiter unterstreicht. Um diesen CAP-vermittelten Effekt auf die Zellmigration zu verstehen, wurden die Signalwege, die an der Homöostase und Regeneration des Gewebes beteiligt sind, insbesondere der HIPPO-Signalweg, untersucht. Dabei wurde eine Hochregulation auf Transkriptionsebene von Signalmolekülen in GM Fbs nach CAP-Behandlung beobachtet.

YAP ist der zentrale nukleare Vermittler des HIPPO-Signalwegs. YAP wurde sowohl in HaCaT Zellen als auch in GM Fbs hochreguliert. Die wichtigsten nachgeschalteten Effektoren des HIPPO-Signalwegs (CTGF und Cyr61) waren in dermalen Fibroblasten sowohl auf Transkriptions- als auch auf Proteinebene hochreguliert. Die Verabreichung des Antioxidans NAC konnte jedoch die CAP-vermittelte Wundheilung hemmen und die

Genexpression der nachgeschalteten HIPPO-Effektoren aufheben. Diese Ergebnisse bestätigen, dass die Hochregulation der YAP-CTGF-CYR61-Achse auf CAP-erzeugte Redoxspezies zurückzuführen ist. In HaCaT-Zellen allein wurden sowohl CTGF als auch Cyr61 minimal transkribiert. Obwohl CTGF in HaCaT-Zellen (Proteinspiegel) nur minimal nachgewiesen wurde, blieb Cyr61 unentdeckt. Dies zeigt erneut die Bedeutung des parakrinen cross talks zwischen Fibroblasten und Keratinozyten.

Die Kokultur unter Einbeziehung von Fibroblasten zeigte eine beschleunigte Migrationsrate im Vergleich zur HaCaT-Monokultur, was einen *cross talk* zwischen diesen beiden Zelltypen nahelegt. Daher wurde die Monokultur von HaCaT Zellen mit CAP-behandeltem und unbehandeltem Fibroblasten-konditioniertem Medium inkubiert. Interessanterweise beobachteten wir eine im Vergleich mit der nach Inkubation mit unbehandelten Medien deutlich verbesserte Zellmigrationsrate der HaCaT-Zellen bei Inkubation mit CAP-behandelten Fibroblasten-konditionierten Medien. Bei der Untersuchung wurde bei CAP-Behandlung in den Fibroblasten-konditionierten Medien eine Induktion der CTGF- und Cyr61-Sekretion beobachtet. Darüber hinaus könnte die Exposition gegenüber rekombinantem CTGF und Cyr61 auch die HaCaT-Zellmigration signifikant verbessern, was bestätigt, dass die CAP-vermittelte beschleunigte Zellmigration auf die Aktivierung der YAP-CTGF-Cyr61-Achse zurückzuführen ist.

Zusammenfassend ergab diese Studie einen völlig neuen mechanistischen Einblick in die CAP-vermittelte Wundheilung. Zusammen mit der Regulation mehrerer ECM-Moleküle, aktiviert CAP einen regenerativen Signalweg, nämlich den HIPPO-Signalweg in dermalen Fibroblasten zu Beginn der Wundheilung. Dermale Fibroblasten steuern eine parakrine Wechselwirkung, indem sie CTGF und Cyr61 in unmittelbarer Nähe der Wunde sekretieren, was zu einer beschleunigten Keratinozytenmigration und Wundheilung in der Kokultur führt.

9. References

1.   Sterry, W., *Kurzlehrbuch Dermatologie.* Unter Mitarb. von Czai, 2011.

2.   Gordon Betts, J., et al., *OpenStax, Anatomy & Physiology.* 2016.

3.   Delavary, B.M., et al., *Macrophages in skin injury and repair.* Immunobiology, 2011. **216**(7): p. 753-762.

4.   Martin, P., *Wound healing--aiming for perfect skin regeneration.* Science, 1997. **276**(5309): p. 75-81.

5.   Yazdanpanah, L., et al., *Literature review on the management of diabetic foot ulcer.* World J Diabetes, 2015. **6**(1): p. 37-53.

6.   Akbik, D., et al., *Curcumin as a wound healing agent.* Life sciences, 2014. **116**(1): p. 1-7.

7.   Azzimonti, B., et al., *Manipulating the healing response*, in *Wound Healing Biomaterials*. 2016, Elsevier. p. 101-116.

8.   Falanga, V., *Wound healing and its impairment in the diabetic foot.* The Lancet, 2005. **366**(9498): p. 1736-1743.

9.   Singer, A.J., et al., *Cutaneous wound healing.* New England journal of medicine, 1999. **341**(10): p. 738-746.

10.   Cañedo-Dorantes, L., et al., *Skin acute wound healing: a comprehensive review.* International journal of inflammation, 2019.

11.   Li, J., et al., *Pathophysiology of acute wound healing.* Clinics in dermatology, 2007. **25**(1): p. 9-18.

12.   Simpson, D.M., et al., *The neutrophilic leukocyte in wound repair: a study with antineutrophil serum.* The Journal of clinical investigation, 1972. **51**(8): p. 2009-2023.

13.   Noli, C., et al., *The mast cell in wound healing.* Veterinary dermatology, 2001. **12**(6): p. 303-313.

14.   Kunkel, S.L., et al., *Stimulus specific induction of monocyte chemotactic protein-1 (MCP-1) gene expression*, in *Chemotactic Cytokines*. 1991, Springer. p. 65-71.

15.   Sherry, B., et al., *Resolution of the two components of macrophage inflammatory protein 1, and cloning and characterization of one of those components, macrophage inflammatory protein 1 beta.* The Journal of experimental medicine, 1988. **168**(6): p. 2251-2259.

16.   Postlethwaite, A., et al., *Collagen-and collagen peptide-induced chemotaxis of human blood monocytes.* The Journal of experimental medicine, 1976. **143**(6): p. 1299-1307.

17.   Wynn, T.A., et al. *Macrophages: master regulators of inflammation and fibrosis.* in *Seminars in liver disease.* 2010. © Thieme Medical Publishers.

18.   Duscher, D., et al., *Fibroblast-specific deletion of hypoxia inducible factor-1 critically impairs murine cutaneous neovascularization and wound healing.* Plastic and reconstructive surgery, 2015. **136**(5): p. 1004.

19.   Greaves, N.S., et al., *Current understanding of molecular and cellular mechanisms in fibroplasia and angiogenesis during acute wound healing.* Journal of dermatological science, 2013. **72**(3): p. 206-217.

20.   Rezvani, H.R., et al., *Loss of epidermal hypoxia-inducible factor-1α accelerates epidermal aging and affects re-epithelialization in human and mouse.* Journal of cell science, 2011. **124**(24): p. 4172-4183.

21.   Murdoch, C., et al., *Hypoxia regulates macrophage functions in inflammation.* The Journal of Immunology, 2005. **175**(10): p. 6257-6263.

22.   Willenborg, S., et al., *CCR2 recruits an inflammatory macrophage subpopulation critical for angiogenesis in tissue repair.* Blood, The Journal of the American Society of Hematology, 2012. **120**(3): p. 613-625.

23.   Skuli, N., et al., *Endothelial HIF-2α regulates murine pathological angiogenesis and revascularization processes.* The Journal of clinical investigation, 2012. **122**(4): p. 1427-1443.

24.   Eelen, G., et al., *Endothelial cell metabolism in normal and diseased vasculature.* Circulation research, 2015. **116**(7): p. 1231-1244.

25.   Verrecchia, F., et al., *Transforming growth factor-β signaling through the Smad pathway: role in extracellular matrix gene expression and regulation.* Journal of Investigative Dermatology, 2002. **118**(2): p. 211-215.

26.   Opneja, A., et al., *Contribution of platelets, the coagulation and fibrinolytic systems to cutaneous wound healing.* Thrombosis research, 2019.179: p. 56-63

27.   Attinger, C.E., et al., *Clinical approach to wounds: debridement and wound bed preparation including the use of dressings and wound-healing adjuvants.* Plastic and reconstructive surgery, 2006. **117**(7S): p. 72S-109S.

28.   Demidova-Rice, T.N., et al., *Low-level light stimulates excisional wound healing in mice.* Lasers in Surgery and Medicine: The Official Journal of the American Society for Laser Medicine and Surgery, 2007. **39**(9): p. 706-715.

29.   Stojadinovic, A., et al., *Topical advances in wound care.* Gynecologic oncology, 2008. **111**(2): p. S70-S80.

30.   Woo, K., et al., *The edge effect: current therapeutic options to advance the wound edge.* Advances in skin & wound care, 2007. **20**(2): p. 99-117.

9. References

31.   Loots, M.A., et al., *Differences in cellular infiltrate and extracellular matrix of chronic diabetic and venous ulcers versus acute wounds.* Journal of Investigative Dermatology, 1998. **111**(5): p. 850-857.

32.   Beidler, S.K., et al., *Inflammatory cytokine levels in chronic venous insufficiency ulcer tissue before and after compression therapy.* J Vasc Surg, 2009. **49**(4): p. 1013-20.

33.   Gohel, M.S., et al., *The relationship between cytokine concentrations and wound healing in chronic venous ulceration.* J Vasc Surg, 2008. **48**(5): p. 1272-7.

34.   Trengove, N.J., et al., *Mitogenic activity and cytokine levels in non-healing and healing chronic leg ulcers.* Wound Repair Regen, 2000. **8**(1): p. 13-25.

35.   Wallace, H.J., et al., *Levels of tumor necrosis factor-alpha (TNF-alpha) and soluble TNF receptors in chronic venous leg ulcers--correlations to healing status.* J Invest Dermatol, 1998. **110**(3): p. 292-6.

36.   Bekeschus, S., et al., *Distinct cytokine and chemokine patterns in chronic diabetic ulcers and acute wounds.* Experimental dermatology, 2017. **26**(2): p. 145-147.

37.   Bader, M.S., *Diabetic foot infection.* Am Fam Physician, 2008. **78**(1): p. 71-9.

38.   Demidova-Rice, T.N., et al., *Acute and impaired wound healing: pathophysiology and current methods for drug delivery, part 1: normal and chronic wounds: biology, causes, and approaches to care.* Advances in skin & wound care, 2012. **25**(7): p. 304.

39.   James, G.A., et al., *Biofilms in chronic wounds.* Wound Repair and regeneration, 2008. **16**(1): p. 37-44.

40.   Schierle, C.F., et al., *Staphylococcal biofilms impair wound healing by delaying reepithelialization in a murine cutaneous wound model.* Wound Repair and Regeneration, 2009. **17**(3): p. 354-359.

41.   Usui, M.L., et al., *Keratinocyte migration, proliferation, and differentiation in chronic ulcers from patients with diabetes and normal wounds.* Journal of Histochemistry & Cytochemistry, 2008. **56**(7): p. 687-696.

42.   Stojadinovic, O., et al., *Molecular pathogenesis of chronic wounds: the role of β-catenin and c-myc in the inhibition of epithelialization and wound healing.* The American journal of pathology, 2005. **167**(1): p. 59-69.

43.   Kuo, P.-C., et al., *Glycated type 1 collagen induces endothelial dysfunction in culture.* In Vitro Cellular & Developmental Biology-Animal, 2007. **43**(10): p. 338-343.

44.   Death, A.K., et al., *High glucose alters matrix metalloproteinase expression in two key vascular cells: potential impact on atherosclerosis in diabetes.* Atherosclerosis, 2003. **168**(2): p. 263-269.

45.   Liao, H., et al., *Cells and tissue interactions with glycated collagen and their relevance to delayed diabetic wound healing.* Biomaterials, 2009. **30**(9): p. 1689-1696.

46.   Cano Sanchez, M., et al., *Targeting Oxidative Stress and Mitochondrial Dysfunction in the Treatment of Impaired Wound Healing: A Systematic Review.* Antioxidants (Basel, Switzerland), 2018. **7**(8): p. 98.

47.   Nouvong, A., et al., *Reactive oxygen species and bacterial biofilms in diabetic wound healing.* Physiological genomics, 2016. **48**(12): p. 889-896.

48.   Rojas, A.I., et al., *Patients with chronic leg ulcers show diminished levels of vitamins A and E, carotenes, and zinc.* Dermatologic Surgery, 1999. **25**(8): p. 601-604.

49.   Mudge, B.P., et al., *Role of glutathione redox dysfunction in diabetic wounds.* Wound Repair and Regeneration, 2002. **10**(1): p. 52-58.

50.   Grether-Beck, S., et al., *Activation of transcription factor AP-2 mediates UVA radiation-and singlet oxygen-induced expression of the human intercellular adhesion molecule 1 gene.* Proceedings of the National Academy of Sciences, 1996. **93**(25): p. 14586-14591.

51.   Brenneisen, P., et al., *Central role of Ferrous/Ferric iron in the ultraviolet B irradiation-mediated signaling pathway leading to increased interstitial collagenase (matrix-degrading metalloprotease (MMP)-1) and stromelysin-1 (MMP-3) mRNA levels in cultured human dermal fibroblasts.* Journal of Biological Chemistry, 1998. **273**(9): p. 5279-5287.

52.   Stricklin, G., et al., *Oxidant-mediated inactivation of TIMP.* Matrix (Stuttgart, Germany). Supplement, 1992. **1**: p. 325.

53.   Wenk, J., et al., *Stable overexpression of manganese superoxide dismutase in mitochondria identifies hydrogen peroxide as a major oxidant in the AP-1-mediated induction of matrix-degrading metalloprotease-1.* Journal of Biological Chemistry, 1999. **274**(36): p. 25869-25876.

54.   Wlaschek, M., et al., *Singlet oxygen is an early intermediate in cytokine-dependent ultraviolet-A induction of interstitial collagenase in human dermal fibroblasts in vitro.* FEBS letters, 1997. **413**(2): p. 239-242.

55.   Larouche, J., et al., *Immune Regulation of Skin Wound Healing: Mechanisms and Novel Therapeutic Targets.* Advances in Wound Care, 2018. 7(**7**) : p. 209-231.

56.   Bekeschus, S., *Effects of cold physical plasma on human leukocytes.* 2015.

57.   Pan, D., *The hippo signaling pathway in development and cancer.* Developmental cell, 2010. **19**(4): p. 491-505.

58.   Justice, R.W., et al., *The Drosophila tumor suppressor gene warts encodes a homolog of human myotonic dystrophy kinase and is required for the control of cell shape and proliferation.* Genes & development, 1995. **9**(5): p. 534-546.

59.   Xu, T., et al., *Identifying tumor suppressors in genetic mosaics: the Drosophila lats gene encodes a putative protein kinase.* Development, 1995. **121**(4): p. 1053-1063.

60.   Kango-Singh, M., et al., *Shar-pei mediates cell proliferation arrest during imaginal disc growth in Drosophila.* Development, 2002. **129**(24): p. 5719-5730.

61.   Tapon, N., et al., *salvador Promotes both cell cycle exit and apoptosis in Drosophila and is mutated in human cancer cell lines.* Cell, 2002. **110**(4): p. 467-478.

62.   Harvey, K.F., et al., *The Drosophila Mst ortholog, hippo, restricts growth and cell proliferation and promotes apoptosis.* Cell, 2003. **114**(4): p. 457-67.

63.   Udan, R.S., et al., *Hippo promotes proliferation arrest and apoptosis in the Salvador/Warts pathway.* Nature cell biology, 2003. **5**(10): p. 914-920.

64.   Wu, S., et al., *hippo encodes a Ste-20 family protein kinase that restricts cell proliferation and promotes apoptosis in conjunction with salvador and warts.* Cell, 2003. **114**(4): p. 445-456.

65.   Lai, Z.-C., et al., *Control of cell proliferation and apoptosis by mob as tumor suppressor, mats.* Cell, 2005. **120**(5): p. 675-685.

66.   Mao, B., et al., *Hippo signaling in stress response and homeostasis maintenance.* Acta Biochim Biophys Sin, 2015. **47**(1): p. 2-9.

67.   Callus, B.A., et al., *Association of mammalian sterile twenty kinases, Mst1 and Mst2, with hSalvador via C-terminal coiled-coil domains, leads to its stabilization and phosphorylation.* The FEBS journal, 2006. **273**(18): p. 4264-4276.

68.   Chan, E.H., et al., *The Ste20-like kinase Mst2 activates the human large tumor suppressor kinase Lats1.* Oncogene, 2005. **24**(12): p. 2076-2086.

69.   Praskova, M., et al., *MOBKL1A/MOBKL1B phosphorylation by MST1 and MST2 inhibits cell proliferation.* Current Biology, 2008. **18**(5): p. 311-321.

70.   Dong, J., et al., *Elucidation of a universal size-control mechanism in Drosophila and mammals.* Cell, 2007. **130**(6): p. 1120-1133.

71.   Lei, Q.-Y., et al., *TAZ promotes cell proliferation and epithelial-mesenchymal transition and is inhibited by the hippo pathway.* Molecular and cellular biology, 2008. **28**(7): p. 2426-2436.

72.   Zhao, B., et al., *Inactivation of YAP oncoprotein by the Hippo pathway is involved in cell contact inhibition and tissue growth control.* Genes & development, 2007. **21**(21): p. 2747-2761.

73.   Hergovich, A., et al., *NDR kinases regulate essential cell processes from yeast to humans.* Nature reviews Molecular cell biology, 2006. **7**(4): p. 253-264.

74.   Zhao, B., et al., *A coordinated phosphorylation by Lats and CK1 regulates YAP stability through SCFβ-TRCP.* Genes & development, 2010. **24**(1): p. 72-85.

75.   Luo, X., et al., *NUP37, a positive regulator of YAP/TEAD signaling, promotes the progression of hepatocellular carcinoma.* Oncotarget, 2017. **8**(58): p. 98004-98013.

76.   Chan, S.W., et al., *A role for TAZ in migration, invasion, and tumorigenesis of breast cancer cells.* Cancer research, 2008. **68**(8): p. 2592-2598.

77.   Pobbati, A.V., et al., *Structural and functional similarity between the Vgll1-TEAD and the YAP-TEAD complexes.* Structure, 2012. **20**(7): p. 1135-1140.

78.   Zhao, B., et al., *TEAD mediates YAP-dependent gene induction and growth control.* Genes & development, 2008. **22**(14): p. 1962-1971.

79.   Boopathy, G.T., et al., *Role of hippo pathway-Yap/Taz signaling in angiogenesis.* Frontiers in cell and developmental biology, 2019. **7**: p. 49

80.   Lau, L.F., et al., *The CCN family of angiogenic regulators: the integrin connection.* Experimental cell research, 1999. **248**(1): p. 44-57.

81.   Chen CC, L.L., *Functions and mechanisms of action of CCN matricellular proteins.* Int J Biochem Cell Biol, 2010. **41**: p. 771–783.

82.   Lehtinen, M.K., et al., *A conserved MST-FOXO signaling pathway mediates oxidative-stress responses and extends life span.* Cell, 2006. **125**(5): p. 987-1001.

83.   Shao, D., et al., *A functional interaction between Hippo-YAP signalling and FoxO1 mediates the oxidative stress response.* Nature communications, 2014. **5**(1): p. 1-10.

84.   Wu, H., et al., *The Ets transcription factor GABP is a component of the hippo pathway essential for growth and antioxidant defense.* Cell reports, 2013. **3**(5): p. 1663-1677.

85.   Tumaneng, K., et al., *YAP mediates crosstalk between the Hippo and PI(3)K–TOR pathways by suppressing PTEN via miR-29.* Nature cell biology, 2012. **14**(12): p. 1322-1329.

86.   Zhang, X., et al., *Yes-associated protein (YAP) binds to HIF-1α and sustains HIF-1α protein stability to promote hepatocellular carcinoma cell glycolysis under hypoxic stress.* Journal of experimental & clinical cancer research : CR, 2018. **37**(1): p. 216-216.

87.   Lee, M.J., et al., *YAP and TAZ regulate skin wound healing.* J Invest Dermatol, 2014. **134**(2): p. 518-525.

88.   Elbediwy, A., et al., *Integrin signalling regulates YAP and TAZ to control skin homeostasis.* Development, 2016. **143**(10): p. 1674-1687.

89.   Lipson, K.E., et al. *CTGF is a central mediator of tissue remodeling and fibrosis and its inhibition can reverse the process of fibrosis.* in *Fibrogenesis & tissue repair.* 2012. Springer.

90.   Alfaro, M.P., et al, *A physiological role for connective tissue growth factor in early wound healing.* Lab Invest, 2013. **93(1)**: p. 81-95.

91.   Brigstock, D.R., *Regulation of angiogenesis and endothelial cell function by connective tissue growth factor (CTGF) and cysteine-rich 61 (CYR61).* Angiogenesis, 2002. **5**(3): p. 153-165.

92.   Fan, W.H., et al., *Connective tissue growth factor (CTGF) stimulates vascular smooth muscle cell growth and migration in vitro.* Eur J Cell Biol, 2000. **79**(12): p. 915-23.

93.   Yang, Z., et al., *Connective tissue growth factor stimulates the proliferation, migration and differentiation of lung fibroblasts during paraquat-induced pulmonary fibrosis.* Molecular Medicine Reports, 2015. **12**: p. 1091-1097

94.   Liu, L.d., et al., *The repairing effect of a recombinant human connective-tissue growth factor in a burn-wounded rhesus-monkey (Macaca mulatta) model.* Biotechnology and applied biochemistry, 2007. **47**(2): p. 105-112.

95.   Henshaw, F.R., et al., *Topically applied connective tissue growth factor/CCN2 improves diabetic preclinical cutaneous wound healing: potential role for CTGF in human diabetic foot ulcer healing.* J Diabetes Res, 2015. **2015**: p. 236238.

96.   Kapoor, M., et al., *Connective tissue growth factor promoter activity in normal and wounded skin.* Fibrogenesis & tissue repair, 2008. **1**(1): p. 3.

97.   Chen, C.C., et al., *The angiogenic factors Cyr61 and connective tissue growth factor induce adhesive signaling in primary human skin fibroblasts.* J Biol Chem, 2001. **276**(13): p. 10443-52.

98.   Schober, J.M., et al., *Identification of a novel integrin alphaMbeta2 binding site in CCN1 (CYR61), a matricellular protein expressed in healing wounds and atherosclerotic lesions.* J Biol Chem 2003. **278**: p. 25808–25815.

99.   Yang, R., et al., *Biological functions and role of CCN1/Cyr61 in embryogenesis and tumorigenesis in the female reproductive system.* Molecular medicine reports, 2018. **17**(1): p. 3-10.

100.   Zhang, F., et al., *The matricellular protein Cyr61 is a key mediator of platelet-derived growth factor-induced cell migration.* Journal of Biological Chemistry, 2015. **290**(13): p. 8232-8242.

101.   Qin, Z., et al., *CCN1 Domain-specific Stimulation of Matrix Metalloproteinase-1 Expression Through αVβ3 Integrin in Human Skin Fibroblasts.* Journal of Biological Chemistry, 2013: p. jbc. M112. 424358.

102.   Jun, J.-I., et al., *The matricellular protein CCN1 induces fibroblast senescence and restricts fibrosis in cutaneous wound healing.* Nature cell biology, 2010. **12**(7): p. 676-685.

103.   Qin, Z., et al., *Oxidant exposure induces cysteine-rich protein 61 (CCN1) via c-Jun/AP-1 to reduce collagen expression in human dermal fibroblasts.* PLoS One, 2014. **9**(12): p. e115402.

104.   Mao, B., et al., *Hippo signaling in stress response and homeostasis maintenance.* Acta Biochim Biophys Sin (Shanghai), 2015. **47**(1): p. 2-9.

105.   Goldston, R.J., et al., *Plasmaphysik: eine Einführung*. 1998: Vieweg.

106.   Langmuir, I., *Oscillations in Ionized Gases*. Proc Natl Acad Sci U S A, 1928. **14**(8): p. 627-37.

107.   Kaufmann, M., *Plasma physics and fusion research. 2. rev.* 2013.

108.   von Woedtke, T., et al., *Plasma Medicine: A field of applied redox biology.* in vivo, 2019. **33**(4): p. 1011-1026.

109.   Heinlin, J., et al., *Plasma applications in medicine with a special focus on dermatology.* J Eur Acad Dermatol Venereol, 2011. **25**(1): p. 1-11.

110.   Parker, G., *Encyclopedia of materials: science and technology.* 2001.

111.   Weltmann, K.-D., et al., *The future for plasma science and technology.* Plasma Processes and Polymers, 2019. **16**(1): p. 1800118.

112.   Meichsner, J., et al., *Nonthermal plasma chemistry and physics*. 2012: CRC Press.

9. References

113.   Stoffels, E., et al., *Plasma needle: a non-destructive atmospheric plasma source for fine surface treatment of (bio) materials.* Plasma Sources Science and Technology, 2002. **11**(4): p. 383.

114.   Von Woedtke, T., et al., *Plasmas for medicine.* Physics Reports, 2013. **530**(4): p. 291-320.

115.   Lu, X., et al., *Reactive species in non-equilibrium atmospheric-pressure plasmas: Generation, transport, and biological effects.* Physics Reports, 2016. **630**: p. 1-84.

116.   Weltmann, K., et al., *Plasma medicine—current state of research and medical application.* Plasma Physics and Controlled Fusion, 2016. **59**(1): p. 014031.

117.   Bernhardt, T., et al., *Plasma medicine: Applications of cold atmospheric pressure plasma in dermatology.* Oxidative medicine and cellular longevity, 2019. **2019**.

118.   Kieft, I.E., et al., *Plasma treatment of mammalian vascular cells: a quantitative description.* IEEE transactions on plasma science, 2005. **33**(2): p. 771-775.

119.   Metelmann, H.-R., et al., *Comprehensive clinical plasma medicine: cold physical plasma for medical application*. 2018: Springer.

120.   Arndt, S., et al., *Comparing two different plasma devices kINPen and Adtec SteriPlas regarding their molecular and cellular effects on wound healing.* Clinical Plasma Medicine, 2018. **9**: p. 24-33.

121.   Arndt, S., et al., *Cold atmospheric plasma, a new strategy to induce senescence in melanoma cells.* Experimental Dermatology, 2013. **22**(4): p. 284-289.

122.   Hirst, A.M., et al., *Low temperature plasmas as emerging cancer therapeutics: the state of play and thoughts for the future.* Tumour Biol, 2016. **37**(6): p. 7021-31.

123.   Schmidt, A., et al., *Nrf2 signaling and inflammation are key events in physical plasma-spurred wound healing.* Theranostics, 2019. **9**(4): p. 1066-1084.

124.   Daeschlein, G., et al., *In vitro susceptibility of multidrug resistant skin and wound pathogens against low temperature atmospheric pressure plasma jet (APPJ) and dielectric barrier discharge plasma (DBD).* Plasma Processes and Polymers, 2014. **11**(2): p. 175-183.

125.   Daeschlein, G., et al., *In vitro susceptibility of important skin and wound pathogens against low temperature atmospheric pressure plasma jet (APPJ) and dielectric barrier discharge plasma (DBD).* Plasma Processes and Polymers, 2012. **9**(4): p. 380-389.

126.   Daeschlein, G., et al., *Antibacterial activity of an atmospheric pressure plasma jet against relevant wound pathogens in vitro on a simulated wound environment.* Plasma Processes and Polymers, 2010. **7**(3-4): p. 224-230.

127.   Guo, L., et al., *Mechanism of virus inactivation by cold atmospheric-pressure plasma and plasma-activated water.* Applied and environmental microbiology, 2018. **84**(17): p. e00726-18.

128.   Maisch, T., et al., *Decolonisation of MRSA, S. aureus and E. coli by cold-atmospheric plasma using a porcine skin model in vitro.* PloS one, 2012. **7**(4): e34610

129.   Brehmer, F., et al., *Alleviation of chronic venous leg ulcers with a hand-held dielectric barrier discharge plasma generator (PlasmaDerm® VU-2010): results of a monocentric, two-armed, open,*

prospective, randomized and controlled trial (NCT 01415622). Journal of the European Academy of Dermatology and Venereology, 2015. **29**(1): p. 148-155.

130. Daeschlein, G., et al., *Skin and wound decontamination of multidrug-resistant bacteria by cold atmospheric plasma coagulation.* JDDG: Journal der Deutschen Dermatologischen Gesellschaft, 2015. **13**(2): p. 143-149.

131. Isbary, G., et al., *Successful and safe use of 2 min cold atmospheric argon plasma in chronic wounds: results of a randomized controlled trial.* British Journal of Dermatology, 2012. **167**(2): p. 404-410.

132. Isbary, G., et al., *A first prospective randomized controlled trial to decrease bacterial load using cold atmospheric argon plasma on chronic wounds in patients.* British Journal of Dermatology, 2010. **163**(1): p. 78-82.

133. Ulrich, C., et al., *Clinical use of cold atmospheric pressure argon plasma in chronic leg ulcers: A pilot study.* Journal of wound care, 2015. **24**(5): p. 196-203.

134. Kalghatgi, S., et al., *Endothelial cell proliferation is enhanced by low dose non-thermal plasma through fibroblast growth factor-2 release.* Annals of biomedical engineering, 2010. **38**(3): p. 748-757.

135. Arndt, S., et al., *Cold atmospheric plasma (CAP) changes gene expression of key molecules of the wound healing machinery and improves wound healing in vitro and in vivo.* PloS one, 2013. **8**(11).

136. Haertel, B., et al., *Differential effect of non-thermal atmospheric-pressure plasma on angiogenesis.* Orléans-France, 2014: p. 152.

137. Haertel, B., et al., *Non-thermal atmospheric-pressure plasma possible application in wound healing.* Biomolecules & therapeutics, 2014. **22**(6): p. 477.

138. Ngo, M.H.T., et al., *Increased Fibroblast Cell Proliferation and Migration Using Atmospheric N2/Ar Micro-Plasma for the Stimulated Release of Fibroblast Growth Factor-7.* Plasma Processes and Polymers, 2014. **11**(1): p. 80-88.

139. Lendeckel, D., et al., *Proteomic changes of tissue-tolerable plasma treated airway epithelial cells and their relation to wound healing.* BioMed research international, 2015. **2015**.

140. Choi, J., et al., *Skin renewal activity of non-thermal plasma through the activation of β-catenin in keratinocytes.* Scientific reports, 2017. **7**(1): p. 1-11.

141. Kang, S.U., et al., *N2 non-thermal atmospheric pressure plasma promotes wound healing in vitro and in vivo: Potential modulation of adhesion molecules and matrix metalloproteinase-9.* Experimental dermatology, 2017. **26**(2): p. 163-170.

142. Schmidt, A., et al., *A cold plasma jet accelerates wound healing in a murine model of full-thickness skin wounds.* Experimental dermatology, 2017. **26**(2): p. 156-162.

143. Schmidt, A., et al., *Redox for repair: cold physical plasmas and Nrf2 signaling promoting wound healing.* Antioxidants, 2018. **7**(10): p. 146.

144. Schmidt, A., et al., *Identification of the molecular basis of non-thermal plasma-induced changes in human keratinocytes.* Plasma Medicine, 2013. **3**(1-2).

145. Barton, A., et al., *Nonthermal plasma increases expression of wound healing related genes in a keratinocyte cell line.* Plasma Medicine, 2013. **3**(1-2).

146. Ngo Thi, M.H., et al., *Enhancement of angiogenesis and epithelialization processes in mice with burn wounds through ROS/RNS signals generated by non-thermal N2/Ar micro-plasma.* Plasma Processes and Polymers, 2014. **11**(11): p. 1076-1088.

147. Weltmann, K.D., et al. , *Low temperature plasma applications in medicine.* Europhysics News, 2016. **47**(5-6): p. 39-42.

148. Wirtz, M., et al., *Actinic keratoses treated with cold atmospheric plasma.* Journal of the European Academy of Dermatology and Venereology, 2018. **32**(1): p. e37-e39.

149. Emmert, S., et al., *Atmospheric pressure plasma in dermatology: Ulcus treatment and much more.* Clinical Plasma Medicine, 2013. **1**(1): p. 24-29.

150. Cha, S., et al., *Plasma in dentistry.* Clinical plasma medicine, 2014. **2**(1): p. 4-10.

151. Bekeschus, S., et al., *The plasma jet kINPen–A powerful tool for wound healing.* Clinical Plasma Medicine, 2016. **4**(1): p. 19-28.

152. Schmidt, A., et al., *One Year Follow-Up Risk Assessment in SKH-1 Mice and Wounds Treated with an Argon Plasma Jet.* Int J Mol Sci, 2017. **18(4)**.

153. Wende, K., et al., *Risk assessment of a cold argon plasma jet in respect to its mutagenicity.* Mutat Res Genet Toxicol Environ Mutagen, 2016. **798-799**: p. 48-54.

154. Reuter, S., et al., *Detection of ozone in a MHz argon plasma bullet jet.* Plasma Sources Science and Technology, 2012. **21**(3): p. 034015.

155. Winter, J., et al., *Feed gas humidity: a vital parameter affecting a cold atmospheric-pressure plasma jet and plasma-treated human skin cells.* Journal of Physics D: Applied Physics, 2013. **46**(29): p. 295401.

156. Lieberman, M.A., et al., *Principles of plasma discharges and materials processing*. 2005: John Wiley & Sons.

157. Reuter, S., et al., *Controlling the ambient air affected reactive species composition in the effluent of an argon plasma jet.* IEEE Transactions on Plasma Science, 2012. **40**(11): p. 2788-2794.

158. Dunnill, C., et al., *Reactive oxygen species (ROS) and wound healing: the functional role of ROS and emerging ROS-modulating technologies for augmentation of the healing process.* Int Wound J, 2017. **14**(1): p. 89-96.

159. Görlach, A., *Redox regulation of the coagulation cascade.* Antioxidants & redox signaling, 2005. **7**(9-10): p. 1398-1404.

160. Krjukov, A.A., et al., *Activation of redox-systems of monocytes by hydrogen peroxide.* Biofactors, 2006. **26**(4): p. 283-292.

161. Driscoll, K.E., et al., *Mitochondrial-derived oxidants and quartz activation of chemokine gene expression*, in *Biological Reactive Intermediates VI*. 2001, Springer. p. 489-496.

162. Shi, M.M., et al., *Regulation of macrophage inflammatory protein-1 mRNA by oxidative stress.* Journal of Biological Chemistry, 1996. **271**(10): p. 5878-5883.

163. Fraticelli, A., et al., *Hydrogen peroxide and superoxide modulate leukocyte adhesion molecule expression and leukocyte endothelial adhesion.* Biochimica et Biophysica Acta (BBA)-Molecular Cell Research, 1996. **1310**(3): p. 251-259.

164. Hong, Y.-H., et al., *Hydrogen peroxide-mediated transcriptional induction of macrophage colony-stimulating factor by TGF-beta1.* The Journal of Immunology, 1997. **159**(5): p. 2418-2423.

165. Saccani, A., et al., *Redox regulation of chemokine receptor expression.* Proceedings of the National Academy of Sciences, 2000. **97**(6): p. 2761-2766.

166. Nishio, E., et al., *The involvement of reactive oxygen species and arachidonic acid in α1-adrenoceptor-induced smooth muscle cell proliferation and migration.* British journal of pharmacology, 1997. **121**(4): p. 665-670.

167. Ranjan, P., et al., *Redox-dependent expression of cyclin D1 and cell proliferation by Nox1 in mouse lung epithelial cells.* Antioxidants & redox signaling, 2006. **8**(9-10): p. 1447-1459.

168. Sen, C.K., et al., *Oxidant-induced vascular endothelial growth factor expression in human keratinocytes and cutaneous wound healing.* Journal of Biological Chemistry, 2002. **277**(36): p. 33284-33290.

169. Roy, S., et al., *Dermal wound healing is subject to redox control.* Molecular therapy, 2006. **13**(1): p. 211-220.

170. Schäfer, G., et al., *Oxidative stress regulates vascular endothelial growth factor-A gene transcription through Sp1-and Sp3-dependent activation of two proximal GC-rich promoter elements.* Journal of Biological Chemistry, 2003. **278**(10): p. 8190-8198.

171. Arndt, S., et al., *Effects of cold atmospheric plasma (CAP) on ss-defensins, inflammatory cytokines, and apoptosis-related molecules in keratinocytes in vitro and in vivo.* PLoS One, 2015. **10**(3): p. e0120041.

172. Bundscherer, L., et al., *Impact of non-thermal plasma treatment on MAPK signaling pathways of human immune cell lines.* Immunobiology, 2013. **218**(10): p. 1248-55.

173. Wende, K., et al., *Atmospheric pressure plasma jet treatment evokes transient oxidative stress in HaCaT keratinocytes and influences cell physiology.* Cell Biol Int, 2014. **38**(4): p. 412-25.

174. Bekeschus, S., et al., *Redox Stimulation of Human THP-1 Monocytes in Response to Cold Physical Plasma.* Oxid Med Cell Longev, 2016. **2016**: p. 5910695.

175. Kramer, A., et al., *Cold Physical Plasmas in the Field of Hygiene-Relevance, Significance, and Future Applications.* Plasma Process Polymer, 2015. **12**: p. 1410-1422.

9. References

176.   Schmidt, A., et al., *A cold plasma jet accelerates wound healing in a murine model of full-thickness skin wounds.* Exp Dermatol, 2017. **26**(2): p. 156-162.

177.   Jindam, A., et al., *Nrf2: A promising trove for diabetic wound healing.* Annals of translational medicine, 2017. **5**(23).

178.   Schmidt, A., et al., *Non-thermal plasma activates human keratinocytes by stimulation of antioxidant and phase II pathways.* J Biol Chem, 2015. **290**(11): p. 6731-50.

179.   Livak, K.J., et al., *Analysis of relative gene expression data using real-time quantitative PCR and the 2(-Delta Delta C(T)) Method.* Methods, 2001. **25**(4): p. 402-8.

180.   Wende, K., et al., *Identification of the biologically active liquid chemistry induced by a nonthermal atmospheric pressure plasma jet.* Biointerphases, 2015. **10**(2): p. 029518.

181.   Loo, A.E., et al., *Effects of hydrogen peroxide on wound healing in mice in relation to oxidative damage.* PLoS One, 2012. **7**(11): p. e49215.

182.   Stamm, A., et al., *In vitro wound healing assays–state of the art.* BioNanoMaterials, 2016. **17**(1-2): p. 79-87.

183.   Loo, A.E., et al., *Mechanism of hydrogen peroxide-induced keratinocyte migration in a scratch-wound model.* Free Radic Biol Med, 2011. **51**(4): p. 884-92.

184.   Das, T., et al., *A molecular mechanotransduction pathway regulates collective migration of epithelial cells.* Nature Cell Biology, 2015. **17**(3): p. 276-287.

185.   Loo, A.E.K., et al., *Effects of hydrogen peroxide in a keratinocyte-fibroblast co-culture model of wound healing.* Biochemical and Biophysical Research Communications, 2012. **423**(2): p. 253-258.

186.   Maas-Szabowski, N., et al., *Keratinocyte growth regulation in defined organotypic cultures through IL-1-induced keratinocyte growth factor expression in resting fibroblasts.* J Invest Dermatol, 2000. **114**(6): p. 1075-84.

187.   Wang, Z., et al., *Enhanced keratinocyte proliferation and migration in co-culture with fibroblasts.* PLoS One, 2012. **7**(7): p. e40951.

188.   Seo, G.Y., et al., *A Novel Synthetic Material, BMM, Accelerates Wound Repair by Stimulating Re-Epithelialization and Fibroblast Activation.* Int J Mol Sci, 2018. **19**(4).

189.   Seo, G.Y., et al., *TMF and glycitin act synergistically on keratinocytes and fibroblasts to promote wound healing and anti-scarring activity.* Experimental and Molecular Medicine, 2017. **49**.

190.   Nyström, A., et al., *Collagen VII plays a dual role in wound healing.* The Journal of clinical investigation, 2013. **123**(8): p. 3498-3509.

191.   Hattori, N., et al., *MMP-13 plays a role in keratinocyte migration, angiogenesis, and contraction in mouse skin wound healing.* The American journal of pathology, 2009. **175**(2): p. 533-546.

192.   Knäuper, V., et al., *Biochemical characterization of human collagenase-3.* Journal of Biological Chemistry, 1996. **271**(3): p. 1544-1550.

193.   Knäuper, V., et al., *Cellular mechanisms for human procollagenase-3 (MMP-13) activation Evidence that MT1-MMP (MMP-14) and gelatinase a (MMP-2) are able to generate active enzyme.* Journal of Biological Chemistry, 1996. **271**(29): p. 17124-17131.

194.   Tornavaca, O., et al., *ZO-1 controls endothelial adherens junctions, cell–cell tension, angiogenesis, and barrier formation.* Journal of Cell Biology, 2015. **208**(6): p. 821-838.

195.   Schmidt, A., et al., *Periodic Exposure of Keratinocytes to Cold Physical Plasma: An In Vitro Model for Redox-Related Diseases of the Skin.* Oxidative medicine and cellular longevity, 2016. **2016**: p. 9816072-9816072.

196.   Houreld, N.N., et al., *Cell Adhesion Molecules are Mediated by Photobiomodulation at 660 nm in Diabetic Wounded Fibroblast Cells.* Cells, 2018. **7**(4): p. 30.

197.   Gorbanev, Y., et al., *Analysis of short-lived reactive species in plasma–air–water systems: the dos and the do nots*. 2018. p. 13151-13158.

198.   Haertel, B., et al., *Differential influence of components resulting from atmospheric-pressure plasma on integrin expression of human HaCaT keratinocytes.* BioMed research international, 2013. **2013**: p. 761451-761451.

199.   Ezeriņa, D., et al., *N-acetyl cysteine functions as a fast-acting antioxidant by triggering intracellular H2S and sulfane sulfur production.* Cell chemical biology, 2018. **25**(4): p. 447-459. e4.

200.   Aldini, G., et al., *N-Acetylcysteine as an antioxidant and disulphide breaking agent: the reasons why.* Free radical research, 2018. **52**(7): p. 751-762.

201.   Ramaesh, T., et al., *Effects of N-acetylcysteine on matrix metalloproteinase-9 secretion and cell migration of human corneal epithelial cells.* Eye (Lond), 2012. **26**(8): p. 1138-44.

202.   Mao, G., et al., *N-acetyl-L-cysteine increases MnSOD activity and enhances the recruitment of quiescent human fibroblasts to the proliferation cycle during wound healing.* Molecular biology reports, 2016. **43**(1): p. 31-39.

203.   Sato, N., et al., *N-Acetyl cysteine (NAC) inhibits proliferation, collagen gene transcription, and redox stress in rat palatal mucosal cells.* Dent Mater, 2009. **25**(12): p. 1532-40.

204.   Kopp, J., et al., *N-acetyl-L-cysteine abrogates fibrogenic properties of fibroblasts isolated from Dupuytren's disease by blunting TGF-beta signalling.* Journal of cellular and molecular medicine, 2006. **10**: p. 157-65.

205.   Glady, A., et al., *Involvement of NADPH oxidase 1 in UVB-induced cell signaling and cytotoxicity in human keratinocytes.* Biochemistry and biophysics reports, 2018. **14**: p. 7-15.

206.   Redondo, P., et al., *N-acetylcysteine downregulates vascular endothelial growth factor production by human keratinocytes in vitro.* Arch Dermatol Res, 2000. **292**(12): p. 621-8.

207.   Kaushik, A.K., et al., *Metabolomic profiling identifies biochemical pathways associated with castration-resistant prostate cancer.* J Proteome Res, 2014. **13**(2): p. 1088-100.

9. References

208. Schmidt, A., et al., *Cold Physical Plasma Modulates p53 and Mitogen-Activated Protein Kinase Signaling in Keratinocytes.* Oxidative Medicine and Cellular Longevity, 2019. **2019**: p. 16.

209. Liu, J.-R., et al., *Low temperature plasma promoting fibroblast proliferation by activating the NF-κB pathway and increasing cyclinD1 expression.* Scientific Reports, 2017. **7**(1): p. 11698.

210. Paromov, V., et al., *The influence of N-acetyl-L-cysteine on oxidative stress and nitric oxide synthesis in stimulated macrophages treated with a mustard gas analogue.* BMC cell biology, 2008. **9**(1): p. 33.

211. Spagnuolo, G., et al., *Effect of N-acetyl-L-cysteine on ROS production and cell death caused by HEMA in human primary gingival fibroblasts.* Biomaterials, 2006. **27**(9): p. 1803-1809.

212. Shome, D., et al., *The HIPPO Transducer YAP and Its Targets CTGF and Cyr61 Drive a Paracrine Signalling in Cold Atmospheric Plasma-Mediated Wound Healing.* Oxidative Medicine and Cellular Longevity, 2020. **2020**.

213. Rognoni, E., et al., *The Roles of YAP/TAZ and the Hippo Pathway in Healthy and Diseased Skin.* Cells, 2019. **8**(5): p. 411.

214. Wang, Y., et al., *The Hippo pathway in tissue homeostasis and regeneration.* Protein Cell, 2017. **8**(5): p. 349-359.

215. Xiao, L., et al., *KIBRA regulates Hippo signaling activity via interactions with large tumor suppressor kinases.* Journal of Biological Chemistry, 2011. **286**(10): p. 7788-7796.

216. Wada, K.I., et al., *Hippo pathway regulation by cell morphology and stress fibers.* Development, 2011. **138**(18): p. 3907-3914.

217. Dupont, S., et al., *Role of YAP/TAZ in mechanotransduction.* Nature, 2011. **474**(7350): p. 179-183.

218. Ege, N., et al., *Quantitative analysis reveals that actin and Src-family kinases regulate nuclear YAP1 and its export.* Cell systems, 2018. **6**(6): p. 692-708. e13.

219. Elosegui-Artola, A., et al., *Force triggers YAP nuclear entry by regulating transport across nuclear pores.* Cell, 2017. **171**(6): p. 1397-1410. e14.

220. Manning, S.A., et al., *Dynamic fluctuations in subcellular localization of the Hippo pathway effector yorkie in vivo.* Current Biology, 2018. **28**(10): p. 1651-1660. e4.

221. Park, S.-K., et al., *Hydrogen peroxide is a novel inducer of connective tissue growth factor.* Biochemical and biophysical research communications, 2001. **284**(4): p. 966-971.

222. Matsuda, S., et al., *Induction of connective tissue growth factor in retinal pigment epithelium cells by oxidative stress.* Japanese journal of ophthalmology, 2006. **50**(3): p. 229-234.

223. Aguiar, D.P., et al., *New strategy to control cell migration and metastasis regulated by CCN2/CTGF.* Cancer cell international, 2014. **14**(1): p. 61.

224. Francischetti, I.M., et al., *Cyr61/CCN1 displays high-affinity binding to the somatomedin B 1–44 domain of vitronectin.* PLoS One, 2010. **5**(2).

225. Tsai, C.-C., et al., *Alteration of connective tissue growth factor (CTGF) expression in orbital fibroblasts from patients with Graves' ophthalmopathy.* PLoS One, 2015. **10**(11).

226. Murphy-Marshman, H., et al., *Antioxidants and NOX1/NOX4 inhibition blocks TGFβ1-induced CCN2 and α-SMA expression in dermal and gingival fibroblasts.* PloS one, 2017. **12**(10).

227. Wu, Y., et al., *Rapamycin upregulates connective tissue growth factor expression in hepatic progenitor cells through TGF-β-Smad2 dependent signaling.* Frontiers in pharmacology, 2018. **9**: p. 877.

228. Qin, Z., et al., *Oxidant exposure induces cysteine-rich protein 61 (CCN1) via c-Jun/AP-1 to reduce collagen expression in human dermal fibroblasts.* PLoS One, 2014. **9**(12).

229. Minhas, U., et al., *Pattern of expression of CCN family members Cyr61, CTGF and NOV in human acute and chronic wounds.* Experimental and therapeutic medicine, 2011. **2**(4): p. 641-645.

230. Seher, A., et al., *Gene expression profiling of connective tissue growth factor (CTGF) stimulated primary human tenon fibroblasts reveals an inflammatory and wound healing response in vitro.* Mol Vis, 2011. **17**: p. 53-62.

231. Seher, A., et al., *Gene expression profiling of connective tissue growth factor (CTGF) stimulated primary human tenon fibroblasts reveals an inflammatory and wound healing response in vitro.* Molecular vision, 2011. **17**: p. 53-62.

232. Kiwanuka, E., et al., *CCN2 is transiently expressed by keratinocytes during re-epithelialization and regulates keratinocyte migration in vitro by the ras-MEK-ERK signaling pathway.* The Journal of surgical research, 2013. **185**.

233. Seo, G.Y., et al., *A Novel Synthetic Material, BMM, Accelerates Wound Repair by Stimulating Re-Epithelialization and Fibroblast Activation.* International journal of molecular sciences, 2018. **19**(4): p. 1164.

234. Horiba, M., et al., *Cytoprotective effects of mild plasma-activated medium against oxidative stress in human skin fibroblasts.* Scientific reports, 2017. **7**: p. 42208.

235. Madan, E., et al., *FAT1 is a novel upstream regulator of HIF1α and invasion of high grade glioma.* International journal of cancer, 2016. **139**(11): p. 2570-2582.

236. Al-Greene, N.T., et al., *Four jointed box 1 promotes angiogenesis and is associated with poor patient survival in colorectal carcinoma.* PloS one, 2013. **8**(7): p. e69660-e69660.

List of Tables

List of Figures

117

Supplementary Data

Figure i. Representative figure of cell migration assay of coculture with the ratio of 1:5 for GM Fbs: HaCaT cells. 10,000 GM Fbs and 50,000 HaCaT cells were seeded in the image lock plate 24 hours prior to the experiment. Cells were starved for about 18-20 hours and treated with 10s or 30s direct CAP treatment or incubated with untreated, 10s, 30s and 60s of CAP treated medium (indirect treatment). Compared to untreated control, indirect treatment (all 10, 30 and 60s) improved cell migration of the coculture. But direct treatment could not improve the cell migration compared to untreated control.
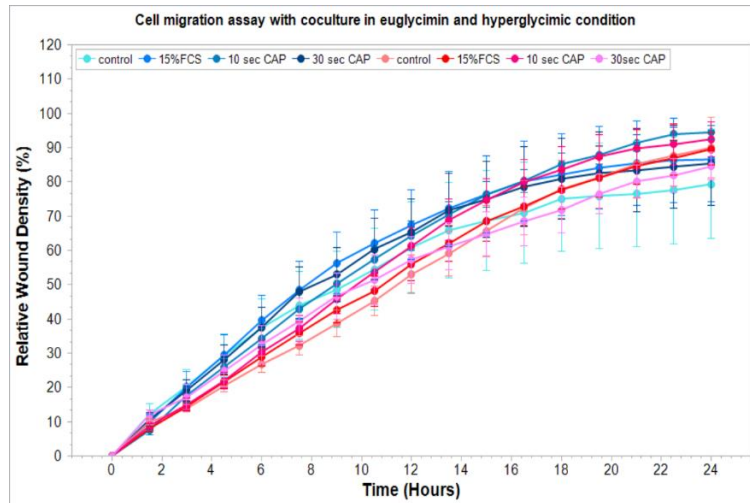
Figure ii. Representative figure of cell migration assay of coculture in euglycimic and hyperglycemic condition. The blue lines correspond to euglycimic condition and the pink lines to hyperglycemic condition. For euglycemic condition, normal RPMI containing 2gm/1000ml of D glucose was used. For hyperglycemia, additional 2.5gm glucose was added in the medium. Cell migration assay was performed with untreated, 15% FCS medium, 10s and 30s CAP treated medium. No significant difference in cell migration was observed between euglycemic and hyperglycemic condition.
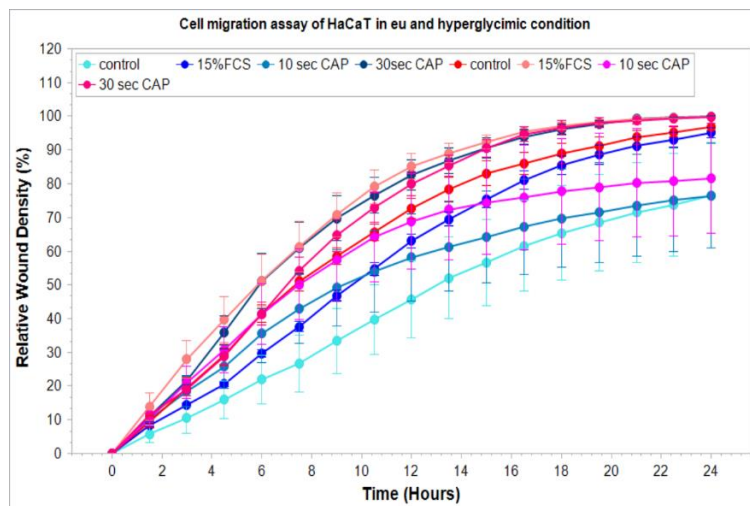
Figure iii. Representative figure of cell migration assay of HaCaT cells in euglycimic and hyperglycemic condition. The blue lines correspond to euglycemic condition and the pink lines to hyperglycemic condition. Cell migration assay was performed with untreated, 15% FCS medium, 10s and 30s CAP treated medium. Cell migration tends to be faster in hyperglycemic condition compared to euglycemic condition.
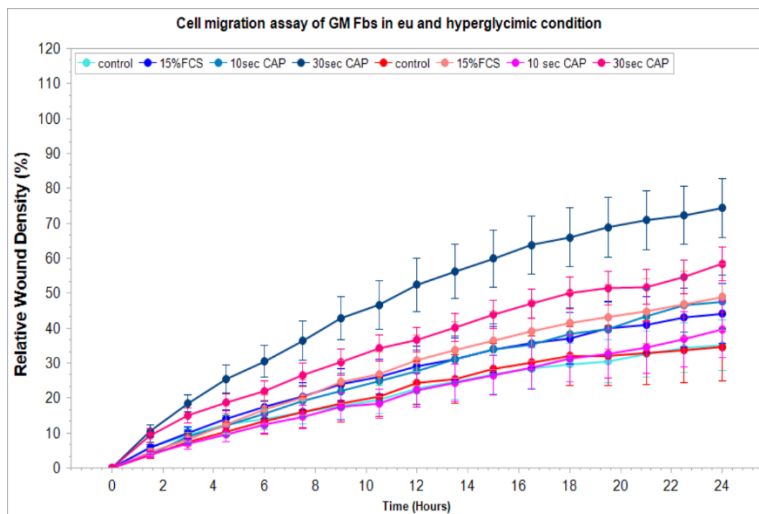
Figure iv. Representative figure of cell migration assay of GM Fbs in euglycimic and hyperglycemic condition. The blue lines correspond to euglycimic condition and the pink lines to hyperglycemic condition. Cell migration assay was performed with untreated, 15% FCS medium, 10s and 30s CAP treated medium. No significant difference in cell migration was observed between euglycemic and hyperglycemic condition.
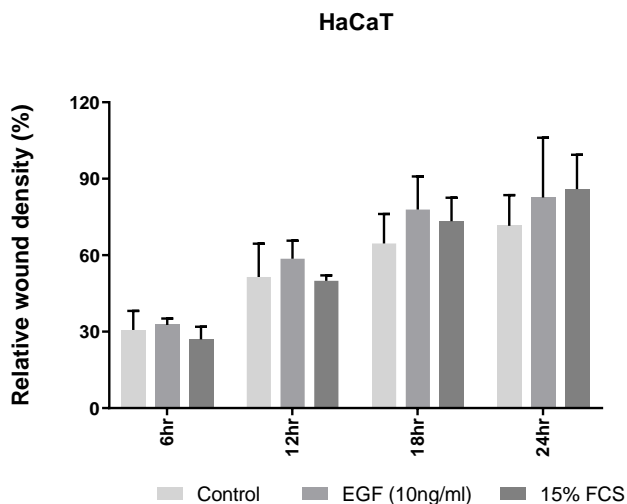
Figure v. Summation of relative wound density of HaCaT monoculture with untreated, 10ng/ml EGF and 15% FCS stimulation. Migration assay was monitored at 6, 12, 18 and 24 hours. Compared to control, EGF and 15% FCS accelerates cell migration, though not significant. Data is presented as mean $\pm$ SD from three independent experiments, each in triplicate. Statistical analysis was carried out with two-way ANOVA.
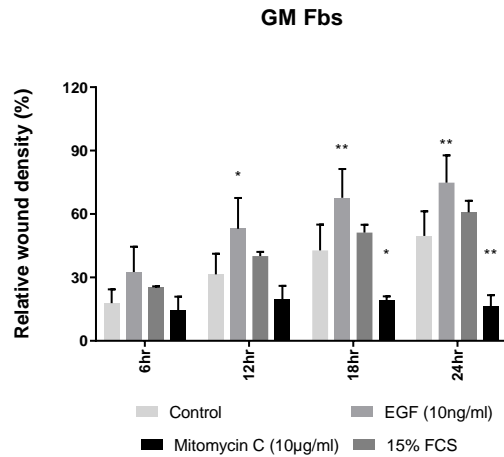
GM Fbs

Figure vi. Summation of relative wound density of GM Fbs with untreated (control), 10ng/ml EGF, 15% FCS and 10µg/ml Mitomycin C stimulation. Migration assay was monitored at 6, 12, 18 and 24 hours. Compared to control, EGF significantly accelerates cell migration. Mitomycin C also significantly decelerates the cell migration. Data is presented as mean ± SD from three independent experiments, each in triplicate. Statistical analysis was carried out with two-way ANOVA.
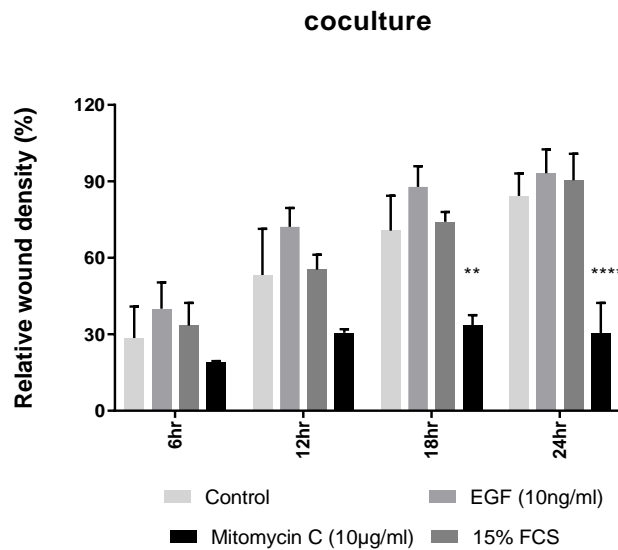
coculture

Figure vii. Summation of relative wound density of coculture with untreated (control), 10ng/ml EGF, 15% FCS and 10µg/ml Mitomycin C stimulation. Migration assay was monitored at 6, 12, 18 and 24 hours. Compared to control, EGF accelerates cell migration, though not significant. Mitomycin C significantly decelerates the cell migration. Data is presented as mean ± SD from three independent experiments, each in triplicate. Statistical analysis was carried out with two-way ANOVA.

(A)
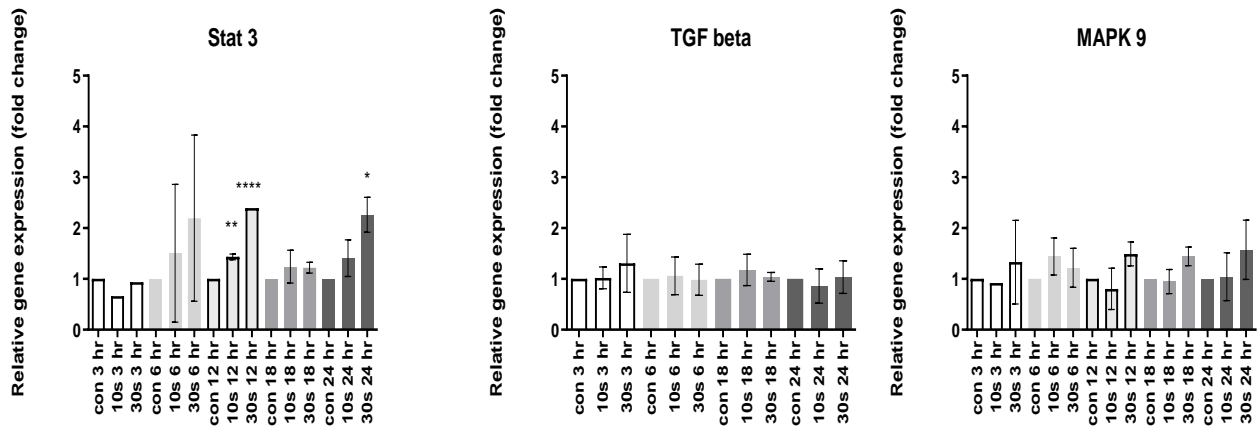
(B)
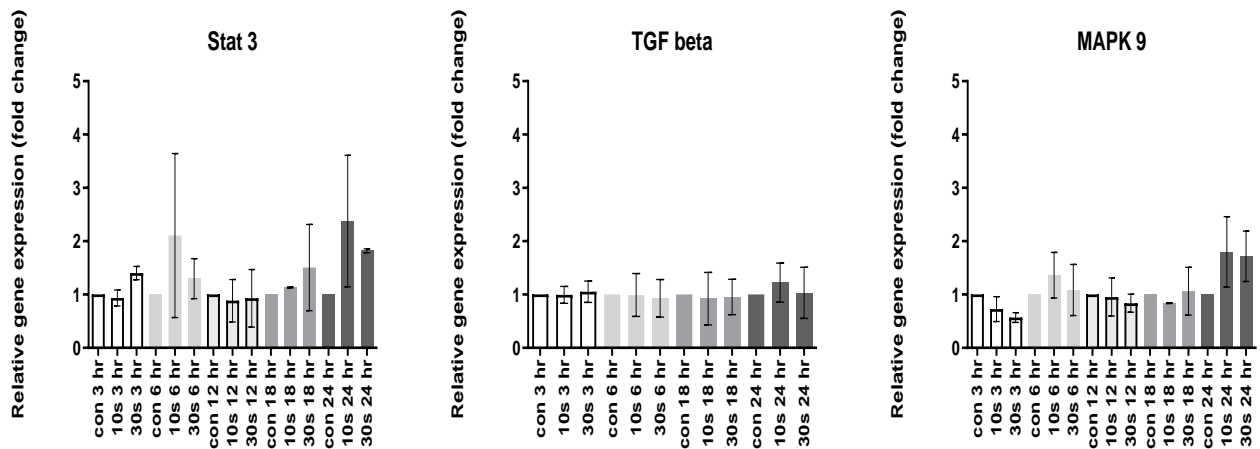
Figure viii. Relative fold change of mRNA expression upon CAP treatment in GM Fbs (A) and HaCaT cells (B). Cells were treated for 10s, 30s and 60s. 3, 6, 12, 18 and 24 hours after the treatment RNA was isolated, cDNA was prepared and gene expression analysis for Stat3, TGF beta and MAPK 9 was carried out. Data is presented as mean ± SD from two independent experiments. Statistical analysis was performed using one-way ANOVA, along with normalization to the untreated control.
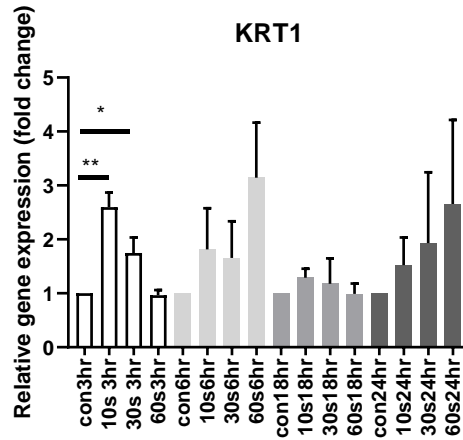
Figure ix. Relative mRNA expression of Keratin-1 (KRT-1) 3, 6, 18 and 24 hours after indirect CAP treatment. HaCaT cells were treated for 10s, 30s and 60s. Compared to control, both 10s and 30s could significantly increase the KRT-1 mRNA expression at 3 hours. Data is presented as mean ± SD from three independent experiments. Statistical analysis was carried out with one-way ANOVA.
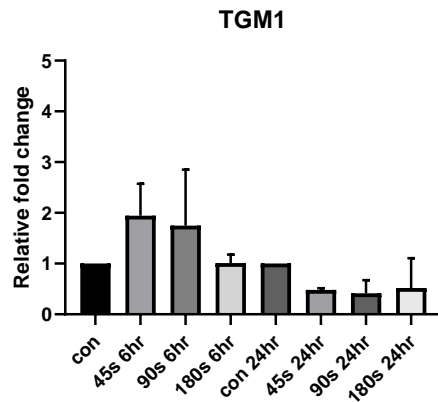
Figure x. Relative mRNA expression of Transglutaminase 1 (TGM-1) 6 and 24 hours after direct CAP treatment. HaCaT cells were directly treated for 45s, 60s and 180s. Compared to control, both 45s and 90s could increase the TGM-1 mRNA expression at 6 hours. Data is presented as mean ± SD from three independent experiments. Statistical analysis was carried out with one-way ANOVA.

Supplementary Data

Table 1. Analyzed genes by RT^2 PCR Profiler array-HIPPO signaling pathway.

Position	Unigene	Refseq	Symbol	Description
A01	Hs.514581	NM_001614	ACTG1	Actin, gamma 1
A02	Hs.528051	NM_133265	AMOT	Angiomotin
A03	Hs.503594	NM_130847	AMOTL1	Angiomotin like 1
A04	Hs.426312	NM_016201	AMOTL2	Angiomotin like 2
A05	Hs.141125	NM_004346	CASP3	Caspase 3, apoptosis-related cysteine peptidase
A06	Hs.244723	NM_001238	CCNE1	Cyclin E1
A07	Hs.727669	NM_057749	CCNE2	Cyclin E2
A08	Hs.126135	NM_201253	CRB1	Crumbs homolog 1 (Drosophila)
A09	Hs.710092	NM_173689	CRB2	Crumbs homolog 2 (Drosophila)
A10	Hs.150319	NM_139161	CRB3	Crumbs homolog 3 (Drosophila)
A11	Hs.631725	NM_001893	CSNK1D	Casein kinase 1, delta
A12	Hs.474833	NM_001894	CSNK1E	Casein kinase 1, epsilon
B01	Hs.199850	NM_003737	DCHS1	Dachsous 1 (Drosophila)
B02	Hs.655664	NM_017639	DCHS2	Dachsous 2 (Drosophila)
B03	Hs.226483	NM_006729	DIAPH2	Diaphanous homolog 2 (Drosophila)
B04	Hs.292549	NM_004087	DLG1	Discs, large homolog 1 (Drosophila)
B05	Hs.118640	NM_004422	DVL2	Dishevelled, dsh homolog 2 (Drosophila)
B06	Hs.481371	NM_005245	FAT1	FAT tumor suppressor homolog 1 (Drosophila)
B07	Hs.591255	NM_001447	FAT2	FAT tumor suppressor homolog 2 (Drosophila)
B08	Hs.98523	NM_0010087 81	FAT3	FAT tumor suppressor homolog 3 (Drosophila)
B09	Hs.563205	NM_024582	FAT4	FAT tumor suppressor homolog 4 (Drosophila)
B10	Hs.39384	NM_014344	FJX1	Four jointed box 1 (Drosophila)
B11	Hs.655675	NM_004466	GPC5	Glypican 5
B12	Hs.731417	NM_022740	HIPK2	Homeodomain interacting protein kinase 2
C01	Hs.58877	NM_031935	HMCN1	Hemicentin 1
C02	Hs.655832	NM_198086	AJUBA	Jub, ajuba homolog (Xenopus laevis)
C03	Hs.549084	NM_004690	LATS1	LATS, large tumor suppressor, homolog 1 (Drosophila)
C04	Hs.78960	NM_014572	LATS2	LATS, large tumor suppressor, homolog 2 (Drosophila)
C05	Hs.621057	NM_014240	LIMD1	LIM domains containing 1
C06	Hs.740619	NM_153713	LIX1L	Lix1 homolog (mouse)-like
C07	Hs.513983	NM_004140	LLGL1	Lethal giant larvae homolog 1 (Drosophila)
C08	Hs.514477	NM_004524	LLGL2	Lethal giant larvae homolog 2 (Drosophila)
C09	Hs.720220	NM_005578	LPP	LIM domain containing preferred translocation partner in lipoma

131

* Table continued in the next page

C10	Hs.125503	NM_002753	MAPK10	Mitogen-activated protein kinase 10
C11	Hs.526754	NM_002398	MEIS1	Meis homeobox 1
C12	Hs.691454	NM_173468	MOB1B	MOB1, Mps One Binder kinase activator-like 1A (yeast)
D01	Hs.602092	NM_018221	MOB1A	MOB1, Mps One Binder kinase activator-like 1B (yeast)
D02	Hs.169378	NM_003829	MPDZ	Multiple PDZ domain protein
D03	Hs.652312	NM_022474	MPP5	Membrane protein, palmitoylated 5 (MAGUK p55 subfamily member 5)
D04	Hs.655432	NM_020998	MST1	Macrophage stimulating 1 (hepatocyte growth factor-like)
D05	Hs.202453	NM_002467	MYC	V-myc myelocytomatosis viral oncogene homolog)
D06	Hs.187898	NM_000268	NF2	Neurofibromin 2 (merlin)
D07	Hs.462348	NM_015102	NPHP4	Nephronophthisis 4
D08	Hs.131489	NM_019619	PARD3	Par-3 partitioning defective 3 homolog (C. elegans)
D09	Hs.654920	NM_032510	PARD6G	Par-6 partitioning defective 6 homolog gamma (C. elegans)
D10	Hs.580547	NM_001099771	POTEF	POTE ankyrin domain family, member F
D11	Hs.491440	NM_001009552	PPP2CB	Protein phosphatase 2, catalytic subunit, beta isozyme
D12	Hs.467192	NM_014225	PPP2R1A	Protein phosphatase 2, regulatory subunit A, alpha
E01	Hs.380372	NM_018461	PPP2R2D	Protein phosphatase 2, regulatory subunit B, delta
E02	Hs.478199	NM_002740	PRKCI	Protein kinase C, iota
E03	Hs.496255	NM_002744	PRKCZ	Protein kinase C, zeta
E04	Hs.688910	NM_005401	PTPN14	Protein tyrosine phosphatase, non-receptor type 14
E05	Hs.631504	NM_014737	RASSF2	Ras association (RalGDS/AF-6) domain family member 2
E06	Hs.522895	NM_032023	RASSF4	Ras association (RalGDS/AF-6) domain family member 4
E07	Hs.463041	NM_012102	RERE	Arginine-glutamic acid dipeptide (RE) repeats
E08	Hs.642842	NM_021818	SAV1	Salvador homolog 1 (Drosophila)
E09	Hs.436329	NM_182706	SCRIB	Scribbled homolog (Drosophila)
E10	Hs.604588	NM_005900	SMAD1	SMAD family member 1
E11	Hs.738869	NM_006281	STK3	Serine/threonine kinase 3
E12	Hs.472838	NM_006282	STK4	Serine/threonine kinase 4
F01	Hs.597434	NM_020791	TAOK1	TAO kinase 1
F02	Hs.291623	NM_004783	TAOK2	TAO kinase 2
F03	Hs.644420	NM_016281	TAOK3	TAO kinase 3
F04	Hs.409911	NM_000116	TAZ	Tafazzin
F05	Hs.655331	NM_021961	TEAD1	TEA domain family member 1 (SV40 transcriptional enhancer factor)

F06	Hs.515534	NM_003598	TEAD2	TEA domain family member 2
F07	Hs.485205	NM_003214	TEAD3	TEA domain family member 3
F08	Hs.94865	NM_003213	TEAD4	TEA domain family member 4
F09	Hs.743990	NM_175610	TJP1	Tight junction protein 1 (zona occludens 1)
F10	Hs.50382	NM_004817	TJP2	Tight junction protein 2 (zona occludens 2)
F11	Hs.137569	NM_003722	TP63	Tumor protein p63
F12	Hs.284217	NM_005786	TSHZ1	Teashirt zinc finger homeobox 1
G01	Hs.473117	NM_173485	TSHZ2	Teashirt zinc finger homeobox 2
G02	Hs.278436	NM_020856	TSHZ3	Teashirt zinc finger homeobox 3
G03	Hs.248164	NM_005430	WNT1	Wingless-type MMTV integration site family, member 1
G04	Hs.585010	NM_001080436	WTIP	Wilms tumor 1 interacting protein
G05	Hs.484047	NM_015238	WWC1	WW and C2 domain containing 1
G06	Hs.477921	NM_015472	WWTR1	WW domain containing transcription regulator 1
G07	Hs.503692	NM_006106	YAP1	Yes-associated protein 1
G08	Hs.643544	NM_003404	YWHAB	Tyrosine 3-monooxygenase/tryptophan 5-monooxygenase activation protein, beta polypeptide
G09	Hs.513851	NM_006761	YWHAE	Tyrosine 3-monooxygenase/tryptophan 5-monooxygenase activation protein, epsilon polypeptide
G10	Hs.74405	NM_006826	YWHAQ	Tyrosine 3-monooxygenase/tryptophan 5-monooxygenase activation protein, theta polypeptide
G11	Hs.492407	NM_003406	YWHAZ	Tyrosine 3-monooxygenase/tryptophan 5-monooxygenase activation protein, zeta polypeptide
G12	Hs.523710	NM_032283	ZDHHC18	Zinc finger, DHHC-type containing 18
H01	Hs.520640	NM_001101	ACTB	Actin, beta
H02	Hs.534255	NM_004048	B2M	Beta-2-microglobulin
H03	Hs.592355	NM_002046	GAPDH	Glyceraldehyde-3-phosphate dehydrogenase
H04	Hs.412707	NM_000194	HPRT1	Hypoxanthine phosphoribosyltransferase 1
H05	Hs.546285	NM_001002	RPLP0	Ribosomal protein, large, P0
H06	N/A	SA_00105	HGDC	Human Genomic DNA Contamination
H07	N/A	SA_00104	RTC	Reverse Transcription Control
H08	N/A	SA_00104	RTC	Reverse Transcription Control
H09	N/A	SA_00104	RTC	Reverse Transcription Control
H10	N/A	SA_00103	PPC	Positive PCR Control
H11	N/A	SA_00103	PPC	Positive PCR Control
H12	N/A	SA_00103	PPC	Positive PCR Control

Supplementary Data

Table 2. Fold regulation of HIPPO signaling genes in GM Fbs (RT^2 array)

Gene	Fold regulation	p value	Fold regulation	p value
ACTG1	1.62	0.874869	2.19	0.517911
AMOT	1.30	0.998960	2.19	0.598629
AMOTL1	1.53	0.774328	4.16	0.105547
AMOTL2	1.48	0.849396	3.90	0.090454
CASP3	1.41	0.814566	3.37	0.061797
CCNE1	1.48	0.682665	3.13	0.067478
CCNE2	1.45	0.638782	2.83	0.048263
CRB1	1.10	0.865559	1.03	0.932514
CRB2	1.03	0.672360	1.11	0.659797
CRB3	-1.50	0.320552	-1.63	0.363436
CSNK1D	1.53	0.235158	1.27	0.554796
CSNK1E	1.49	0.449675	1.65	0.329587
DCHS1	3.93	0.435280	13.01	0.339051
DCHS2	1.06	0.795637	3.80	0.181995
DIAPH2	1.45	0.638400	2.01	0.229300
DLG1	1.38	0.858911	2.17	0.279271
DVL2	1.37	0.782985	2.61	0.112809
FAT1	1.52	0.582935	3.39	0.047915
FAT2	2.03	0.752296	3.84	0.201613
FAT3	1.55	0.952331	4.80	0.067670
FAT4	1.54	0.750252	2.31	0.288413
FJX1	2.02	0.860189	5.95	0.085925
GPC5	-1.16	0.982058	2.04	0.383451
HIPK2	1.38	0.716161	3.80	0.112353
HMCN1	1.48	0.358973	1.31	0.562095
AJUBA	1.38	0.718700	1.36	0.745014
LATS1	1.38	0.729821	4.76	0.030073
LATS2	1.51	0.646429	4.25	0.063708
LIMD1	1.58	0.939951	2.84	0.292172
LIX1L	1.64	0.807102	2.78	0.315281
LLGL1	1.46	0.871232	2.72	0.251759
LLGL2	1.55	0.696967	2.45	0.220092
LPP	1.53	0.487055	3.13	0.065169
MAPK10	1.94	0.275996	1.21	0.960824
MEIS1	1.27	0.651731	1.22	0.954104
MOB1B	1.46	0.888892	3.88	0.137801
MOB1A	1.43	0.762460	3.05	0.100418
MPDZ	1.50	0.668981	1.75	0.460211
MPP5	1.43	0.819766	3.10	0.125213
MST1	1.07	0.940090	1.59	0.310818
MYC	1.50	0.553440	1.96	0.208274
NF2	1.40	0.802972	4.03	0.031044
NPHP4	1.29	0.293442	-1.35	0.561039

* Table continued in the next page   134

PARD3	1.16	0.940164	1.95	0.336930
PARD6G	1.40	0.461229	1.53	0.334145
POTEF	-1.31	0.563080	2.28	0.108282
PPP2CB	1.64	0.390416	2.43	0.090477
PPP2R1A	1.68	0.480073	2.06	0.282850
PPP2R2D	1.54	0.802021	4.66	0.053238
PRKCI	1.64	0.773106	2.85	0.206932
PRKCZ	1.69	0.621061	2.17	0.323039
PTPN14	1.50	0.790166	2.44	0.474564
RASSF2	1.45	0.648155	2.29	0.216716
RASSF4	1.21	0.773764	1.51	0.707979
RERE	1.60	0.333979	1.63	0.305134
SAV1	1.54	0.538410	1.82	0.290866
SCRIB	1.40	0.668939	4.79	0.083976
SMAD1	1.49	0.702622	2.74	0.163789
STK3	1.78	0.810184	2.73	0.370386
STK4	1.64	0.750085	3.89	0.173296
TAOK1	1.13	0.666718	2.48	0.147607
TAOK2	1.14	0.968689	3.67	0.128899
TAOK3	-1.26	0.482525	1.67	0.217684
TAZ	1.20	0.827108	1.60	0.385994
TEAD1	1.06	0.958445	3.06	0.125905
TEAD2	1.28	0.823072	2.22	0.198271
TEAD3	1.17	0.813578	2.14	0.144745
TEAD4	1.07	0.994433	2.17	0.063983
TJP1	1.19	0.887092	3.15	0.106808
TJP2	1.09	0.964879	2.77	0.112749
TP63	-1.38	0.366007	1.68	0.105568
TSHZ1	1.02	0.943331	1.87	0.313155
TSHZ2	-1.30	0.615788	1.12	0.859503
TSHZ3	1.36	0.814021	2.31	0.191378
WNT1	-1.08	0.698825	2.53	0.192024
WTIP	1.56	0.838290	3.85	0.058564
WWC1	1.66	0.611361	3.78	0.051908
WWTR1	1.32	0.950449	3.19	0.195357
YAP1	1.30	0.910557	4.35	0.077360
YWHAB	1.15	0.756097	-1.72	0.290050
YWHAE	1.74	0.579597	2.83	0.148402
YWHAQ	1.56	0.594932	1.88	0.366352
YWHAZ	1.25	0.907335	2.67	0.183889
ZDHHC18	1.46	0.921145	4.14	0.147844
ACTB	1.03	0.998372	2.35	0.136226
B2M	-1.06	0.608659	1.14	0.405699
GAPDH	1.07	0.984755	1.67	0.310870
HPRT1	-1.00	0.910039	1.37	0.236489
RPLP0	1.06	0.667574	-1.55	0.015845

Supplementary Data

Table 3. Analyzed genes by RT^2 PCR Profiler array-Extracellular matrix and adhesion molecules.

Position	Unigene	Refseq	Symbol	Description
A01	Hs.643357	NM_006988	ADAMTS1	ADAM metallopeptidase with thrombospondin type 1 motif, 1
A02	Hs.131433	NM_139025	ADAMTS13	ADAM metallopeptidase with thrombospondin type 1 motif, 13
A03	Hs.271605	NM_007037	ADAMTS8	ADAM metallopeptidase with thrombospondin type 1 motif, 8
A04	Hs.502328	NM_000610	CD44	CD44 molecule (Indian blood group)
A05	Hs.461086	NM_004360	CDH1	Cadherin 1, type 1, E-cadherin (epithelial)
A06	Hs.476092	NM_003278	CLEC3B	C-type lectin domain family 3, member B
A07	Hs.143434	NM_001843	CNTN1	Contactin 1
A08	Hs.523446	NM_080629	COL11A1	Collagen, type XI, alpha 1
A09	Hs.101302	NM_004370	COL12A1	Collagen, type XII, alpha 1
A10	Hs.409662	NM_021110	COL14A1	Collagen, type XIV, alpha 1
A11	Hs.409034	NM_001855	COL15A1	Collagen, type XV, alpha 1
A12	Hs.368921	NM_001856	COL16A1	Collagen, type XVI, alpha 1
B01	Hs.172928	NM_000088	COL1A1	Collagen, type I, alpha 1
B02	Hs.508716	NM_001846	COL4A2	Collagen, type IV, alpha 2
B03	Hs.210283	NM_000093	COL5A1	Collagen, type V, alpha 1
B04	Hs.474053	NM_001848	COL6A1	Collagen, type VI, alpha 1
B05	Hs.420269	NM_001849	COL6A2	Collagen, type VI, alpha 2
B06	Hs.476218	NM_000094	COL7A1	Collagen, type VII, alpha 1
B07	Hs.654548	NM_001850	COL8A1	Collagen, type VIII, alpha 1
B08	Hs.410037	NM_001901	CTGF	Connective tissue growth factor
B09	Hs.656653	NM_001903	CTNNA1	Catenin (cadherin-associated protein), alpha 1, 102kDa
B10	Hs.712929	NM_001904	CTNNB1	Catenin (cadherin-associated protein), beta 1, 88kDa
B11	Hs.166011	NM_001331	CTNND1	Catenin (cadherin-associated protein), delta 1
B12	Hs.314543	NM_001332	CTNND2	Catenin (cadherin-associated protein), delta 2 (neural plakophilin-related arm-repeat protein)
C01	Hs.81071	NM_004425	ECM1	Extracellular matrix protein 1
C02	Hs.203717	NM_002026	FN1	Fibronectin 1
C03	Hs.57697	NM_001523	HAS1	Hyaluronan synthase 1
C04	Hs.643447	NM_000201	ICAM1	Intercellular adhesion molecule 1
C05	Hs.644352	NM_181501	ITGA1	Integrin, alpha 1
C06	Hs.482077	NM_002203	ITGA2	Integrin, alpha 2 (CD49B, alpha 2 subunit of VLA-2 receptor)
C07	Hs.265829	NM_002204	ITGA3	Integrin, alpha 3 (antigen CD49C, alpha 3 subunit of VLA-3 receptor)
C08	Hs.440955	NM_000885	ITGA4	Integrin, alpha 4 (antigen CD49D, alpha 4 subunit of VLA-4 receptor)
C09	Hs.505654	NM_002205	ITGA5	Integrin, alpha 5 (fibronectin receptor, alpha polypeptide)
C10	Hs.133397	NM_000210	ITGA6	Integrin, alpha 6
C11	Hs.524484	NM_002206	ITGA7	Integrin, alpha 7
C12	Hs.592472	NM_003638	ITGA8	Integrin, alpha 8
D01	Hs.174103	NM_002209	ITGAL	Integrin, alpha L (antigen CD11A (p180), lymphocyte function-associated antigen 1; alpha polypeptide)
D02	Hs.172631	NM_000632	ITGAM	Integrin, alpha M (complement component 3 receptor 3 subunit)
D03	Hs.436873	NM_002210	ITGAV	Integrin, alpha V (vitronectin receptor, alpha polypeptide, antigen CD51)
D04	Hs.643813	NM_002211	ITGB1	Integrin, beta 1 (fibronectin receptor, beta polypeptide, antigen CD29 includes MDF2, MSK12)

D05	Hs.375957	NM_000211	ITGB2	Integrin, beta 2 (complement component 3 receptor 3 and 4 subunit)
D06	Hs.218040	NM_000212	ITGB3	Integrin, beta 3 (platelet glycoprotein IIIa, antigen CD61)
D07	Hs.632226	NM_000213	ITGB4	Integrin, beta 4
D08	Hs.13155	NM_002213	ITGB5	Integrin, beta 5
D09	Hs.521869	NM_000216	ANOS1	Kallmann syndrome 1 sequence
D10	Hs.270364	NM_005559	LAMA1	Laminin, alpha 1
D11	Hs.200841	NM_000426	LAMA2	Laminin, alpha 2
D12	Hs.436367	NM_000227	LAMA3	Laminin, alpha 3
E01	Hs.650585	NM_002291	LAMB1	Laminin, beta 1
E02	Hs.497636	NM_000228	LAMB3	Laminin, beta 3
E03	Hs.609663	NM_002293	LAMC1	Laminin, gamma 1 (formerly LAMB2)
E04	Hs.83169	NM_002421	MMP1	Matrix metallopeptidase 1 (interstitial collagenase)
E05	Hs.2258	NM_002425	MMP10	Matrix metallopeptidase 10 (stromelysin 2)
E06	Hs.143751	NM_005940	MMP11	Matrix metallopeptidase 11 (stromelysin 3)
E07	Hs.1695	NM_002426	MMP12	Matrix metallopeptidase 12 (macrophage elastase)
E08	Hs.2936	NM_002427	MMP13	Matrix metallopeptidase 13 (collagenase 3)
E09	Hs.2399	NM_004995	MMP14	Matrix metallopeptidase 14 (membrane-inserted)
E10	Hs.80343	NM_002428	MMP15	Matrix metallopeptidase 15 (membrane-inserted)
E11	Hs.546267	NM_005941	MMP16	Matrix metallopeptidase 16 (membrane-inserted)
E12	Hs.513617	NM_004530	MMP2	Matrix metallopeptidase 2 (gelatinase A, 72kDa gelatinase, 72kDa type IV collagenase)
F01	Hs.375129	NM_002422	MMP3	Matrix metallopeptidase 3 (stromelysin 1, progelatinase)
F02	Hs.2256	NM_002423	MMP7	Matrix metallopeptidase 7 (matrilysin, uterine)
F03	Hs.161839	NM_002424	MMP8	Matrix metallopeptidase 8 (neutrophil collagenase)
F04	Hs.297413	NM_004994	MMP9	Matrix metallopeptidase 9 (gelatinase B, 92kDa gelatinase, 92kDa type IV collagenase)
F05	Hs.503878	NM_000615	NCAM1	Neural cell adhesion molecule 1
F06	Hs.514412	NM_000442	PECAM1	Platelet/endothelial cell adhesion molecule
F07	Hs.82848	NM_000450	SELE	Selectin E
F08	Hs.728756	NM_000655	SELL	Selectin L
F09	Hs.73800	NM_003005	SELP	Selectin P (granule membrane protein 140kDa, antigen CD62)
F10	Hs.371199	NM_003919	SGCE	Sarcoglycan, epsilon
F11	Hs.111779	NM_003118	SPARC	Secreted protein, acidic, cysteine-rich (osteonectin)
F12	Hs.185597	NM_003119	SPG7	Spastic paraplegia 7
G01	Hs.313	NM_000582	SPP1	Secreted phosphoprotein 1
G02	Hs.369397	NM_000358	TGFBI	Transforming growth factor, beta-induced, 68kDa
G03	Hs.732539	NM_003246	THBS1	Thrombospondin 1
G04	Hs.371147	NM_003247	THBS2	Thrombospondin 2
G05	Hs.169875	NM_007112	THBS3	Thrombospondin 3
G06	Hs.522632	NM_003254	TIMP1	TIMP metallopeptidase inhibitor 1
G07	Hs.633514	NM_003255	TIMP2	TIMP metallopeptidase inhibitor 2
G08	Hs.644633	NM_000362	TIMP3	TIMP metallopeptidase inhibitor 3
G09	Hs.143250	NM_002160	TNC	Tenascin C
G10	Hs.109225	NM_001078	VCAM1	Vascular cell adhesion molecule 1
G11	Hs.643801	NM_004385	VCAN	Versican
G12	Hs.2257	NM_000638	VTN	Vitronectin
H01	Hs.520640	NM_001101	ACTB	Actin, beta
H02	Hs.534255	NM_004048	B2M	Beta-2-microglobulin
H03	Hs.592355	NM_002046	GAPDH	Glyceraldehyde-3-phosphate dehydrogenase
H04	Hs.412707	NM_000194	HPRT1	Hypoxanthine phosphoribosyltransferase 1
H05	Hs.546285	NM_001002	RPLP0	Ribosomal protein, large, P0

H06	N/A	SA_00105	HGDC	Human Genomic DNA Contamination
H07	N/A	SA_00104	RTC	Reverse Transcription Control
H08	N/A	SA_00104	RTC	Reverse Transcription Control
H09	N/A	SA_00104	RTC	Reverse Transcription Control
H10	N/A	SA_00103	PPC	Positive PCR Control
H11	N/A	SA_00103	PPC	Positive PCR Control
H12	N/A	SA_00103	PPC	Positive PCR Control

Table 4. Fold regulation values of ECM and adhesion molecules in GM Fbs (RT^2 array)

Gene	Fold regulation	p value	Fold regulation	p value
ADAMTS1	1.08	0.716629	3.18	0.000657
ADAMTS13	1.22	0.214722	2.08	0.000381
ADAMTS8	1.04	0.875029	-4.88	0.290210
CD44	1.07	0.825638	2.33	0.004781
CDH1	-1.02	0.834105	-2.49	0.073696
CLEC3B	1.00	0.829559	2.67	0.473928
CNTN1	-1.18	0.688289	2.52	0.002076
COL11A1	-1.11	0.144560	-1.03	0.503835
COL12A1	-1.13	0.684349	2.06	0.007246
COL14A1	-1.05	0.795726	1.43	0.329908
COL15A1	1.01	0.980629	2.54	0.017258
COL16A1	-1.08	0.511838	-1.15	0.314720
COL1A1	-1.02	0.999016	1.33	0.010823
COL4A2	1.08	0.718169	2.53	0.000601
COL5A1	-1.06	0.978819	2.10	0.020984
COL6A1	1.01	0.926112	2.37	0.042276
COL6A2	1.06	0.899037	2.93	0.005369
COL7A1	1.08	0.942082	4.35	0.002748
COL8A1	1.06	0.897411	2.71	0.248261
CTGF	1.11	0.230641	1.52	0.001767
CTNNA1	-1.01	0.977866	1.05	0.831960
CTNNB1	-1.07	0.960761	1.99	0.276861
CTNND1	-1.16	0.873495	1.16	0.847328
CTNND2	-1.13	0.759110	3.16	0.027769
ECM1	-1.05	0.507635	-3.31	0.000353
FN1	1.04	0.846784	1.07	0.886545
HAS1	-1.38	0.665626	-1.00	0.865533
ICAM1	1.12	0.551947	1.68	0.003033
ITGA1	-1.20	0.045952	-1.04	0.287498
ITGA2	-1.22	0.588610	1.75	0.061550
ITGA3	1.05	0.906710	2.19	0.098243
ITGA4	1.02	0.954204	1.13	0.898875
ITGA5	1.06	0.275005	1.23	0.003283
ITGA6	1.10	0.688693	1.41	0.076085
ITGA7	1.07	0.751566	1.28	0.164202

* Table continued in the next page

ITGA8	1.08	0.982173	-1.38	0.309784
ITGAL	1.16	0.893386	-1.19	0.492917
ITGAM	1.45	0.640931	-2.43	0.338333
ITGAV	-1.09	0.868592	1.03	0.980124
ITGB1	-1.04	0.951223	-1.13	0.549479
ITGB2	1.06	0.766786	2.03	0.017578
ITGB3	1.09	0.939581	1.53	0.382498
ITGB4	-1.04	0.993354	2.44	0.006163
ITGB5	1.07	0.838545	1.65	0.060925
ANOS1	1.99	0.189812	1.87	0.179485
LAMA1	-1.12	0.870136	-1.13	0.527754
LAMA2	-1.11	0.680183	1.36	0.019186
LAMA3	-1.41	0.389514	-1.35	0.234136
LAMB1	-1.01	0.950916	-2.21	0.000980
LAMB3	-1.17	0.925566	-1.64	0.276904
LAMC1	1.06	0.799835	1.53	0.047127
MMP1	1.44	0.180722	-1.44	0.041934
MMP10	1.03	0.896231	1.26	0.946052
MMP11	-1.08	0.590878	-1.44	0.056597
MMP12	1.22	0.790079	-776.57	0.147875
MMP13	1.04	0.854088	2.10	0.000847
MMP14	1.08	0.842745	4.64	0.014415
MMP15	-1.04	0.959207	1.34	0.850521
MMP16	1.03	0.940767	1.87	0.010016
MMP2	1.00	0.952308	-1.14	0.098753
MMP3	2.00	0.156489	3.20	0.010258
MMP7	-1.16	0.701597	1.01	0.881719
MMP8	1.09	0.785713	-2.69	0.245800
MMP9	1.18	0.976326	-1.19	0.441894
NCAM1	-1.07	0.923377	-1.31	0.393670
PECAM1	-1.16	0.969688	-2.31	0.385806
SELE	1.21	0.578405	-1.66	0.158296
SELL	1.05	0.827656	1.51	0.144048
SELP	-1.00	0.914596	-1.70	0.190495
SGCE	-1.13	0.243119	-1.58	0.007591
SPARC	-1.03	0.903766	1.03	0.729354
SPG7	-1.01	0.986861	1.72	0.036354
SPP1	-1.03	0.829655	1.15	0.610870
TGFBI	-1.06	0.341270	1.42	0.009024
THBS1	1.07	0.808687	2.95	0.000895
THBS2	1.02	0.876191	1.56	0.008256
THBS3	-1.23	0.239864	1.73	0.007719
TIMP1	1.05	0.936888	1.55	0.526719
TIMP2	-1.04	0.983904	2.32	0.054272
TIMP3	-1.04	0.777419	1.36	0.065055
TNC	1.02	0.830104	-1.04	0.505713
VCAM1	-1.08	0.846195	-2.47	0.195074

VCAN	1.16	0.897723	3.84	0.050823
VTN	-1.01	0.867357	2.07	0.016908
ACTB	-1.01	0.960792	1.95	0.059943
B2M	1.00	0.955797	-1.09	0.077184
GAPDH	1.03	0.884993	1.43	0.070255
HPRT1	-1.01	0.937612	-1.12	0.323585
RPLP0	-1.02	0.971180	-2.29	0.077020

Acknowledgements

First, I am grateful to Prf. Katharina Riedel and Prf. Michael Lalk for their guidance, trust and support of my PhD project. The fruitful discussions on the scientific results, their encouragement and advice motivated me in my PhD. Next, I would like to express my deepest gratitude to Dr. Kai Masur for giving me the opportunity to work in his group and supervising me in this interesting new topic 'Plasma Medicine'. He supported me throughout my work and gave me the scientific freedom to self-manage my work whenever required. Thank you for trusting on my ability and being positive on 'trying out experiments'. Next, I would like to thank Prf. Thomas von Woedtke for his constant encouragement on my project and his advice and thorough comments on the manuscript. It was quite reassuring to know that he is always up for discussions.

I further would like to thank my colleagues Liane Kantz and Felix Nießner for solving my experimental glitches. In addition, cheers to Anke Schmidt for giving directions on all real time related queries, Jan Wilm Lackmann for helpful discussions. I am thankful to my present and former group members Maria, Marieke, Vladimir for always putting up a positive atmosphere in the office. I would also like to appreciate all other researchers and colleagues at INP for their help and support.

Further, I am thankful to all my fellow PhDs in ZIK (Giuliana, Gabri, Marie, Basti, Johanna, Christina, Ramona, Juliana) for making my life a bit more colorful and enjoyable in Greifswald. Especially Giuliana, for being my go to person in Greifswald! My friends from Berlin, who always made me feel at home. The weekend trips to Berlin have given me a constant moral boost to continue my PhD here.

A big shout out to my whole family and friends from all over the world for being a part of my life and making it so much better!

Last but not the least, I am forever indebted to my parents for supporting me and believing me in all the decisions that I have taken in my life. The constant encouragement that I received from them have driven me to continue my studies abroad. Even though they are far way, I can always feel their love and support.

Finally, words will fall short to say thanks to my husband Wrijupan, who have stood like a pillar beside me for this last decade. Thank you for cheering me when it is needed, supporting me in difficult decisions, for believing me and most importantly for bearing with me through all the ups and downs in life. Thank you for being there!